Risk Assessment of Constraint Relaxation Practices

Final Project Report

M-34

Power Systems Engineering Research Center

Empowering Minds to Engineer
the Future Electric Energy System

Risk Assessment of Constraint Relaxation Practices

Final Project Report

Project Team
Kory W. Hedman, Project Leader
Arizona State University

Vijay Vittal
Arizona State University

James McCalley
Iowa State University

Graduate Students
Ahmed Salloum
Jonghwan Kwon
Yousef M. Al-Abdullah
Arizona State University

Xian Guo
Iowa State University

PSERC Publication 17-07

October 2017

For information about this project, contact

Kory W. Hedman
Arizona State University
School of Electrical, Computer, and Energy Engineering
P.O. BOX 875706
Tempe, AZ 85287-5706
Phone: 480 965-1276
Fax: 480 965-0745
Email: kory.hedman@asu.edu

Power Systems Engineering Research Center

The Power Systems Engineering Research Center (PSERC) is a multi-university Center conducting research on challenges facing the electric power industry and educating the next generation of power engineers. More information about PSERC can be found at the Center's website: http://www.pserc.org.

For additional information, contact:

Power Systems Engineering Research Center
Arizona State University
527 Engineering Research Center
Tempe, Arizona 85287-5706
Phone: 480-965-1643
Fax: 480-727-2052

Acknowledgements

This is the final report for the Power Systems Engineering Research Center (PSERC) research project titled “Risk Assessment of Constraint Relaxation Practices” (project M-34). This project is an extension of the prior PSERC research project, M-29.

We express our appreciation for the support provided by PSERC industry members and collaborators, including: Doug Bowman (SPP); Thomas Burns (SPP); Jay Caspary (SPP); Hong Chen (PJM); Yonghong Chen (MISO); Vikas Dawar (NYISO); Erik Ela (EPRI); Bob Entriken (EPRI); David Gray (GE); Garry Gu (GE); Melanie Hill (SPP); Muhammad Marwali (NYISO); Catherine Mooney (SPP); Nivad Navid (PG&E); Mahendra Patel (EPRI); Jim Price (CAISO); Harvey Scribner (SPP); Feng Zhao (ISONE).

Executive Summary

Today, system operators employ constraint relaxations practices, which allow certain constraints to be relaxed for penalty prices, in their market models. The prior research, PSERC project M-29, investigated the impacts of constraint relaxations on market solutions, reliability, and stability of the system while acknowledging the presence of the out-of-market correction phase that corrects constraint relaxations that occur within dispatch models. This research extends the prior work based on confirmation from industry advisors that these constraint relaxations can and do occur in real-time (i.e., actual) operations. The primary goal of this research is to analyze the impacts of constraint relaxations that propagate into actual operations. The analysis will include reliability analysis, stability analysis, risk-based analysis, as well as market economic analysis.

The report is presented in two parts.

Part I: Analyzing the Impacts of Constraint Relaxations in Real-Time Operations

Part I of the final report on PSERC project M-34 focuses on following concerns raised by industry advisors: 1) treatment of pre-contingency relaxations versus post-contingency relaxations; 2) the impact of constraint relaxations when accounting for probabilities of contingencies; 3) thermal transmission constraint relaxation staircase curve that considers the impact of the duration and magnitude of these relaxations; 4) the effect of operating reserve relaxations on system *N*-1 security. The research shows that:

- Constraint relaxations do occur in real-time operations.
- Relaxations in energy market models have negative effects on real-time system performance in general.
- Pre-contingency (base-case) relaxations encountered voltage violations caused by the limited availability of reactive power as a result of committing fewer generating units in the relaxed cases.
- Post-contingency constraint relaxations are much less likely to appear in the realtime system as line flow violations compared to base-case relaxations.
- Allowing base-case and post-contingency constraint relaxations simultaneously had the largest impact on real-time system performance.
- A risk-based penalty price determination approach that avoids (or limits) relaxing high-risk lines, based on outage frequency and the impact on system operational security, resulted in decreased total relaxations magnitude and reduced voltage violations.
- An online penalty price determination model provides staircase penalty prices for thermal constraint relaxations while accounting for the magnitude and duration of the relaxations simultaneously; the numerical analysis shows that the proposed approach can help system operators to reduce or eliminate the operator's manual intervention to cope with model infeasibility or possible risk on the transmission assets. This also helps reduce the discretionary changes imposed by market operators and provides added transparency for market participants.

- There was no trend or statistical significance in how much the reserve relaxations on system *N*-1 security costs; market solutions with reserve relaxations can have *N*-1 violations not only due to a lack of reserves, but also the approximate nature of the reserve requirement.

Part II: Risked-based Predictive Constraint Relaxation

Volume II of the final report on PSERC project M-34 reviews and investigates insights of industry-based constraint relaxation (CR) practice aligning with security constrained economic dispatch (SCED); it proposes and illustrates the methodology of risk-based predictive constraint relaxation to solve infeasibilities. Volume II summarizes the state of art of industry-based CR practice and statistics of the CR practice, which lays the foundation of this research.

A central concept developed in this volume is that, under conditions of CR, significant system maneuverability is gained through estimation of conductor temperature as flows vary from one market interval to another. This maneuverability occurs as a result of the increased line capacity obtained via the delay in conductor temperature change as flows change; it is safe because the temperature calculations are conservatively computed. The ability to conservatively compute temperature as a function of loading and time is built into the formulation of predictive risk-based constraint relaxation (P-RBCR). P-RBCR minimizes risk and cost during situations when one or more flows are approaching or exceeding what is considered to be their flow limit.

Specifically, this report addresses the following:

- Constraint relaxation practices are observed with high occurrences in real-time operations, both under pre-contingency and post-contingency conditions; we summarize CR statistics from several ISOs to show that CRs usually occur with very high influence on the markets, often causing locational marginal prices (LMPs) to spike.
- Shifting from power flow limits to conductor temperature limits increases dispatching flexibility.
- Use of conductor temperature limits for CR decisions over a specific time interval, i.e., a sequence of 5-minute market solutions, requires the initial temperature and conductor loading for that time-interval
- Risk, as used in this report, is a probabilistic metric quantifying the effects on system security level of heavy circuit loading; it can be applied to both pre- and post-contingency operating conditions; it can be computed using either power flow or conductor temperature.
- The methodology of P-RBCR is free of penalty price; the determination of appropriate penalty price has been a challenging issue facing ISOs, as it results in excessively high operational risk if too low and LMP spikes if too high.
- The CR decisions proposed by P-RBCR are less risky and more cost-efficient than that from the industry-based CR methodology.
- We have illustrated the P-RBCR approach on two systems. The first is a small IEEE test system; it provides conceptual insight into the performance of P-RBCR relative to the method currently employed within the industry. The second is a system developed using

public data to reflect the topology, conditions, and some actual constraint relaxations of the network managed by the New York ISO; this system illustrates the performance of P-RBCR in situations that are reasonable captures of those faced by the market operators of one ISO.

Project Publications:

[1] Y. Al-Abdullah, M. Abdi-Khorsand, and K. W. Hedman, "Analyzing the impacts of out of-market corrections," *2013 IREP Symposium*, pp. 1-10, Crete, Greece, Aug. 2013.

[2] Y. M. Al-Abdullah, M. Abdi-Khorsand, and K. W. Hedman, "The role of out-of-market corrections in day-ahead scheduling," *IEEE Transactions on Power Systems*, vol. 30, no. 4, pp. 1937-1946, Jul. 2015.

[3] Y. M. Al-Abdullah, A. Salloum, K. W. Hedman, and V. Vittal, "Analyzing the impacts of constraint relaxation practices in electric energy markets," *IEEE Transactions on Power Systems*, vol. 31, no. 4, pp. 2566-2577, Oct. 2015.

[4] X. Guo and J. McCalley, "Risk-based constraint relaxation for security constrained economic dispatch," *North American Power Symposium*, 2015.

[5] A. Salloum, Y. M. Al-Abdullah, K. W. Hedman, and V. Vittal, "Risk-based penalty price determination procedure for transmission constraint relaxations," *International Conference on Probabilistic Methods Applied to Power Systems (PMAPS)*, 2016.

[6] X. Guo and J. McCalley, "Risk-based constraint relaxation with high penetration of wind resources," *Intelligent System Applications to Power Systems (ISAP) Conference*, 2017.

[7] J. Kwon and K. W. Hedman, "Offline penalty price determination method for transmission thermal constraint relaxations," *Electric Power Systems Research*, accepted for publication, Aug. 2017.

[8] X. Guo and J. McCalley, "Risk-based predictive constraint relaxation," *IEEE Transactions on Power Systems*, to be submitted.

Student Theses:

[1] Yousef M. Al-Abdullah, *Energy Market Transparency: Analyzing the Impacts of Constraint Relaxation and Out-of-Market Correction Practices in Electric Energy Markets*, Ph.D. Dissertation, Arizona State University, Tempe AZ, Mar. 2016.

[2] Ahmed Salloum, *Impacts of Base-Case and Post-Contingency Constraint Relaxations on Static and Dynamic Operational Security*, Ph.D. Dissertation, Arizona State University, Tempe AZ, Mar. 2016.

[3] Jonghwan Kwon, *Performance Enhancement of Power System Operation and Planning through Advanced Advisory Mechanisms*, Ph.D. Dissertation, Arizona State University, Tempe AZ, expected in Nov. 2017.

[4] Xian Guo, *Constraint Relaxation and Cascading Contingency Monitoring: A Risk-Based Approach*, Ph.D. Dissertation, Iowa State University, Ames IA, expected in Dec. 2017.

Part I

Analyzing the Impacts of Constraint Relaxations in Real-Time Operations

Ahmed Salloum
Jonghwan Kwon
Yousef M. Al-Abdullah
Kory W. Hedman
Vijay Vittal

Arizona State University

For information about this project, contact

Kory W. Hedman
Arizona State University
School of Electrical, Computer, and Energy Engineering
P.O. BOX 875706
Tempe, AZ 85287-5706
Phone: 480 965-1276
Fax: 480 965-0745
Email: kory.hedman@asu.edu

Power Systems Engineering Research Center

The Power Systems Engineering Research Center (PSerc) is a multi-university Center conducting research on challenges facing the electric power industry and educating the next generation of power engineers. More information about PSerc can be found at the Center's website: http://www.pserc.org.

For additional information, contact:

Power Systems Engineering Research Center
Arizona State University
527 Engineering Research Center
Tempe, Arizona 85287-5706
Phone: 480-965-1643
Fax: 480-272-2052

Notice Concerning Copyright Material

Table of Contents

List of Figures

List of Tables

Nomenclature

Indices and Sets

g	Index of generators, $g \in G$.
$g(n)$	Set of generators connected to node n.
$H(g)$	Set of hydro-generators.
i	Index of generator segments, $i \in I$.
j	Index of penalty price segments, $j \in J$.
k	Index of transmission lines, $k \in K$.
n	Index for buses, $n \in N$.
t	Index for time periods, $t \in T$.
$\delta^+(n)$	Set of lines specified as to node n.
$\delta^-(n)$	Set of lines specified as from node n.

Parameters

B_k	Electrical susceptance of line k.
B_{im}	Imaginary part of admittance of element between i and m.
C^{ED}	End of service cost.
c_{gi}^{OP}	Operational cost of unit g (\$/MWh) segment i.
c_g^{NL}	No-load cost of unit g.
c_g^{SD}, c_g^{SU}	Shutdown and startup cost of unit g.
C^{NS}, C_x^{NS}	Penalty price for non-spinning reserve; fixed-price and staircase-price relaxations.
C^{SP}, C_x^{SP}	Penalty price for spinning reserve; fixed-price and staircase-price relaxations.
d	Conductor diameter.
D_i	Operating durations at relaxation point i.
D_{nt}	Demand at bus n in period t.

D_{T_c}	Duration of operations in hours at temperature T_c.
D_i^{eq}	Equivalent operating duration at relaxation point i.
Deg_T	Loss of tensile strength of a conductor.
Deg_{al}^{+}	Maximum degradation level of aluminum strands.
deg_i^{al}	Marginal degradation effect at each relaxation point.
FS_g	Indicator for unit g as a fast-start unit.
G_{im}	Real part of admittance of element between i and m.
h^{+}	Accumulated operation history at the maximum temperature.
$LODF_{kz}$	Line outage distribution factor for flow on line k with the loss of line z.
mC_P	Total heat capacity of conductor.
P_{gi}^{Limit}	Max output of unit g for segment i.
P_g^{+}	Max output of unit g.
P_g^{-}	Minimum output of unit g.
P_i	Penalty price for each staircase segment i.
F_k^{+}	Thermal rating of transmission line k.
F_k	Unplanned outage frequency of line k.
OL_j^{norm}	Normalized post-contingency overload on line j.
OL_j^{post}	Post-contingency overload on line j.
OL_{MAX}^{post}	Absolute maximum post-contingency overload for all contingencies.
$PTDF_{nk}^{REF}$	Power transfer distribution factor for an injection at n sent to the reference bus, for flow on line k.
Q_c	Forced convection heat loss.
Q_i	Reactive power consumed at bus i.
Q_R	Radiated heat loss.
Q_S	Solar heat gain.

$i^2R(T_c)$	Joule heating from the line flow at the line temperature T_c.
R_g^{HR}, R_g^{10}	Max hourly and 10-min ramp rates of unit g.
RS_{al}	Residual tensile strength of an aluminum strand.
Si	Complex power consumed at bus i.
$\overline{SL_\iota}$	Length of each segment i of staircase penalty price scheme.
STR_{al}	Initial strength of aluminum strands.
STR_{st}	Initial strength of steel cores.
STR_T	Initial strength of a conductor.
T_C	Line temperature.
T^+	Predetermined maximum temperature.
T_i	Anticipated temperatures at relaxation point i.
T_a	Ambient temperature.
UT_g, DT_g	Minimum up time and down time of unit g.
α	Percent of total supply required for operating reserve.
β	Percent of non-hydro supply required for operating reserve.

Variables

f_k	Real power flow on line k.
P_{git}	Real power output for unit g, segment i, period t.
p_{gt}	Total real power output for unit g in period t.
q_g	Total reactive power output for unit g in period t.
q_k	Reactive power flow on line k.
P_{nt}^{inj}	Net power injection at bus n for time period t.
r_{gt}^{NS}	Non-spinning reserve for unit g in period t.
r_{gt}^{SP}	Scheduled spinning reserve for unit g in period t.

r_t^{total}	Total system-wide operating reserve in period t.
R_{kj}	Risk index associated with line k outage and line j overload.
r_t^{req}	Required level of spinning reserve in period t.
s_{kt}^{k+}, s_{kt}^{k-}	Violation in the flow limits of line k in period t.
s_t^{SP}, s_t^{NS}	Violation in the operating reserve in period t.
u_{gt}	Unit commitment binary variable for unit g in period t.
v_i	Voltage at bus i.
v_{gt}, w_{gt}	Startup and shutdown variables for unit g in period t respectively.
θ_{nt}	Voltage angle at bus n in period t.

Terms

AC	Alternating Current
ACOPF	Alternating Current Optimal Power Flow
ACSR	Alloy Aluminum Conductor Steel Reinforced
CAISO	California ISO
CEA	Canadian Electricity Association
DCOPF	Direct Current Optimal Power Flow
DR	Constraint Relaxations
ERCOT	Electric Reliability Council of Texas
FMP	Flowgate Marginal Price
ISO	Independent System Operator
ISONE	ISO New England
LMP	Locational Marginal Price
LODF	Line Outage Distribution Factor
MISO	Midcontinent ISO
MMS	Market Management Systems

NERC	North American Electric Reliability Corporation
NYISO	New York ISO
OPF	Optimal Power Flow
PJM	Pennsylvania-New Jersey-Maryland Interconnection
PTDF	Power Transfer Distribution Factor
RTO	Regional Transmission Organization
RTS	Reliability Test System
RUC	Reliability Unit Commitment
SCED	Security Constrained Economic Dispatch
SCUC	Security Constrained Unit Commitment
SPP	Southwest Power Pool
TCDC	Transmission Constraint Demand Curve
TCR	Thermal Constraint Relaxations

1. Introduction

1.1. Research Premise

To ensure a reliable and continuous supply of electric energy in the most efficient manner, system operators manage generation fleet, which has complex operating requirements, while maintaining system synchronism, managing transmission assets and meeting stringent reliability standards. To do this, system operators solve various market models, which are typically optimization problems. Moreover, system operators employ constraint relaxations practices, which allow certain constraints to be relaxed for penalty prices, in their market model. That is, instead of strictly adhering to all the approximated system constraints, market operators treat certain constraints as soft constraints by adding slack variables into the constraints and penalty term multiplying the slack variable into the objective function.

Constraint relaxations that occur within dispatch models, such as security constrained unit commitment (SCUC), are generally corrected before the actual real-time dispatch. That is, a required operating limit, or constraint, may be violated within a mathematical model but, with the operator's out-of-market correction, the limit is still enforced during actual operations. However, based on confirmation from industry advisors from the prior project, PSerc Project M-29, these relaxations can and do occur in real-time. This research is an extension of the PSerc Project M-29 by specifically focusing on the situations when these relaxations occur in real-time operations.

1.2. Research Scope

Market models to date approximate complex operating, reliability, and transmission requirements while trying to optimize the dispatch of the generation fleet. Most common approximations include a linearized direct current power flow, linear ramping constraints, and proxy reserve requirements. Moreover, system operators enable constraint relaxation by introducing slack variables along with penalty prices on the corresponding slack variables. Approximated system conditions inherent in market models require additional adjustment processes, including reliability unit commitment and out-of-market corrections. The prior research, PSerc Project M-29, investigated the impacts of constraint relaxations on market solutions, reliability, and stability of the system. This research extends the prior work by focusing on the constraint relaxations that occur in real-time operations. The primary goal of this research is to analyze the impacts of constraint relaxations that propagate into actual operations. The analysis will include reliability analysis, stability analysis, risk-based analysis, as well as market economic analysis. This research focuses on following tasks:

- Treatment of pre-contingency (base case) relaxations versus post-contingency relaxations.
- The impact of constraint relaxations when accounting for probabilities of contingencies.
- Thermal transmission constraint relaxation staircase curve that considers the impact of the duration and magnitude of the constraint relaxations.
- The effect of operating reserve relaxations on N-1 security.

1.3. Report Organization

The rest of part one of this two-part report is summarized as follows. Chapter 2 presents background material regarding power system scheduling, such as optimal power flow (OPF), direct current optimal power flow (DCOPF), and SCUC, and constraint relaxations (CR). Also, Chapter 2 presents a summary and description of thermal constraint relaxation practices in the industry. Chapter 3 investigates the impacts of post-contingency constraint (emergency limits) relaxations on real-time system performance and energy markets. Chapter 4 introduces a risk-based penalty price determination approach that considers the impact of constraint relaxations when accounting for the probability of contingencies. Chapter 5 presents an online-based penalty price determination model for thermal constraint relaxations; the model determines staircase penalty prices based on the marginal degradation effect along with the conductor temperature anticipation. The model simultaneously captures the impact of magnitude and the duration of the relaxations and provides the penalty prices to a real-time security constrained economic dispatch (SCED) model at each execution interval. Chapter 6 investigates the effects of two different penalty price schemes for reserve relaxations on *N*-1 security and market outcomes. Finally, the conclusions are presented in Chapter 7.

2. Background

This chapter provides the background knowledge necessary to understand the technical details in the subsequent chapters. First, this chapter reviews the modeling of OPF and SCUC in Chapter 2.1. Second, this chapter introduces constraint relaxation practices in Chapter 2.2 and industry practices regarding transmission thermal constraint relaxation practices in Chapter 2.3.

2.1. Power System Scheduling

2.1.1. Alternating Current Optimal Power Flow

The OPF problem, generally, tries to minimize the total production cost in the power system subject to the system and resource constraints. These constraints include line power flows, bus voltage magnitudes, bus voltage angles as well as generator capacities and ampacities of the line.

The AC formulation of the OPF problem (ACOPF) uses the AC power flow equations in the constraints. Due to the non-convexity of the problem, obtaining a solution for large-scale ACOPF problems efficiently is challenging despite the development of nonlinear algorithms. The general mathematical formulation of the ACOPF problem takes the following form:

$$\text{Min } \sum_g (c_g^{OP} p_g) \tag{2.1}$$

$$\sum_g p_g + \sum_{\forall \delta^-(n)} f_k - \sum_{\forall \delta^+(n)} f_k = D_n \qquad \forall n \tag{2.2}$$

$$\sum_{\forall \Omega_G^n} q_g + \sum_{\forall \delta^-(n)} q_k - \sum_{\forall \delta^+(n)} q_k = Q_n \qquad \forall n \tag{2.3}$$

$$\| f_k^2 + q_k^2 \| \le S_k^+ \qquad \forall k \tag{2.4}$$

$$P_g^- \le p_g \le P_g^+ \qquad \forall g \tag{2.5}$$

$$Q_g^- \le q_g \le Q_g^+ \qquad \forall g \tag{2.6}$$

$$V_n^- \le v_n \le V_n^+ \qquad \forall n \tag{2.7}$$

$$\theta^- \le \theta_n - \theta_m \le \theta^+ \qquad \forall k \tag{2.8}$$

where the complex power flow equations for a line *k*, connecting bus *n* and *m* can be derived as following equations.

$$f_k = v_n^2 G_{ik} - v_n v_m (G_{ik} \cos(\theta_n - \theta_m) + B_{ik} \sin(\theta_n - \theta_m)) \tag{2.9}$$

$$q_k = -v_n^2 B_{ik} - v_n v_m (G_{ik} \sin(\theta_n - \theta_m) - B_{ik} \cos(\theta_n - \theta_m)) \tag{2.10}$$

In the above formulation for the ACOPF, the optimization variables are the active and reactive power generations, bus voltage magnitude, and angles. The total production cost is usually used as the objective function. The equality constraints (2.2) and (2.3) represent the power balance at each bus. It is important to note that, in the above formulation, the power generation is

represented by power injection to the grid, and the bus loads are in the receiving reference. The inequality constraints (2.4) represent limits on the apparent power flow in the line. The active and reactive power generation is bounded by (2.5) and (2.6) respectively. The proxy of power system stability bounds is enforced in (2.7) and (2.8) as the voltage magnitude and angle constraints.

2.1.2. Direct Current Optimal Power Flow

The DC formulation of the OPF problem (DCOPF) is a linearized version of the ACOPF model, which uses the linearized power flow equations. This approximation provides acceptable results for the day-ahead market processes while significantly reducing the time and computing resources required to solve large-scale optimization problems. The DC power flow approximation is based on the following assumptions [1]-[2]:

1) Neglecting the reactive power – voltage (Q-V) component of the regular AC power flow. This results in a completely linear, non-iterative, power flow algorithm. However, this approximation implies that DC power flow is only good for calculating real power flows on transmission lines and transformers and does not provide any information about the reactive power flows or the voltage profiles.

2) All voltages throughout the system are assumed to have an absolute magnitude of 1.0 p.u. This approximation makes the real power flow independent of voltage magnitudes and, therefore, the real power flow is only affected by branches impedances and voltage angles.

3) Nonlinear thermal losses are neglected by neglecting branch resistances.

4) The difference between voltage angles is assumed to be small enough to use the small angle trigonometric approximation: $(\cos(\theta_i - \theta_j) \approx 1)$, $(\sin(\theta_i - \theta_j) \approx (\theta_i - \theta_j))$.

The original non-convex ACOPF problem can be transformed into a linear programming model, as long as the objective is linear. It should be noted here that these approximations are not necessarily found in all DC power flow formulations. Some of these approximations may not be used in order to achieve a more accurate and realistic solution. For instance, if real power losses are known, these losses can be incorporated in the DC model by adding them to the system loads. The general mathematical formulation of the ACOPF problem takes the following form:

$$\text{Min } \sum_g (C_g p_g) \tag{2.11}$$

$$\sum_{\forall \Omega_G^n} p_g + \sum_{\forall \Omega_K^{n-}} f_k - \sum_{\forall \Omega_K^{n+}} f_k = D_n \qquad \forall n \tag{2.12}$$

$$f_k - B_k(\theta_n - \theta_m) = 0 \qquad \forall k \tag{2.13}$$

$$F_k^+ \le f_k \le F_k^+ \qquad \forall k \tag{2.14}$$

$$P_g^- \le p_g \le P_g^+. \qquad \forall g \tag{2.15}$$

2.1.3. Security Constrained Unit Commitment

The security constrained unit commitment model, used for this study, is a deterministic mixed integer program, which resembles the deterministic SCUC that is used in day-ahead market models. Its solution is used to produce the day-ahead market solution. The model presented is a mixed integer linear program, with the objective of,

$$minimize\ \sum_g \sum_t \left(c_g^{op} P_{gt} + c_g^{NL} u_{gt} + c_g^{SU} v_{gt} + c_g^{SD} w_{gt}\right). \quad (2.16)$$

The total system cost (2.16) is represented by linear cost term in $c_g^{op} P_{gt}$, where c_g^{op} is the linear fixed cost and P_{gt} is the supply for each generator during each time period. The fixed costs are represented by binary variables (whose value could only be 0 or 1) in u_{gt}, v_{gt}, and w_{gt}, which represent the generator status, startup indicator, and shutdown indicator. Therefore, the term $c_g^{NL} u_{gt}$ represents the fixed no-load cost term and $c_g^{SU} v_{gt} + c_g^{SD} w_{gt}$ represent the startup and shutdown costs, respectively.

The binary variables v_{gt} and w_{gt} are related to the status binary, u_{gt}, which represents the periods that a unit is committed. A generator turned on during a specific time period is represented by the binary v_{gt}, the startup variable, whereas a de-committed generator is represented by w_{gt}, the shutdown variable.

$$v_{gt} \geq u_{gt} - u_{gt-1} \qquad \forall g, t \quad (2.17)$$

$$w_{gt} \geq u_{gt-1} - u_{gt} \qquad \forall g, t \quad (2.18)$$

The SCUC replicates generator operating constraints. For example, the minimum and maximum production levels are represented by the parameters P_g^{min} and P_g^{max} respectively. In (2.19) and (2.20), a committed generator must be between its minimum and maximum production level. The variable r_{gt}^{SP} represents the spinning reserve acquired for a given generator during a specific time period and, therefore, the production level plus the spinning reserve must be less than the maximum supply level since, in the event of a contingency, a generator cannot provide power greater than its maximum production level. Thus, the reserve acquired plus the production level must be less than the maximum production level. These operational constraints are represented below,

$$P_{gt} \geq P_g^{-} u_{gt} \qquad \forall g, t \quad (2.19)$$

$$P_{gt} + r_{gt}^{SP} \leq P_g^{+} u_{gt}. \qquad \forall g, t \quad (2.20)$$

Operational generator requirements extend beyond minimum and maximum production levels. Another set of requirements include minimum time up and down that a committed/de-committed generator has after a unit has been turned on or off. This is represented in (2.21) and (2.22), where the summation of the startup and shutdown binary variable is over the minimum up and down time requirement, respectively.

$$\sum_{s=t-UT_g-1}^{t} v_{gs} \leq u_{gt} \qquad \forall g, t \quad (2.21)$$

$$\sum_{s=t-DT_g-1}^{t} w_{gs} \leq 1 - u_{gt} \qquad \forall g, t \quad (2.22)$$

Another generator operational constraint included in the SCUC is the hourly ramp rate. For simplicity, startup and shutdown ramp rates are assumed to be the generator's max production level, P_g^{max}. The ramp up and down constraints, using only hourly ramp rates, are shown in (2.23) and (2.24),

$$u_{gt-1} R_g^{HR} + v_{gt} P_g^{+} \geq P_{gt} - P_{gt-1} \qquad \forall g, t \quad (2.23)$$

$$u_{gt} R_g^{HR} + w_{gt} P_g^{+} \geq P_{gt-1} - P_{gt}. \qquad \forall g, t \quad (2.24)$$

Apart from generator operational constraints, the unit commitment model seeks to ensure *N*-1 reliable dispatch by also acquiring reserve. Committed generators could have their production level reduced to provide spinning reserve in the case of a contingency. Reserve could also be provided in the form of non-spinning reserve from fast-start generators. The total reserve acquired from the system during a given time period must be at least 7% of the total demand during that specific hour and greater than the largest generator production level plus any spinning reserve acquired from that generator, represented in (2.25) and (2.26). The total reserve acquired is also constrained to be at least half from spinning reserve, shown in (2.27). Furthermore, the total reserve for the given time period is also constrained to 7% of the total load.

$$r_t^{total} \geq \sum_n 0.07\, D_{nt} \qquad \forall n, t \quad (2.25)$$

$$r_t^{total} \geq P_{gt} + r_{gt}^{SP} \qquad \forall g, t \quad (2.26)$$

$$\sum_g r_{gt}^{SP} \geq 0.5\, r_t^{total} \qquad \forall t \quad (2.27)$$

The amount of spinning reserve acquired for a committed unit is further constrained by the emergency ramp rate of the specific generator. This restriction is needed because, in case of a contingency, a generator can only move within the emergency ramp rate. Any spinning reserve acquired in the unit commitment model must be also be constrained to the emergency ramp rate.

$$r_{gt}^{SP} \leq R_g^{10} u_{gt} \qquad \forall g, t \quad (2.28)$$

Non-spinning reserve can only be acquired by fast-start generators. A binary parameter FS_g is set to 1 to indicate a fast-start generator and 0 otherwise. Paired with this binary parameter, the non-spinning reserve acquired is constrained between a generator's minimum and maximum production levels for units that are not committed.

$$0 \leq r_{gt}^{NS} \leq R_g^{10}\left(1 - u_{gt}\right) FS_g \qquad \forall g, t \quad (2.29)$$

$$r_{gt}^{NS} \leq P_g^{+}\left(1 - u_{gt}\right) FS_g \qquad \forall g, t \quad (2.30)$$

Based on a DCOPF, the transmission network included in the unit commitment model are constrained by (2.31) to (2.32), where (2.33) is a node balance constraint. Alternatively, the line flow constraints could be formulated with the power transfer distribution factors (PTDFs) of the transmission network.

$$f_{kt} - B_k(\theta_{nt} - \theta_{mt}) = 0 \qquad \forall k, t \quad (2.31)$$

$$-F_k^+ \leq f_{kt} \leq F_k^+ \qquad \forall k, t \quad (2.32)$$

$$\sum_{k\epsilon\delta^+(n)} f_{kt} - \sum_{k\epsilon\delta^-(n)} f_{kt} + \sum_{g\epsilon g(n)} p_{gt} = D_{nt} \qquad \forall n, t \quad (2.33)$$

$$u_{gt}, v_{gt}, w_{gt} \in \{0,1\} \qquad \forall g, t \quad (2.34)$$

There are several forms and modifications that can be made to better represent the system. For example, there are several different reserve requirement rules that could be used in an attempt to guarantee *N*-1 reliability, but these reserve requirements do not necessarily guarantee reliability.

2.2. Constraint Relaxations

Power systems are among the largest and most complex systems in the world. System operators must manage generation scheduling while considering complex operational requirements and strict physical restrictions, to ensure a reliable supply of electric energy. To do this, system operators solve various market models, which are typically optimization problems. SCUC, SCED, and reliability unit commitment (RUC) are examples of these procedures. The electric power network is represented in these energy market models as a linear approximate DC system. This approximation is required in order to solve the optimization problems associated with the energy market operations without incurring prohibitive processing times and complexity. The constraint relaxation process, which is defined as allowing certain constraints in the optimization problem to be violated for a set penalty price, is considered as a type of approximation. That is, instead of strictly adhering to all the approximated system conditions, market operators treat certain constraints as soft constraints by adding slack variables into the constraints and penalty term into the objective function. Reference [3] presents a summary of CR practices in the industry and investigates the impacts of CR practices on markets and system security.

CR practices provide several benefits to market operators and participants. First, CR practices help market operators to obtain a solution within given time limits even if one or more of original (non-relaxed) constraints cannot be satisfied by available resources. Secondly, CR practices can provide gains in market surplus. Lastly, CR practice allows market operators to limit market prices (shadow prices). The electric energy markets in the US use shadow prices, such as locational marginal prices (LMPs) or flowgate marginal prices (FMPs), for market settlements. Originally, many independent system operators (ISOs) employed bid caps to limit market prices; however, this practice does not place a maximum cap on the dual variables (e.g., LMPs). Instead, by employing CR practices, the shadow prices are capped by the assigned penalty price [3]. For instance, when a node balance constraint is relaxed, its LMP will be limited by the assigned penalty price.

2.3. Thermal Constraint Relaxation: Industry Practices

Thermal constraint relaxations (TCR) allow a line flow to exceed the steady state line rating for a certain penalty price. Typically, exceeding the steady state operating level is only allowed for emergency situations for a limited time to avoid load interruptions. However, many ISOs already

implemented similar CR practices in their market models. This section introduces the current industry practices regarding TCR and associated penalty prices.

In sum, each ISO has a different attitude to utilize the CR practices. Also, the current industry practices for determining penalty prices are neither transparent nor systematic; rather, the current process relies on operator's judgments and stakeholders' agreements. Moreover, few ISOs does not provide information regarding their CR procedures and penalty price parameters which could raise concerns regardig market transparency.

2.3.1. Midcontinent ISO

Midcontinent ISO (MISO) sets marginal value limit of each transmission constraint in both day-ahead and real-time market through the transmission constraint demand curves (TCDC). First, MISO grouping transmission lines into two categories. The group one is classified based on the voltage level. A two-step TCDC is used for group one constraints to consider the impact of relaxation magnitude. Constraints that do not respond well to group one TCDCs are assigned to group two. Moreover, MISO operators can temporarily override group one or two TCDCs based on operating conditions. For example, when overloading is occurring for two or more consecutive dispatch intervals, MISO may temporarily override TCDCs. The shape and magnitude of an override TCDC are determined based on the current costs and capabilities of available resources that impact the transmission constraint. [4]

The TCDCs does not reflect what CR activations would cause to the system or transmission assets. Instead, TCDCs are determined as a mean to control power flows. Also, it is not clear how group one and two TCDCs differ each other. Moreover, the TCDCs does not change with magnitude and duration of constraint relaxations systematically. Rather, MISO operators temporary overrides TCDCs to handle exceptional situations.

2.3.2. Pennsylvania-New Jersey-Maryland Interconnection

Pennsylvania-New Jersey-Maryland Interconnection (PJM) uses a default penalty factor of $2,000/MWh regardless of voltage level of transmission constraints. The determination of the penalty factor is based on a historical constraints control analysis. PJM overrides penalty factor based on system operating condition. However, PJM does not allow the penalty factor to set the shadow price of a constraint. That is, PJM adjusts transmission ratings so that market model itself does not experience any line overloading and, as a result, transmission penalty factors does not affect shadow price of the constraints [5].

2.3.3. Electric Reliability Council of Texas

Electric Reliability Council of Texas (ERCOT) sets a fixed penalty price for TCR in the base case and contingency case as presented in Table 2.1. The penalty prices are determined based on the maximum LMP congestion component and shift factors [6]. However, the fixed penalty price scheme does not provide a meaningful way to distinguish the magnitude or duration of relaxations.

Table 2.1 Penalty prices for TCR in ERCOT

Base Case Voltage Violation	*N*-1 Constraint Violation		
	69 kV	138 kV	345 kV
$5,000	$2,800	$3,500	$4,500

2.3.4. New York ISO

New York ISO (NYISO) adjusts transmission ratings when power flows exceed the original rating. First, NYISO solves the market model with graduated transmission demand curve for specific transmission constraints and $4,000 for remaining constraints. Then, if any line flow level is greater than the original limit, NYISO set a relaxed limit equal to the relaxed flow plus 0.2 MW. In this case, penalty price does not affect market clearing prices since the market model will not experience overloading after operator's adjustment on transmission ratings. However, when the marginal re-dispatch cost is greater than penalty price, NYISO sets market clearing prices by penalty prices [7]. Table 2.2 presents the detailed penalty price information.

Although NYISO has a staircase penalty price scheme, the main purpose is to find a relaxed line flow which could be used to adjust the transmission rating. Also, the penalty prices do not capture the duration of relaxations. Lastly, the penalty price determination process is not publicly available.

Table 2.2 Penalty prices for TCR in NYISO

Graduated Transmission Demand Curve			Penalty Prices for Remaining Constraints
First 5 MWs	Next 15 MWs	Thereafter	
$350	$2,350	$4,000	$4,000

2.3.5. California ISO

California ISO (CAISO) has lowered the real-time scheduling run TCR penalty price factor from $5,000 to $1,500 in 2013. In 2016, CAISO proposed a new tiered approach for TCR with the penalty prices for the scheduling run based on the voltage level and magnitude of relaxation as presented in Table 2.3. Setting the lower price at first tier aims to promote efficient real-time market dispatch for small amounts of constraint violation. CAISO assumes that the relaxations occur within the first segment is less than the operational margin and does not have an impact on assets. The two-tiered CAISO's penalty price scheme for TCR seems to capture the magnitude of relaxations; however, the shape of the penalty price scheme does not capture the duration of relaxations [8].

Table 2.3 Penalty prices for TCR in CAISO

Voltage Level	230 kV and above		115 kV and lower	
Constraint Relaxation Level	Below 2 %	2% or more	Below 2 %	2 % or more
Penalty Price	$750	$1,500	$500	$1,000

2.3.6. Southwest Power Pool

Southwest Power Pool (SPP) utilizes the violation relaxation limits for spinning reserve requirements, operating constraints, resource ramp constraints, global power balance constraint, and resource capacity constraints. SPP implemented five-tiered penalty price scheme with 1 % segment length for the first four tiers as presented in Table 2.4. However, the step-size of segment and amount of price increases at each step is exactly same. Although a common belief is that a penalty price scheme with a higher number of segments would provide a better reflection of the actual impact of the relaxations, the process of the penalty price determination is also important. Also, the penalty price scheme of SPP does not capture the duration of constraint relaxations [9].

Table 2.4 Penalty prices for TCR in SPP

Loading Level	100 % - 101 %	101 % - 102 %	102 % - 104 %	103 % - 104 %	Thereafter
Penalty Price	$500	$750	$1,000	$1,250	$1,500

2.4. Conclusions

Reliable and economic deployment of a generation fleet to satisfy demand is a complex problem. ISOs solve complex unit commitment and economic dispatch models to determine appropriate resources to deploy at various time stages. Due to the complexity of power systems, several approximations are made within optimization models, including approximations of the transmission network with a linearized formulation known as the DCOPF instead of the more realistic ACOPF formulation. Furthermore, approximations occur in these models by relaxing specific constraints in the model, i.e., the constraint is allowed to be violated based on a predetermined penalty price. By doing so, the ISO receives several benefits, including the ability to manage prices and clear the market as well as the potential to obtain gains in social welfare (market surplus).

3. Post-Contingency Constraint Relaxations Analysis

3.1. Introduction

In this chapter, the investigation of constraint relaxations is extended to include post-contingency constraint relaxations. The purpose of this work is to investigate the impact of base-case and post-contingency constraint relaxations in energy market models on the real-time AC system performance and total generation costs. Although theoretically any constraint can be relaxed, only the thermal limits on the branches were considered in this study because these relaxations can be physically realized in the real-time system and have direct impact on security and reliability. Two types of constraint relaxations are considered in this study:

- Base-case relaxations: where the normal, continuous thermal ratings (Rate-A) are allowed to be relaxed
- Post-contingency relaxations: where the relaxations are allowed for emergency thermal ratings (Rate-C) following a contingency

In order to compare the impact of each type of these relaxations separately, as well as when both types are allowed simultaneously, four scenarios were investigated:

- No relaxation allowed
- Base-case relaxations only
- Post-contingency relaxations only
- Base-case and post-contingency relaxations allowed

The results from DC and AC analysis for each scenario were used to investigate the impact of each relaxation type on system security and reliability. Moreover, different penalty prices were also used for each scenario in order to investigate the correlation between penalty prices and real-time violations for each type of constraint relaxation. Since constraint relaxations also affect the total production cost, a thorough comparison between production costs for each scenario and for different penalty prices was also conducted.

In order to capture the direct effect of constraint relaxations on system security and reliability, the IEEE Reliability Test System (RTS) test case was utilized [10]. The test case was represented in the DC market model to obtain the SCUC solutions, and it was represented in PSS/E as well to capture AC and nonlinear characteristics such as reactive power, voltage magnitude and angles, and thermal losses. Different combinations of base-case and post-contingency relaxations were investigated. The same analysis was conducted twice for each scenario, once for cases with constraint relaxations and another time for cases that do not have any relaxations while ensuring analysis consistency.

3.2. Benders' Decomposition

Benders' decomposition is one of the commonly used mathematical decomposition techniques in solving particular large-scale optimization problems. The main idea of Benders' decomposition and other multistage optimization algorithms, is to partition the decision making process into several stages as opposed to the traditional approach of considering all variables and constraints simultaneously by solving a monolithic optimization problem. The decision making process usually consists of one or more optimization problems along with feasibility checks. For optimization problems with the appropriate structure, decomposition techniques usually reap significant computational benefits because typically the computation complexity growth of these large scale problems is not linear [11]. Moreover, Benders' decomposition facilitates the use of parallel computing which in turn could provide flexibility and utilize available computing resources efficiently [11]-[12]. However, Benders' decomposition serves its purpose only for certain types of problems as will be explained in the forthcoming discussion. Benders' decomposition is used in power systems decision problems such as security constraints unit commitment and maintenance scheduling, as well as other applications [11], [13].

Since the mathematics of Benders' decomposition is beyond the scope of this work, a brief description of Benders' decomposition mechanism is presented here. The first component of Benders' decomposition is the master problem. The master problem is usually an optimization problem that could be of various types, such as: linear programing (LP), mixed integer programming (MIP) or nonlinear programming (NL). Depending on the structure of the decomposition the master problem evaluates a lower bound solution by solving for all variables or for a subset of variables. The master problem therefore has fewer constraints or variables or both. The solution is then fixed and passed to the sub-problems to check its feasibility and optimality in case sub-optimization problems are present [13].

In a feasibility sub-problem the initial solution is checked against additional constraints. The goal of the feasibility check is to ensure that for the generated master problem solution, there exists a feasible solution for the sub-problem. In the event of infeasibility, the dual information is used to introduce additional constraints on the master problem to ensure feasibility in the next iteration. These additional constraints are called Benders' feasibility cuts. Therefore, sub-problems in Benders' decomposition are required to be convex problems in order to ensure that the generated cuts create a new feasibility region for the master problem that would remove the related violations in the next iteration [11]. The feasibility check is performed by introducing slack variables to relax the coupling constraints. The problem is considered feasible only if the summation of these slack variables is zero. After passing the feasibility check the sub-optimization problems evaluate the upper limit solution and modify the master problem through optimality Benders' cuts if the gap between the lower and upper limits exceeds a predefined value. Typically, this entire process is performed iteratively until a feasible solution within a desired optimality gap is obtained. It should be noted here that the application and structure of the problem dictate whether both feasibility and sub-optimization slave problems are required or just one of them. Moreover, depending on the relationship between sub-problems, decomposition can be either time (sequential) or functional based [11].

Benders' decomposition efficiency and, even viability, rely on the ability to distinguish the variables and their separability in order to form the master and slave problems. An efficient and successful decomposition synthesizes Benders' cuts that rule out a large class of trial values in the master problem. This is critical because Benders' cuts add additional constraints to the master problem at each iteration. Therefore, adding an excessive number of additional constraints would increase the size of the master problem to the point where the decomposition loses its purpose or even makes the problem more complicated. Hence, Benders' decomposition efficiency relies on the localization of variables, i.e. the ability to separate the variables among the constraints in a way that generates sub-problems with strong intra-coupling and weak inter-coupling correlation [14].

3.3. SCUC Model with Base-Case and Post-Contingency Relaxations

Using Benders' decomposition, the SCUC problem was split into two sub-problems. The first part (master problem) is a regular base-case SCUC problem. Solving the master problem determines the status and dispatch of each generating unit. The base-case SCUC solution is then passed on to the second sub-problem (slave problem) where post-contingency feasibility is checked. The slave problem generates feasibility cuts and passes them to the master problem for each infeasible contingency. These feasibility cuts act as additional constraints in the master problem and therefore reduce the feasibility region for the next SCUC solution. This process is iterative and will continue till a SCUC solution that is feasible for all contingencies is achieved.

The SCUC formulation is modified to allow both, base-case and post-contingency relaxations. Typically, relaxations are allowed by adding a slack variable to the constraint to be relaxed, and adding that slack multiplied by the penalty price to the objective function. Base-case relaxations were allowed in that manner since the objective function and relaxed constraints exist in the same sub-problem (master problem) as shown in Appendix A, Equation A.1 and Equation A.19. However, since the slave problem is merely a feasibility check for post-contingency conditions, the post-contingency relaxation decision cannot be made by the slave problem. Therefore, the slack variables were added to the feasibility cuts that are passed to the master problem as shown by Equation A.38 and Equation A.40. The post-contingency slack variables are also multiplied by the post-contingency penalty price and added to the main objective function. The post-contingency slack variables are sent back to the slave problem as fixed parameters in order for the relaxed lines to pass the post-contingency feasibility check as shown in Equations A.27, A.28, A.35, and A.36. The complete SCUC formulations (master and slave sub-¬problems) are presented in Appendix A.

3.4. Market Model Results

Using the security constrained unit commitment formulation presented in Appendix A, the day-ahead SCUC solutions (i.e. 24-hours solutions) were obtained for different scenarios. First, a non-relaxed SCUC solution was attained in order to be used as a benchmark for both, total production costs and system performance. Two base-case relaxed SCUC solutions were then achieved using two different penalty prices of values \$150/MWh and \$180/MWh. For the sake of comparison, a SCUC solution with post-contingency relaxation was performed using a penalty

price of $150/MWh (identical to base-case relaxation scenario). However, it was noticed that there were fewer post-contingency line relaxations -number and magnitude- compared to base-case relaxations. Therefore, another post-contingency SCUC solution was obtained using a penalty price of $30/MWh. Finally, a SCUC solution was obtained allowing both base-case and post-contingency relaxations, using penalty prices of $150/MWh and $30/MWh for base-case and post-contingency respectively. The SCUC problem was formed in AMPL and solved using Gurobi solver with a MIP gap of 0.1%. Table 3.1 presents the different relaxations scenarios as well as line relaxations details (number and magnitude) over the 24 hours and the total production cost.

Table 3.1 Relaxation scenarios summary

	No relax-ations	Base-case		Post-contingency		Base-case and Post-contingency
		Penalty price: 180	Penalty price: 150	Penalty price: 150	Penalty price: 30	Penalty price: Base: 30; Post: 150
Total cost %	100%	99.63%	99.09%	98.27%	97.87%	96.85%
Number of relaxed lines	-	18	31	12	14	Base: 36; Post: 22
Max. relaxation magnitude	-	9.5% (30MW)	16% (50MW)	2.2% (12.7MW)	6% (33.5MW)	Base: 14% (44MW); Post: 6% (33.5MW)

As can be seen in Table 3.1the total production cost dropped to 99.63% of the original (non-relaxed) case for base-case relaxations using a penalty price of $180/MWh. This relaxation resulted in a total of 18 relaxations with the highest relaxation being 9.5% beyond the line normal thermal rating. Decreasing the base-case penalty price to $150/MWh resulted in reducing the total production cost to 99.09% of the non-relaxed price. However, this relatively small reduction in total production costs was accompanied by a significant increase in the number and magnitude of line relaxations. Decreasing the base-case penalty price to $150/MWh has caused the line relaxations (violations) to rise to 31 relaxations with the maximum value being 16% above the line thermal rating. The base-case penalty price was not decreased below $150/MWh because of the excessive and unrealistic relaxations that would appear at lower penalty prices.

As for post-contingency relaxations, it can be noted from Table 3.1 that using a penalty price of $150/MWh caused total production cost to drop to 98.27% of the original price. This reduction was caused by relaxing the emergency thermal limits of 12 lines with a maximum violation of 2.2% beyond the line emergency thermal rating. Remarkably, the post-contingency penalty factor could be significantly reduced allowing for further reduction in total production costs without introducing unreasonable line flow violations. The total production cost was reduced to 97.87% of the original cost when a post-contingency penalty price of $30/MWh was used. Using this relatively low penalty price resulted in 14 line relaxations with the highest violation being 6% beyond the emergency thermal line rating.

Allowing both, base-case and post-contingency line relaxations together resulted in the lowest total production cost as well as the highest number and magnitude of line flow violations. The

penalty prices used were $150/MWh and $30/MWh for base-case and post-contingency line relaxations, respectively. Using these penalty prices the total production cost was reduced to 96.85% of the original cost. This reduction in cost was accompanied with 36 line flow relaxations in base-case with the highest relaxation being 14% beyond line normal thermal limits, and 22 line flow relaxations in post-contingency with the highest relaxation being 6% beyond line emergency thermal limits.

3.5. Base-Case AC Analysis

In order to investigate the impacts of line relaxations in the DC market model on real-time steady-state security and reliability, the SCUC solutions were used to obtain AC solutions using PSS/E. Therefore, the test case (RTS-96) was modeled in PSS/E using the same data used in the DC market model. Moreover, generators economic data and other constraints used to solve the SCUC were modeled in PSS/E in order to run ACOPF. Using ACOPF rather than just an AC power-flow provides several advantages, such as:

- Distribute losses among committed units economically and consistently
- Control reactive power generation to ensure acceptable voltage levels throughout the system
- Identify infeasibilities in the system and quantify their sensitivities (severities)

The different scenarios presented in Chapter 3.1 were simulated in PSS/E. The DC SCUC solution was used as a starting point for the ACOPF. Five different time periods (hours) were chosen for AC analysis. Those hours were chosen in a manner that guarantees the inclusion of significant amount of line relaxations for both, base-case and post-contingency scenarios. Those hours also comprise peak load, medium load, and light load hours. Table 3.2 summarizes the steady state line flow and voltage violations in the ACOPF solution for the different scenarios considered. From Table 3.2 it can be seen that even with no relaxations there were voltage and line flow violations. These violations are expected because of the approximations incorporated in the DC market model. In order to remove those violations and attain a completely feasible AC case, additional units need to be turned on. In this work no additional units were turned on in order to keep the operation conditions as close as possible to market solution.

Voltage and line flow violations are increased when constraint relaxations are allowed. As can be seen from Table 3.2 almost all base-case relaxations were translated into line flow violation in the AC case. The only exception was time period 19 in which only one violation appeared in AC solution. This exception can be explained again by the existing approximations in the DC market solution which result in slightly different AC solution. This also proves that relaxations in the market model could be considered another form of approximation and do not necessarily result in real-time violations all the time, provided that those relaxations are limited in number and magnitude. Table 3.2 also shows a noticeable increase in the number of voltage violations. These voltage violations are caused mainly by the fewer number of generators committed in the relaxed solution which resulted in less reactive power availability.

As for post-contingency relaxations, none of the line relaxations from the market solution appeared in real-time. This shows that post-contingency line relaxations have no direct adverse

effect on real-time line flows. However, voltage violations increased in real-time due to the reduced number of committed generators.

When base-case and post-contingency relaxations are both allowed more real-time line flow and voltage violations are observed. Base-case relaxations directly affect line flow violations as well as voltage violations, while post-contingency relaxations have a major impact on voltage violations. Therefore, when base-case and post-contingency relaxations are both allowed, the real-time AC case would encounter line flow violations as well as depressed voltage levels caused by reactive power deficiency.

Table 3.2 Base-case violations

	No relaxation					Base-case (PP: 150)				
Time period	*7*	*8*	*11*	*19*	*22*	*7*	*8*	*11*	*19*	*22*
Voltage violations	2	2	0	0	2	2	3	2	1	3
Flow violations	0	0	0	1	0	0	2	2	1	1
Number of relaxations	-	-	-	-	-	-	2	2	2	1
Maximum relaxation	-	-	-	-	-	-	7.4%	15.9%	10.5%	0.16%
	Post-contingency (PP: 30)					Base-case/Post-contingency (PP: 150/30)[1]				
Time period	*7*	*8*	*11*	*19*	*22*	*7*	*8*	*11*	*19*	*22*
Voltage violations	6	3	2	0	4	7	5	2	2	3
Flow violations	0	0	0	0	0	0	1	3	3	2
Number of relaxations	4	2	1	-	2	-/4	2/3	3/1	3/1	2/7
Maximum relaxation	2.9%	6%	-	-	2.3%	-/ 2.9%	5.7/ 6%	8.7/ 1.5%	12.4/ 0.54%	3.2/ 4.6%

3.6. Post-Contingency AC Analysis

In order to investigate the base-case and post-contingency relaxations impact on the system following a credible contingency event, a full-blown *N*-1 AC contingency analysis was run in PSS/E for each scenario shown in Chapter 3.1. The *N*-1 contingency analysis in this work included all branches (lines and transformers) as well as committed units. Following the loss of a unit the remaining units were re-dispatched according to their inertias.

[1] Base-case and post-contingency number and magnitude of relaxations for this scenario are displayed respectively.

Table 3.3 presents the post-contingency performance of the various considered scenarios. It can be seen that the original case (non-relaxed) was not *N*-1 secure since there were several line flow and voltage violations caused by various contingencies. There were also non-converged contingencies, which implies that the AC power-flow either diverged or the maximum number of iterations was reached before reducing the mismatches to acceptable values for those contingencies. It should be noted here that *N*-1 security could be achieved for this test case by committing additional units, re-dispatching the system, and utilizing other control parameters such as tap settings and shunt devices. However, that is beyond the scope of this work as it is desired to keep the DC market solution as unchanged as possible.

Table 3.3 Post-contingency violations

	No relaxation					Base-case (PP: 150)				
Time period	*7*	*8*	*7*	*8*	*7*	*8*	*7*	*8*	*7*	*8*
Voltage violations	67	48	67	48	67	48	67	48	67	48
Flow violations	9	5	9	5	9	5	9	5	9	5
Not converged	13	9	13	9	13	9	13	9	13	9
Number of relaxations	-	-	-	-	-	-	-	-	-	-
Maximum relaxation	-	-	-	-	-	-	-	-	-	-
	Post-contingency (PP: 30)					Base-case/Post-contingency (PP: 150/30)[2]				
Time period	*7*	*8*	*7*	*8*	*7*	*8*	*7*	*8*	*7*	*8*
Voltage violations	16	22	16	22	16	22	16	22	16	22
Flow violations	2	5	2	5	2	5	2	5	2	5
Not converged	20	21	20	21	20	21	20	21	20	21
Number of relaxations	4	2	4	2	4	2	4	2	4	2
Maximum relaxation	2.9%	6%	2.9%	6%	2.9%	6%	2.9%	6%	2.9%	6%

Similar to AC base-case analysis, base-case and post-contingency relaxations have increased the number of real-time line flow and voltage violations. It should be noted here that despite the decrease in the number of violations for some hours that does not imply better reliability or security conditions because it is always accompanied with an increase in the number of the unsolved (non-converged) cases. Therefore, this implies that violations actually became more severe causing more contingencies not to solve.

[2] Base-case and post-contingency number and magnitude of relaxations for this scenario are displayed respectively

The significant degradation in post-contingency reliability performance when base-case and post-contingency relaxations are both allowed aroused concerns related to excessive line flow violations caused by violations from coinciding from both types of relaxations in a cascading like effect. Therefore, the lines that were relaxed in base-case and post-contingency SCUC solution were identified and their real-time flows were monitored throughout the *N*-1 analysis. Table 3.4 shows those lines.

Table 3.4 Flows on lines relaxed in base-case and post-contingency

Time period 11		
Line	Base-case loading	Post-contingency loading
114-116	110%	120%
214-216	101%	105%
314-316	101%	109%
Time period 19		
114-116	108%	117%
214-216	102%	110%
314-316	103%	95%
Time period 22		
214-216	105%	106%
314-316	101%	91%

As discussed in AC base-case analysis (Chapter 3.3), Table 3.4 shows that lines relaxed in the base-case SCUC solution are always violated in real-time. Table 3.4 also shows the flows on these lines following a contingency event. It can be seen that the violations on some lines have doubled following a contingency, such as line 114-116 in time period 11 and line 114-116 in time period 19 with real-time flow violations of 120% and 117% of the lines emergency thermal limits respectively. This significant increase in line flow violations could easily fall beyond the acceptable relaxation limits and impose serious security problems especially in the occasion of another contingency event taking place (*N*-1-1).

3.7. Conclusion

This work has also investigated the effect of post-contingency constraint relaxations on system performance end energy markets utilizing the RTS-96 test case. The results presented in this work show that relaxations in energy market models have negative effects on real-time system performance in general since constraint relaxations are a form of violations in the market DC model. Base-case relaxations appeared consistently in real-time system as line flow violations. Base-case relaxations are based on the continuous normal thermal ratings of lines, therefore, they appeared as continuous violations in the real-time system. Scenarios that were base-case relaxed also encountered voltage violations caused by the limited availability of reactive power as a result of committing fewer generating units in the relaxed cases. Base-case relaxations have slightly increased the social welfare as they resulted in lower total production costs. Using lower penalty prices for base-case violations resulted in lower production costs. However, lowering the

base-case penalty price below certain values resulted in unrealistic relaxations that would be translated into excessive violations.

Post-contingency constraint relaxations on the other hand were based on the emergency thermal ratings of lines following a contingency. Therefore, post-contingency relaxations appear as line flow violations in real-time system only following the event of a certain contingency. Hence, post-contingency relaxations are much less likely to appear in the real-time system as line flow violations compared to base-case relaxations. However, similar to base-case relaxations, voltage violations appeared in post-contingency relaxed cases because of reactive power deficiency. Post-contingency relaxations showed significant impact on lowering the total production costs. It was also possible to use much lower penalty prices (e.g., $30/MWh) without causing excessive violations because base-case constraints had to be enforced all the time.

Allowing base-case and post-contingency constraint relaxations simultaneously had the largest impact on real-time system performance. Line flow violations caused by base-case relaxations and voltage violations caused by both types of relaxations appeared in real-time system. Moreover, allowing both types of relaxations simultaneously could result in cascading violation events. This could happen when a single line is relaxed in base-case and post-contingency simultaneously. Therefore, that line could encounter large violations as a result of base-case and post-contingency relaxations overlapping at the same time following a specific contingency. A maximum line overload of 120% above the emergency thermal rate was reported when the same lines was relaxed in base-case and post-contingency simultaneously. Allowing both types of relaxations had also the most significant effect on lowering the total production cost, as the total cost was reduced to 96.5% of the non-relaxed cost when base-case and post-contingency constraint relaxations were allowed simultaneously. Penalty prices should be chosen carefully in this scenario, especially base-case penalty price, to ensure that relaxations do not cause excessive real-time violations.

4. Impact of constraint relaxations when accounting for probabilities

4.1. Introduction

Constraint relaxations, by definition, mean that certain security, operational, or financial constraints are allowed to be violated in the energy market models for a pre-determined penalty price. Some of these relaxations are physically unrealizable, such as the node balance constraints. Other relaxations, however, are physically achievable, such as branches thermal limits and, therefore, could appear in the AC real-time system as actual violations. Even physically unrealizable relaxations could appear in the real-time system as violations in other forms since these relaxations are a form of approximation. Therefore, in order to assess the true risk associated with allowing certain constraints to be relaxed, the impact of these relaxations on real-time system performance was investigated. Capturing the impact of constraint relaxations on real-time system performance provides operators with a better understanding on how relaxations in the energy market models are translated into physical violations. This information can be used not only to assess the criticality of constraint relaxations, but also as a basis for determining penalty prices more accurately. In this chapter, power system performance criteria are presented and defined. The methodology of the analysis conducted is discussed, followed by the results.

4.2. Power System Performance Definition

Power system performance is defined by the following concepts:

1) Reliability: North American Electric Reliability Corporation (NERC) defines power system reliability as: "the degree to which the performance of the elements of that system results in power being delivered to consumers within accepted standards and in the amount desired. The degree of reliability may be measured by the frequency, duration, and magnitude of adverse effects on consumer service" [15]. Hence, power system reliability can be regarded as the probability of satisfactory operation over an extended time period.

2) Security: power system security is related to the robustness of the system following imminent disturbances (contingencies). NERC defines power system security as the degree of risk in the power system ability to withstand sudden disturbances such as short circuit faults or the loss of major components, without interruption of customer service. Security, therefore, depends on the system operating conditions as well as the probability of contingent events [16].

3) Stability: power system stability can be defined as "the ability of an electric power system, for a given initial operating condition, to regain a state of operating equilibrium after being subjected to a physical disturbance, with most system variables bounded so that practically the entire system remains intact" [16]. Power system stability depends on the severity and the physical nature of contingent events as well as the system operating conditions.

Power system performance aspects (reliability, security, and stability) are interrelated as all of them refer to system robustness and satisfactory operation. For instance, a power system cannot be considered reliable if it is insecure and it cannot be considered secure if it is unstable. Hence, reliability is the overall objective in power system planning and operation because it spans long period of time and comprises all other aspects. The distinction between power system security and stability is that security is more general, as it factors in the probability of contingent events. Power system security also accounts for contingencies that are not classified as stability events, such as equipment failure or sabotage. Power system security also considers post-contingency operating conditions, such that a system could be stable following a contingency but insecure due to post-contingency overloads or voltage violations.

4.3. Risk Based Penalty Price Constraint Relaxations

Throughout this work, constraint relaxations impacts on system performance were investigated using a single penalty price to allow relaxations in the DC SCUC model, which replicates operators practices related to constraint relaxations. For instance, the PJM original penalty price of 1000 $/MWh for line thermal limits was used. Therefore, all lines were subject to the same penalty price in the day-ahead market model, regardless of the severity of contingencies associated with each line. The static and dynamic security assessment conducted in this work revealed the adverse impacts of potential constraint relaxations on system performance are attributed to two major factors, number of committed generators and the overloading of major transmission lines. Naturally, heavily loaded transmission lines are expected to have higher impact on the system operational security when they are tripped as a result of a contingent event, which is usually initiated by a fault. Tripping a heavily loaded transmission line results in its original power flow being distributed on other routes, which can overload (and even trip) other lines in a cascading sequence. Moreover, high voltage, high capacity transmission corridors consist of long transmission lines. As a result, they have higher probability of being exposed to contingent events, compared to short lines. Therefore, long transmission lines that are heavily loaded should be distinguished in the constraint relaxation process in a manner that prevents or limits relaxing those lines, as they impose high risk to system security when they are overloaded.

4.3.1. High Risk Lines Identification

In order to categorize the transmission lines according to their associated risk on system security, a risk index was defined as:

$$R_{kj} = F_k \times OL_j^{norm} \qquad \forall k, j \quad (4.1)$$

$$OL_j^{norm} = \frac{OL_j^{post}}{OL_{MAX}^{post}} \qquad \forall j \quad (4.2)$$

where, R_{kj} is the risk index associated with line k outage and line j overload, F_k is the frequency of an unplanned outage on line k. F_k is expressed as the number of expected outage events in a

given time period. OL_j^{norm} is the normalized post-contingency overload on line j, and OL_j^{post} and OL_{MAX}^{post} are the post-contingency overload on line j and the absolute maximum post-contingency overload for all contingencies, respectively, in MVA. Therefore, the risk index calculated by (4.1) incorporates both, the frequency (likelihood) of the occurrence of the contingency and, the impact of that contingency on system security. The maximum normalized post-contingency line overload was used in (4.1) as an indication of the impact or severity of a certain contingency, as high post-contingency overloads are expected to result in additional unplanned line outages in a cascading sequence.

The post-contingency operating conditions risk indices for the PJM peak hour were calculated in order to identify the events with high risk indices. A full *N*-1 contingency analysis was conducted on the relaxed PJM peak hour to identify the contingencies that result in post-contingency line overloads (exceed emergency line thermal ratings). The next step in the process of evaluating risk indices was to determine the outage frequency of each line under consideration. The Canadian Electricity Association (CEA) 2012 Annual Report [17] was used to provide statistical and probabilistic information on transmission equipment forced outages. The CEA report used is based on five years (2008 – 2012) of historical data provided by Canadian utilities and operators. The CEA report was chosen for this work because of its comprehensive content and availability. However, other resources that provide similar data for transmission forced outages can be used. In addition, the lengths of transmission lines under consideration had to be estimated since the statistics and data provided by the CEA report are normalized for 100 km of length.

In order to estimate lines length, information such as lines impedance and conductor types and configurations used in the PJM system were utilized [18]. Table 4.1 shows a sample of contingencies and overloaded lines with the highest risk indices. Table 4.1 shows that line length plays a key role in determining the risk index associated with that line since it increases the likelihood of outage occurrence. Moreover, the magnitude of the post-contingency overload also has a direct effect on the risk index as it represents the impact of an outage event. Table 4.1 also shows that the outage of the relaxed line (ID 11001) results in two overloads with high risk indices. This particular line was relaxed in the market solution and had an AC base-case overload of 106% of its normal thermal rating. Therefore, it was desired to attain a relaxed market solution that avoids (or limits) the relaxation of lines that are associated with high risk index outages.

Table 4.1 PJM high risk index outage events

Overloaded line					Contingency					Risk index
Line ID	Voltage base kV	Emergency rating MVA	Maximum flow MVA	Normalized impact	Line ID	Voltage base kV	Line length mi	Base flow MVA	Outage freq. /year	
8253	345	897	912	0.524	8221	765	260	1905	1.15	0.603
11642	345	1718	1740	1.000	8542	765	86	1756	0.51	0.510
6949	345	1552	1626	0.934	6939	345	54	350	0.43	0.402
11474	138	142	254	0.146	11001*	138	171	136	2.64	0.385
11862	138	161	253	0.145	11001*	138	171	136	2.64	0.383
9966	230	626	791	0.455	9826	500	55	1087	0.41	0.187

* Relaxed line

4.3.2. Risk Based SCUC Solution

In order to incorporate the risk index information discussed in the previous subsection, three different penalty prices were defined in the DC SCUC algorithm instead of one. The penalty prices were defined in a manner that discourages the market model from relaxing lines that have high outage frequency, and the lines that have high outage impact. The penalty prices were defined as:

- High risk lines: this category includes transmission lines with thermal ratings greater than 999 MVA and, transmission lines which lengths are greater than 49 miles. A penalty price of 1500 $/MWh for relaxing line thermal limits was assigned for this category. This category includes 18% of the total number of lines.
- Medium risk lines: this category includes transmission lines with thermal ratings greater than 749 MVA and less than 1000 MVA and, transmission lines which lengths are greater than 9 miles and less than 50 miles. A penalty price of 1000 $/MWh for relaxing line thermal limits (original penalty price) was assigned for this category. This category includes 35% of the total number of lines.
- Low risk lines: all other lines are included in this category (thermal ratings less than 750 MVA and, lengths less than 10 miles). A penalty price of 500 $/MWh for relaxing line thermal limits was assigned for this category. This category includes 47% of the total number of lines.

It should be noted that the filters used to create these risk groups are not unique, however, the risk indices analysis presented in the previous subsection provided valuable information on the criteria of lines that are associated with high risk indices outages. For instance, the long lines with high outage frequency and the heavily loaded lines with high outage impact shown in Table 4.1 fell into the high-risk lines group. Moreover, additional risk groups with various penalty prices could be created depending on the system under consideration. Table 4.2 presents relaxations for the SCUC solution with risk based penalty prices. Table 4.2 also lists the relaxations results for the SCUC solution with single penalty price for comparison purposes.

Table 4.2 shows that none of the high risk group lines was relaxed. Out of a total of six relaxed lines, only two lines are considered as medium risk lines, while the rest are in the low risk lines group. On the other hand, when a single penalty price was used, two high-risk lines were relaxed (line IDs: 7557 and 11001). Moreover, although around half of the lines in the system were considered as low risk lines and were assigned low penalty price, the total relaxations magnitude was reduced when risk based penalty prices were used. The total magnitude of relaxations, for all relaxed lines, when risk based penalty prices were used is 81 MW, compared to a total of 119 MW of line relaxations when a single penalty price was used. This result denotes that heavily loaded and long transmission lines are more likely to be relaxed because of their ability to have a noticeable impact on the SCUC solution and operating conditions. As a result, more generating units were committed in the risk based constraint relaxation SCUC solution as an alternative to relax high-risk lines, as will be shown in the next subsection.

Table 4.2 Risk based penalty price relaxations

Risk based penalty price				
Relaxed line ID	Relaxation MW	Line rating MVA	Length mi	Risk group
190	2	553	4.3	Low
1703	51	670	2.7	Low
6470	8	115	45	Medium
6590	7	155	4	Low
7422	8	200	2	Low
7928	5	192	37	Medium
Single penalty price				
190	6	553	4.3	-
1703	4	670	2.7	-
6470	8	115	45	-
7557	85	1009	18	-
11001	2	128	171	-
11255	14	158	27	-

4.3.3. Risk Based Constraint Relaxations AC Analysis

In order to investigate the impacts of using risk based penalty prices on system performance, the market SCUC solution was used to solve an AC power flow. Out-of-market corrections were applied in the form of committing additional generators in order to eliminate active and reactive power mismatches caused by thermal losses and reactive power deficiency. Table 4.3 shows the number of committed generators and voltage violations for the risk based penalty price scenario, compared to the single penalty price and, non-relaxed solutions. It should be noted that the non-relaxed scenario presented in Table 4.3 is not *N*-1 secure in order to ensure comparison consistency with the other scenarios.

Table 4.3 Committed generators and voltage violations (risk based relaxation)

Risk based penalty price		
Committed generators (market)	Added generators	Voltage violations
1878	18	36
Single penalty price		
1837	26	52
No relaxation		
1935	12	6

Table 4.3 shows that fewer base-case voltage violations were reported in the risk based constraint relaxation solution as a result of the larger number of committed generators compared

to single penalty price scenario. Fewer out-of-market generators were also required in the risk based penalty price case. Moreover, none of the high-risk lines (long and high capacity lines) were relaxed when risk based penalty prices were used. Therefore, it can be concluded that using risk based penalty prices can have a positive impact on the system operational security by increasing the number of committed generators and, limit overflow violations.

4.4. Conclusion

Security assessment conducted on the relaxed PJM system indicated that some high capacity transmission lines were relaxed in the market SCUC model and resulted in overloading those lines in the AC real-time solution. However, those high capacity lines tend to have severe impacts on the system security in the event of a fault or forced outage. Moreover, those lines are usually high voltage major transmission corridors that span long distances and should not be violated. Therefore, it was desired to design a risk based penalty price scheme that would avoid (or limit) relaxing high-risk lines. Transmission lines were categorized in three distinctive groups depending on their risk indices. Risk indices were determined depending on the length of the lines (outage frequency) and, the impact on system operational security (post-contingency overloads) following a credible contingency. Increasing the penalty price for high capacity lines resulted in decreasing total relaxations magnitude. The total relaxations magnitude for the risk based penalty price scenario was 81 MW, while a total of 119 MW was reported for the traditional relaxed case. Therefore, more generating units were committed in the risk based penalty price SCUC solution, compared to the traditional single penalty price scenario. As a result, voltage violations were reduced because of the additional reactive power availability. Moreover, none of the high-risk lines (long and high capacity lines) were relaxed when risk based penalty prices were used.

5. Thermal Constraint Relaxation Staircase Curves

In the prior project titled "Constraint Relaxations: Analyzing the Impacts on System Reliability, Dynamics, and Markets (PSerc M-29)", the investigators presented an offline risk-based penalty price determination model, which determines fixed penalty prices for thermal constraint relaxations. The presented model considers probabilistic weather conditions to estimate the degradation risk of a conductor. However, the prior model forecasts the system operating state and weather condition to analyze the risks, which may bring an inaccuracy of the model due to forecasting errors. Moreover, the fixed penalty price scheme used in the prior model does not capture the duration and magnitude of the relaxations. In this chapter, the investigators propose an online penalty price determination model. The primarily objective of this work is to develop a systematic method to define staircase penalty prices that consider the duration and magnitude of the relaxations concurrently on an online basis.

5.1. Background and Motivation

System operators manage the power systems with diverse market optimization models at different time intervals. However, at times, market models have a hard time to get a solution with available resources in the system while respecting all the requirements. Thus, system operators introduce CR practices, which allow specific constraints could be violated with predetermined penalty prices. Theoretically, putting high enough penalty prices would be sufficient to prevent the infeasible situations. However, CR practices also have an impact on shadow prices (i.e., market clearing prices). That is, CR practices could be used to cap market clearing prices. For example, when a node balance constraint is relaxed, the LMP shall be capped by the penalty price of the node balance constraint relaxation. Therefore, it is crucial to set the penalty prices properly. This research proposes following criteria as necessary conditions for determining penalty prices for TCR.

- Penalty prices should reflect what CR practices could cause to the system.
- Penalty prices should be able to capture the magnitude and duration of the relaxations.
- Penalty prices should enable the prioritization of constraints so that constraints that are less significant can be relaxed more frequently than other constraints that are more significant, more important to ensure reliable operations.
- Penalty prices should avoid market price distortion.

Although the prior work in [19] successfully provides a systematic method for determining penalty prices based on the conductor degradation risk on an offline basis, the work does not fully meet the criteria above. First, the model forecasts the system operating state and weather condition to analyze the risks, which may bring an inaccuracy of the model due to forecasting errors. Such inaccuracy could cause market price distortions at times. Second, the fixed penalty price scheme used in the model does not capture the duration and the magnitude of the relaxations. Moreover, as presented in Chapter 2.3, none of the current industry practices on penalty price determination for TCR considers both the magnitude and duration of the

relaxations simultaneously. Although MISO allows the temporary override of penalty prices by operators during exceptional conditions, MISO does not systematically update the prices to reflect the operating condition. Also, the current industry practices do not consider the actual impact of transmission thermal limit violations on assets. This work proposes an online penalty price determination model. The primarily objective of this work is to develop a systematic method to define staircase penalty prices that respect the above criteria. That is, the model considers the duration and magnitude of the relaxations simultaneously on an online basis; moreover, the model captures the trade-off between relaxing transmission thermal limits and its impact on conductor materials.

5.2. Thermal Dynamics of Overhead Conductors

5.2.1. Thermal Behavior of the Overhead Conductors

Transmission line overflows, which are enabled by TCR, can elevate transmission line temperatures that can cause degradations on conductor materials. The overhead conductor thermal dynamics, which balances heating and cooling energies all the times, govern overhead conductor temperatures. The main sources of conductor heating are the line flow, the radiation from the sun, and the reflection from the surroundings. At the same time, the ambient air temperature, wind speed, and radiation of heat from the conductor incur a cooling effect [20]. These heating and cooling energies should be balanced all the times. However, the aspects that influence overhead conductor temperatures vary along a transmission line and are difficult to measure or predict precisely, due to the inherent non-linearity of the conductor thermal dynamics.

The research adopts the IEEE standard model, which will be referred as IEEE standard temperature model throughout this report, for calculating overhead conductor temperatures and thermal ratings at specific weather conditions [21]. The IEEE standard temperature model provides a method for calculating conductor temperature and the thermal capacity in the steady and dynamic states. In the IEEE standard temperature model, the dynamic heat balance equation is expressed as follows,

$$Q_C + Q_R + mC_P \frac{dT_c}{dt} = Q_S + i^2 R(T_c) \tag{5.1}$$

where Q_C is the forced convection heat loss, Q_R is the radiated heat loss, mC_P is the total heat capacity of conductor, Q_S is the solar heat gain, and $i^2R(T_c)$ is the joule heating from the line flow at the line temperature T_c. Convection heat loss mainly depends on wind speed and direction. Higher wind speeds directed perpendicular to a conductor gives a greater cooling effect. Solar heat gain is estimated based on how much solar energy is available as well as the emissivity and absorptivity of a conductor surface. A newly installed conductor typically has a lower emissivity and absorptivity whereas an old conductor has higher values [22]. Therefore, even with fixed line flows, line temperatures can vary based on ambient weather and conductor's physical conditions. The IEEE standard temperature model ignores the corona heating effect, magnetic heating effect, and evaporative cooling effect, which have little impact on the thermal behavior of the conductor. In addition, this equation normally requires repeated calculation due

to its inherent non-linearity. Specific methods to calculate each term in (5.1) can be found in [21].

5.2.2. Effect of High-Temperature Operation on the Overhead Conductor

It is clear that the operation of overhead conductors at elevated temperature can cause damage to the aluminum wires cumulatively and that continued high-temperature operation will significantly reduce the expected service life of the conductor. As the current flowing through a conductor increases, a conductor elongates with the increased temperature. This elongation increases the sag of the conductor, which decreases the ground clearance. If the conductor temperature remains high for an extended and consecutive period, the tensile strength of the conductor may decrease [23]. Although the loss of tensile strength is gradual, it accumulates over time and increases the probability of outages and blackouts [24]. Also, the effects of the elevated temperature operation on the aluminum conductor are irreversible and the damages experienced by the conductor are also cumulative. Note that other factors that may incur negative changes in the conductor's mechanical and electrical properties, such as wind induced vibration and corrosion, are outside of the scope of this study.

The loss of tensile strength of a conductor is caused by the annealing effect. Annealing is the metallurgical process where applied high temperature softens hardened metal resulting in a loss of tensile strength and is a function of both the magnitude of the temperature and the duration of the overheated time. The loss of tensile strength of aluminum conductors, such as Alloy Aluminum Conductor Steel Reinforced (ACSR), is a function of the loss of tensile strength of the aluminum strands compared to the rated strength of both the aluminum and steel wires. Typically, the steel wires will not anneal at temperatures incurred during steady-state and even for emergency operation of ACSR. The degradation of the aluminum strands only partially affects the overall conductor strength since ACSR derives half of its strength from the steel wires and remaining from the aluminum strands.

Some conductors are designed to reduce the effect of annealing on conductor strength by increasing the strength percentage of steel core or using already annealed aluminum strands. For those conductors, however, the maximum temperature can be determined by the thermal capability of connectors, as well as by other accessories. The reference [25] presents the maximum operating temperature of different types of conductors.

The loss of tensile strength due to annealing of the aluminum wires is a temperature and time dependent phenomenon. Predicting such loss requires a complex analysis of the metallurgical aspects of the conductor components as well as probability characteristic of ambient factors that may affect the conductor temperature. The key to approximate the loss of strength over the expected life of the conductor is to predict the time-temperature series that will result in annealing. The projected remaining strength of the conductor can be determined based on such information [25].

Harvey *et al*. [26] derived equations that capture the residual tensile strength of an overhead conductor. The IEEE standard model, which will be referred as IEEE standard degradation model throughout this report, for determining the effects of the high-temperature operation on

conductors adopts the residual conductor strength predictor model in [27]. The IEEE standard degradation model is expressed as follows,

$$RS_{al} = (-0.24T_c + 134){D_{T_c}}^{-(0.001T_c - 0.095)\left(\frac{0.1}{d}\right)} \tag{5.2}$$

$$if\ (-0.24T_c + 134) > 100, use\ 100\ for\ this\ term$$

$$Deg_T = 100 - \left(RS_{al}\left(\frac{STR_{al}}{STR_T}\right) + 109\left(\frac{STR_{st}}{STR_T}\right)\right) \tag{5.3}$$

where RS_{al} is the residual tensile strength of an aluminum strand in percentage with a diameter of d in inches, Deg_T is the loss of tensile strength of a whole conductor in percentage, and D_{T_c} is the duration of operations in hours at temperature T_c in degree. Also, STR_{al}, STR_{st}, STR_T are the initial strength of aluminum strands, steel core, and a whole conductor, respectively. Conductor degradation effects mainly depend on the magnitude and the duration of elevated temperature exposures. Moreover, the number of aluminium strands, their diameter, and the structure of a conductor are other key factors that influence conductor degradation effects. For example, the higher number of aluminium strands, which increases the relative portion of aluminium strands and decreases the relative portion of a steel core, can cause a higher degradation effect for the same temperature exposures, since the impact of an annealing effect that causes a loss of tensile strength of aluminium strands is higher, and the supportive contribution of the steel core is relatively lower.

Note that the presented IEEE standard degradation model was derived for ACSR. It assumes that the loss of tensile strength of stranded conductors is dependent on the diameter of the strand wires. The factor 109 in the presented model accounts for the increased load carried by the steel core as a result of conductor elongation due to the high-temperature operation. Moreover, in applying these equations, the cumulative strength reduction for multiple exposures at the same conductor temperature can be obtained by simply adding up all the hours and calculating the residual strength. For multiple exposures at different conductor temperatures, all exposures should be expressed as an orderly time series of temperatures and converted to an equivalent duration at the highest temperature [27].

This research adopts the IEEE standard degradation model; however, there is no guarantee that a specific method would work perfectly in all cases. Therefore, it would be advisable to investigate different methodologies for given situations.

5.3. Online Penalty Price Determination Model

The main goal of the online penalty price determination model is to provide staircase penalty prices to a real-time SCED model, which typically runs at every 5 minutes. Transmission line overflows, which are enabled by TCR, can elevate transmission line temperatures that can cause degradations on conductor materials. This research utilizes the IEEE standard temperature model and the IEEE standard degradation model to estimate the line temperatures and associated degradation effects. Both IEEE standard models have nonlinear characteristics, which make it hard to incorporate the models into a market optimization model as is. In the prior work in [19],

the work keeps the nonlinearity of the IEEE standard models and applies an offline based methodology to predict conductor degradation effect and set penalty price accordingly. The main reason for such an offline approach was that the IEEE standard degradation model does not provide meaningful information for a short-term period because the model was developed to predict the degradation effect for long-term operations (e.g., hundreds of operating hours at elevated temperature) based on an ordered series of temperature history. Moreover, the IEEE standard degradation model does not consider line temperatures that are lower than 95 °C. That is, for a line temperature lower than 95 °C, the IEEE standard degradation model cannot provide a level of degradation effect, and as a result, the associated impact on the penalty price determination shall be zero.

As mentioned, the primary goal of the proposed online penalty price determination model is to set staircase penalty prices. The design of a staircase penalty price scheme can be classified into the three categories: 1) set the number of segments, 2) define the length of segments, and 3) determine penalty prices for each segment. The main contribution of this work is to set penalty prices for each segment while assuming that there is a base staircase penalty price. The proposed model provides a price adder only if there is a positive anticipated marginal degradation effect due to a line temperature above 95 °C. That is, this study acknowledges the already existing penalty price schemes in the industry; however, this research envisions the enhancement of the existing practices by providing the price adder, which reflects the impact of the duration and magnitude of the relaxations. This functionality can help system operators to reduce or eliminate the operator's manual intervention to cope with model infeasibility or possible risk on the transmission assets. Note that the research does not try to enhance the functionality of the IEEE standard degradation model; instead, this research utilizes the IEEE standard model while trying to tackle the limitations. Figure 5.1 presents the flowchart of the proposed method.

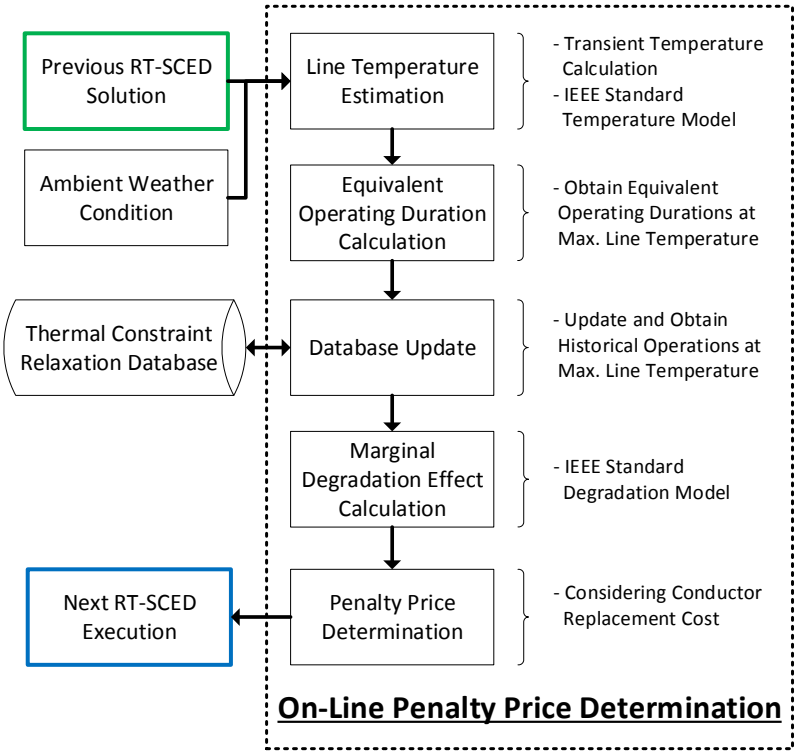

Figure 5.1 Flowchart of the online penalty price determination model.

Although the proposed penalty price determination process is not applied to a market optimization model as a set of constraints, the proposed model can be classified as an online based model since the execution of the model aligns with the real-time operations. Lastly, without loss of generality, it is hard to determine the actual degradation effect of conductors without a detailed physical investigation. A conductor may not suffer from degradations as expected from the proposed studies. There could be multiple reasons including ambient weather condition differences or, more importantly, actual line flow deviations from the DC-based line flow calculation. Therefore, it would be required to evaluate anticipated degradation effects and actual degradation effect routinely so that a penalty price determination process can keep updated based on archived events as well.

5.3.1. Line Temperature Estimation

An estimation of line temperature is an essential part of the proposed penalty price determination model. The work estimates the temperature by utilizing the IEEE standard temperature model. The work considers a transient temperature estimation while assuming step changes in power flow. First, the model calculates the initial line temperature from the previous market model execution. After obtaining the initial temperature, the model anticipates the line temperatures at the relaxation points, where the relaxations begin at each staircase segment, considering the step changes in line flows.

5.3.2. Equivalent Operating Duration Calculation

In the previous step, the model obtained the anticipated temperatures at each relaxation point. The next step is to calculate the conductor degradation effects at each relaxation point. The IEEE standard degradation model is a function of line temperature and operating duration. That is, the model requires an ordered series of temperature and operating duration history to calculate the final level of degradation effect [27]. Instead, this research introduces an operating duration conversion method which maps the temperature and operating duration set of each relaxation point to an equivalent operating duration at predetermined maximum line temperature. Therefore, the entire penalty price determination process, after the operating duration conversion, only deals with the single, maximum, temperature along with different operating durations.

The research makes several assumptions at this point. First, the penalty price determination model only considers the degradation effect on aluminum strands. Thus, the 10 % degradation criterion for a whole conductor, which was used so far throughout this report, is translated into the degradation criterion for aluminum strands accordingly. Let Deg_T^+ and Deg_{al}^+ as the maximum degradation level of a whole conductor and aluminum strands, respectively. Then the Deg_{al}^+ can be obtained as follows,

$$Deg_{al}^+ = (Deg_T^+ - 100)\frac{STR_T}{STR_{al}} + 109\frac{STR_{st}}{STR_{al}} + 100. \quad (5.4)$$

Second, let T^+ as the predetermined maximum temperature, T_i and D_i as the anticipated temperatures and operating durations at relaxation point i, and D_i^{eq} as the equivalent operating duration at relaxation point i. Also, let d as a diameter of an aluminum strand. Then the D_i^{eq} can be obtained from the following equation,

$$D_i^{eq} = \left(\frac{\alpha(T_i)}{\alpha(T^+)} {D_i}^{\beta(T_i)}\right)^{\beta(T^+)^{-1}} \quad \forall i \quad (5.5)$$

where

$$\alpha(T_i) = -0.24T_i + 134 \quad (5.6)$$

$$\beta(T_i) = -(0.001T_i - 0.095)(10d)^{-1}. \quad (5.7)$$

5.3.3. TCR Database Update

The process updates the TCR database with the temperature and operating duration set after the conversion process; therefore, the database only keeps track of operations at the predetermined maximum temperature, T^+. The updated operating history at the maximum temperature will be used as a base to calculate the marginal degradation effect in the next step. Also, the database updating process helps to evaluate anticipated degradation effects from the proposed model and degradation effect from the IEEE standard degradation model.

5.3.4. Marginal Degradation Effect Estimation

At this stage, the model knows the equivalent operation durations at maximum line temperature at each relaxation point. Also, the model knows the accumulated operation history at the maximum temperature. Next step is to calculate the marginal degradation effect at each relaxation point.

First, let h^+ as the accumulated operation history at the maximum temperature. Then, the marginal degradation effect at each relaxation point, deg_i^{al}, can be calculated from the following equation,

$$deg_i^{al} = Deg_{al}\left(T^+, h^+ + D_i^{eq}\right) - Deg_{al}(T^+, h^+) \qquad \forall i \quad (5.8)$$

where

$$Deg_{al}(T, D) = 100 - \alpha(T)D^{\beta(T)}. \qquad (5.9)$$

5.3.5. Penalty Price Calculation

The last step is to set penalty prices at each segment of the staircase penalty price scheme. The model translates the anticipated marginal degradation effect at each segment into a conductor degradation cost. Note that an out-of-service cost is an important factor to consider; however, in this work, such cost is not applied for the sake of complexity. Nevertheless, the conductor replacement cost, which may include the out-of-service cost or not, is a scaling factor. Thus, the proposed penalty price determination model can be extended to incorporate other possible costs. Based on the degradation effects at each relaxation point, the proposed model set penalty prices as follows,

$$P_i = \frac{C^{ED}\left(deg_{i+1}^{al} - deg_i^{al}\right)}{\overline{SL_\iota} \cdot Deg_{al}^+} \qquad \forall i \quad (5.10)$$

where P_i is the penalty price for each staircase segment and $\overline{SL_\iota}$ is the length of each segment. The model assumes that a marginal effect is constant between each segment; thus, the model has another linearization at this point. Ideally, if the model has an infinite number of segments, this model will provide an exact representation of the degradation effect or cost. Thus, this is a trade-off between the accuracy and tractability of the model.

5.4. Numerical Results

5.4.1. Analysis Design

This section presents the evaluation results of the proposed online penalty price determination model. The case study includes the following design and assumptions. First, the analysis assumes a base staircase penalty price scheme that has three segments as presented in Table 5.1. The chosen base staircase penalty price scheme is a combination of the penalty price design of

CAISO and SPP. Second, the study uses a Raven ACSR conductor [28]; Table 5.2 presents the electrical characteristic and capital cost of the conductor. Third, the study considers deterministic weather conditions, as presented in Table 5.3, to estimate the line temperatures. Note that the model can utilize real-time weather condition data if available. Lastly, the study sets the penalty price determination interval as 5 minutes; however, the analysis does not include any market optimization model, such as real-time SCED model. Instead, the analysis assumes hypothetical power flows at each interval and investigates the performance of the penalty price determination model. The proposed model and the IEEE standard models are implemented in Java. All the simulations are performed on the Intel® Core® 2.60 GHz CPU with 16 GB memory.

Table 5.1 Base staircase penalty price scheme

Segment	1	2	3
Length (MW)	15	30	30
Base Price ($)	500	1000	1500

Table 5.2 Raven ACSR conductor data

Structure (Al/St)	6/1
Rate A (MW)	160
Rate B (MW)	214
Rate C (MW)	241
Capital Cost (M$/mile)	0.84
End-of-service Cost (M$/mile)	0.29
Length (mile)	50

Table 5.3 Deterministic weather condition

Wind Speed	2 *ft/s*	Solar Time	12:00 PM
Wind Angle	45 °	Atmosphere	Clear
Elevation	150 *ft*	Line Direction	North-South
Latitude	38.5 °	Ambient Temperature (Summer)	35 °C
Emissivity	0.5	Ambient Temperature (Winter)	15 °C
Absorptivity	0.5		

5.4.2. The Impact of the Magnitude of the Relaxations

The analysis assumes three power flow cases, as presented in Table 5.4, to investigate the impact of the magnitude of relaxations on the penalty price determination. The study uses the summer weather condition from Table 5.3 along with the scheduling time at noon. Case A does not involve relaxations. Case B and Case C have relaxations with different magnitudes. Table 5.5

and Table 5.6 present penalty price adder determination results and the line temperature estimation results, respectively.

Table 5.4 Case study data (Case A-C, power flow, MW)

Interval	1	2	3	4
Case A	80	80	120	120
Case B	140	140	170	170
Case C	160	170	190	220

Table 5.5 Penalty price adder determination results (Case A-C, $)

Interval		1	2	3	4
Case A	Segment 1	-	-	-	-
	Segment 2	-	-	-	-
	Segment 3	611	611	939	1,096
Case B	Segment 1	-	-	-	65
	Segment 2	473	473	840	976
	Segment 3	1,161	1,161	1,181	1,191
Case C	Segment 1	-	126	786	1,073
	Segment 2	910	978	987	1,221
	Segment 3	1,186	1,193	1,204	1,439

Table 5.6 Temperature estimation results (Case A-C, °C)

Interval		1	2	3	4
Case A	Initial	59	59	65	69
	Segment 1	79	79	83	84
	Segment 2	89	89	93	94
	Segment 3	102	102	106	107
Case B	Initial	80	80	88	92
	Segment 1	90	90	94	95
	Segment 2	100	100	104	106
	Segment 3	113	113	118	120
Case C	Initial	90	93	101	117
	Segment 1	94	96	99	107
	Segment 2	105	107	111	118
	Segment 3	119	120	124	132

The results show that the proposed model sets the penalty price adders while capturing the magnitude of the relaxations properly. In Case A, the model only sets the penalty price adders at the last segments. The model anticipates that the line temperatures at the first two segments of Case A shall be lower than 95 °C; as a result, the model sets the price adders to zero. Although the step changes in the line flows between the current line flow, 80 MW, and the line flows at the first two segments, 160 MW and 175 MW, are substantial, the size of the transient temperature increases in 5 minutes are relatively less significant. In Case B, the line flows begin with 140 MW and the relaxations, with the magnitude of 10 MW, occur at the last two intervals. The model sets the penalty price adders for the last two segments at the interval one to three. Also, the model defines the penalty price adders for the entire segments at the last interval. Although there is a relaxation begins at the third interval, the anticipated temperature was lower than 95 °C due to the limited transient temperature increase from the second interval to the third interval. In Case C, due to the relaxations, the model sets the penalty price adders for the almost entire segments at all the intervals. The result shows that the determined penalty price adders increase accordingly based on the magnitude of the relaxations.

5.4.3. The Impact of the Duration of the Relaxations

The study defines additional two cases, as presented in Table 5.7, to investigate the impact of the duration of the relaxations on the penalty price determination. Again, the study assumes a summer weather condition with the scheduling time at noon. The Case D and Case E have continuous relaxations at the last three intervals. Table 5.8 and Table 5.9 present the line temperature estimation and penalty price adder determination results, respectively. The results show that the determined penalty price adders capture the duration of the relaxation properly. In Case D and Case E, the determined penalty price adders increase as the number of consecutive overloading intervals increase.

Table 5.7 Case study data (Case D-E, power flow, MW)

Interval	1	2	3	4	5
Case D	120	120	170	170	170
Case E	150	150	190	190	190

Table 5.8 Temperature estimation results (Case D-E, °C)

Interval		1	2	3	4	5
Case D	Initial	75	75	86	91	93
	Segment 1	87	87	93	95	96
	Segment 2	98	98	103	106	107
	Segment 3	111	111	117	119	120
Case E	Initial	84	84	97	103	106
	Segment 1	92	92	98	100	102
	Segment 2	103	103	109	112	113
	Segment 3	116	116	122	125	127

Table 5.9 Penalty price adder determination results (Case D-E, $)

Interval		1	2	3	4	5
Case D	Segment 1	-	-	-	-	176
	Segment 2	277	277	749	967	979
	Segment 3	1,151	1,151	1,177	1,189	1,194
Case E	Segment 1	-	-	476	860	896
	Segment 2	685	685	984	1,007	1,042
	Segment 3	1,173	1,173	1,200	1,224	1,257

5.4.4. The Impact of the Magnitude and Duration of the Relaxations.

Lastly, the study investigates the impact of the magnitude and duration of the relaxations simultaneously. The analysis defines a hypothetical power flow series, Case F, as presented in Table 5.10. To maintain the consistency, the study adopts a summer weather condition with the scheduling time at noon. Table 5.11 and Figure 5.2 presents the penalty price adder determination result. Also, Figure 5.3 presents the final staircase penalty price scheme after adding the penalty price adders in Table 5.11 to the base staircase penalty price scheme. In Table 5.11 and Figure 5.2, the result shows that the proposed online penalty price determination model sets penalty price adders properly while capturing the magnitude and duration of the relaxations. As a result, the result in Figure 5.3 illustrates that the final staircase penalty price scheme is automatically updated based on the impact of the relaxations.

Table 5.10 Case study data (Case F, power flow, MW)

Interval	1	2	3	4	5	6
Case F	140	140	170	170	150	150
Interval	7	8	9	10	11	12
Case F	150	180	180	190	190	190

Table 5.11 Penalty price adder determination results (Case F, $)

Interval		1	2	3	4	5	6
Case F	Segment 1	-	-	-	65	-	-
	Segment 2	474	474	840	977	832	752
	Segment 3	1,162	1,162	1,182	1,191	1,181	1,177
Interval		7	8	9	10	11	12
Case F	Segment 1	-	222	549	866	898	904
	Segment 2	715	980	985	1,013	1,043	1,049
	Segment 3	1,175	1,196	1,201	1,229	1,258	1,262

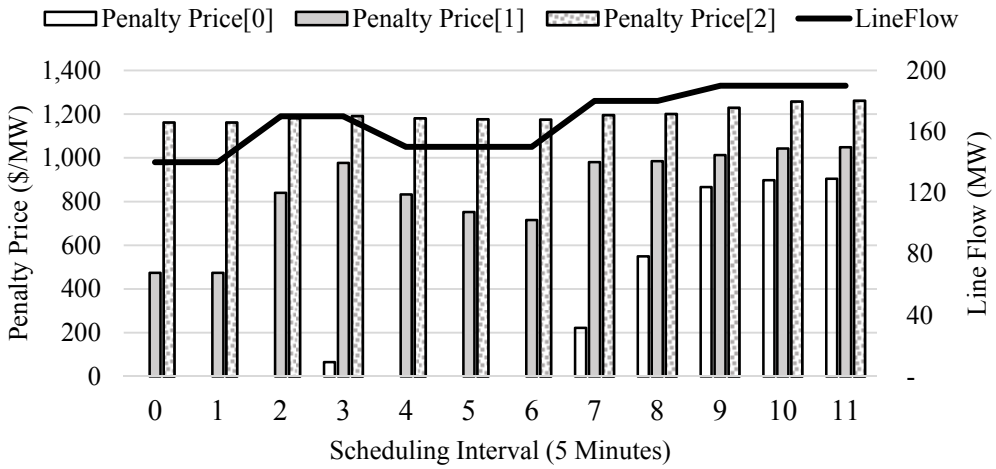

Figure 5.2 Penalty price adder result (Case F).

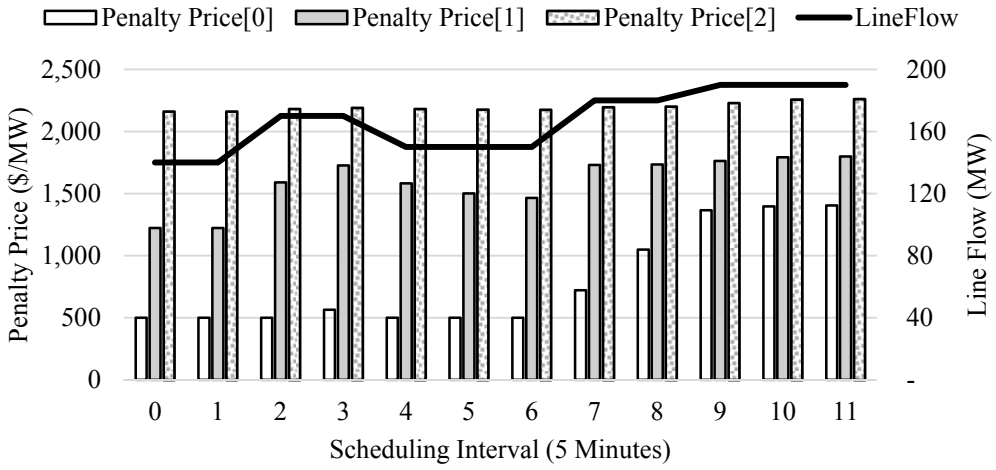

Figure 5.3 Final penalty price result (Case F).

5.5. Conclusion

ISOs employ TCR practices in the market optimization models for various purposes. Such practices can affect the generation fleet as well as market prices. Therefore, it is crucial to set the penalty prices properly. However, the current industry practices on determining penalty prices do not have a systematic methodology and rely on operator's judgment and manual intervention. Also, the currently used penalty price schemes cannot capture the impact of the magnitude and duration of the relaxations simultaneously.

This work proposes an online penalty price determination model. The main goal of the proposed model is to update and provide staircase penalty prices to a real-time SCED model at each execution interval. The model considers the magnitude and duration of the relaxations simultaneously; moreover, the model captures the trade-off between relaxing transmission thermal limits and its impact on conductor materials. The numerical analysis results show that the proposed model can provide an automated and systematic mean to set staircase penalty prices on an online basis.

6. Effects of Reserve Relaxations on *N*-1 Security

6.1. Introduction

Market management systems (MMS) employed by the various ISOs and Regional Transmission Organizations (RTOs) are used to solve unit commitment and determine dispatch decisions. The software employed by the MMS utilizes mixed integer linear programs that approximate the power system under the ISO or RTO's control. Even though the software and algorithmic performance have been improved, the MMS's market model and its solution cannot fully capture all the complexities involved in operating the power system. For example, linear DCOPF is used rather than the more accurate ACOPF. Other approximations include linear ramping constraints and proxy reserve requirements instead of explicitly modeling all contingencies existing in the MMS. Additional complexities result from load uncertainty and, more recently, variable generation.

Not all operating and reliability criteria can be explicitly modeled in the market and will require the proposed day-ahead market model's solution from the MMS to be adjusted. Therefore, an additional adjustment or post-processing phase is needed to correct for the approximations and inaccuracies inherent in market solutions. For example, the market solution must be altered to meet *N*-1 reliability criteria, a NERC standard [29]-[30] stating that the system must be able to withstand the loss of a single bulk element (transmission line or generator). Modification of the day-ahead market solution can be formalized with a process, such as the RUC, or by means of an informal process, such as an out-of-market correction [31]-[32]. The RUC is usually separate from the day-ahead market stage, but some ISOs are considering merging the two market stages [33]-[35].

Additionally, the approximations and inaccuracies characteristic of market models may cause the solution to become infeasible at times. To guarantee feasibility, ISOs and RTOs allow select constraints to be violated or relaxed in their market models, a practice known as constraint relaxation. By adding a slack variable to a specific constraint in the market model, constraint relaxations are incorporated within a market model by the ISO or RTO. Furthermore, the slack variable is then added to the objective function multiplied by a pre-determined penalty price. An example can be viewed in [36].

Including constraint relaxation practices in market models provides several benefits. They allow market operators to manage prices. Previous market designs only included a bid cap, which does not limit the LMPs in the market. Constraint relaxations thus allow market operators to limit the price of energy in the market. By including a slack variable in the node balance constraint in the market, the highest LMP that the market will have is the pre-determined penalty price associated with that slack variable in the objective.

Another benefit is that even small relaxations could potentially allow for substantial gains in market surplus. Requiring market models to strictly enforce approximated constraints in the market can significantly increase costs. Therefore, there is no need to strictly enforce approximated constraints. By including constraint relaxations in the market model, when the

day-ahead market is solved, the market is allowed to choose to relax constraints. However, the model will not readily do so unless the benefit of added flexibility, i.e., the value of the associated dual variable, is greater than the cost of the relaxation. For example, if a constraint causes the market model to be infeasible, had the market model included constraint relaxations, the market model's solution would have allowed the constraint to be relaxed, whereas without this practice the model would not return any solution. Constraint relaxations may allow violations in the market solution, but the constraints themselves at times have caused infeasibilities.

Previous work investigated the effect of constraint relaxations on market outcomes [36] as well as system security performance [37] due to line and nodal constraint relaxations in the market solution. In [38], the effects of pre- and post-contingency transmission line relaxations were investigated.

Most ISOs and RTOs utilize a fixed-price penalty price scheme in their market models, but some prefer a staircase penalty price function [39]. In this work, these two penalty price schemes are explored for constraint relaxations on reserve requirement constraints. In addition, several penalty prices, both fixed-price and staircase penalties, were tested by reporting *N*-1 violations and their effects on market outcomes. A more thorough review of ISO constraint relaxation practices of various ISOs, as well as the impact on the adjustment phase, is given in [36]. Others have investigated methods to obtain an *N*-1 secure solution from a market SCUC with proxy reserve requirements and the effect on market outcomes was detailed in [31]-[32]. Furthermore, in [40], the issue of reserve deliverability was investigated with renewable penetration and a review of ISO practices regarding this issue was examined.

6.2. Procedure

To investigate the potential impact of reserve relaxations on system security and market outcomes, the three area RTS-96 test case [41] was modified to include a 10% reduction in capacity limits for both normal operations and emergency ratings for all 120 transmission lines and transformers. In all other respects, the test case utilized the same data for all 96 generators located across 73 buses, 51 of which included aggregated load.

The RTS-96 test case provides an entire year of load data. To choose representative days, the k-means clustering algorithm in MATLAB [42] was used. This algorithm used the season, the total load, the day type, and the hourly change in load to allocate each day into four different clusters. With this algorithm, the load data was separated into four different clusters and sixteen days were selected from each cluster. Therefore, a total of 64 days were tested across all four clusters.

6.2.1. SCUC without relaxations

A traditional SCUC formulation without relaxations was used for comparison with the relaxed cases. In this section, the SCUC formulation is given in (6.1)-(6.24). The objective (6.1) minimizes total system cost, including the procurement of operating (contingency) reserves. In (6.2)-(6.6), generator operating constraints are represented, including generator capacity and

ramping constraints. The facet defining constraints [43]-[44] regarding unit status, start-up, and shutdown variables are used in (6.7)-(6.9). As a result, from (6.22)-(6.24), only the status variable must be binary while the start-up and shutdown, respectively, can be continuous variables.

The reserve requirements are represented in (6.10)-(6.17). Taking a more conservative approach, the SCUC is required to acquire reserves greater than or equal to 120% of the single largest generator contingency (6.10), which is a modification of CAISO's rules [45]. In (6.11), CAISO's rule, which specifies that the total reserve acquired must be greater than a combination of load (α) and load met by non-hydro resources (β), is still applied. CAISO specifies that operating reserves must exceed 5% of the load met by hydro resources and 7% of load met by non-hydro, which translates to α=0.05, β=0.02 in (6.11). From (6.12), the total reserve is reflected as spinning and non-spinning reserve and from (6.13) the total reserve must obtain at least half from spinning reserve, while (6.14)-(6.17) represent the limits for the spinning and non-spinning reserve acquired.

Finally, the DCOPF formulation is used to represent the network in (6.18)-(6.21). Line flow is calculated using a power transfer distribution factor (PTDF) formulation and a net-injection variable representing the total power flow into or out of a bus for a given period *t*. Note that in (6.21), line outage distribution factors (LODFs) are used to include transmission contingencies in the SCUC formulation [1], [46]. As a result, the dispatch chosen by the SCUC is *N*-1 secure for transmission line contingencies.

$$Minimize \ \sum_g \sum_t \sum_i \left(c_{gi}^{op} P_{git}\right) + \sum_g \sum_t (c_g^{NL} u_{gt} + c_g^{SU} v_{gt} + c_g^{SD} w_{gt}) + \sum_g \sum_t (0.25 c_{gI}^{op} r_{gt}^{sp} + 0.05 c_{gI}^{op} r_{gt}^{NS}) \quad (6.1)$$

$$u_{gt} P_g^{min} \le P_{gt} \le u_{gt} P_g^{max} \qquad \forall g, i = 1, t \quad (6.2)$$

$$0 \le P_{git} \le u_{gt} P_{gi}^{Limit} \qquad \forall g, i, t \quad (6.3)$$

$$P_{gt} = \sum_i P_{git} \qquad \forall g, t \quad (6.4)$$

$$u_{gt-1} R_g^{HR} + v_{gt} R_g^{SU} \ge P_{gt} - P_{gt-1} \qquad \forall g, t \quad (6.5)$$

$$u_{gt} R_g^{HR} + w_{gt} R_g^{SD} \ge P_{gt-1} - P_{gt} \qquad \forall g, t \quad (6.6)$$

$$v_{gt} - w_{gt} = u_{gt} - u_{gt-1} \qquad \forall g, t \quad (6.7)$$

$$\sum_{s=t-UT_g+1}^{t} v_{gs+T} + \sum_{s=t-UT_g+1}^{t} v_{gs} \le u_{gt} \qquad \forall g, t \quad (6.8)$$

$$\sum_{s=t-DT_g+1}^{t} w_{gs+T} + \sum_{s=t-UT_g+1}^{t} w_{gs} \le 1 - u_{gt} \qquad \forall g, t \quad (6.9)$$

$$1.2 P_{gt} + r_{gt}^{SP} \le r_t^{req} \qquad \forall g, t \quad (6.10)$$

$$r_t^{req} \ge \alpha \sum_g P_{gt} + \beta \sum_{g \epsilon H(g)=0} P_{gt} \qquad \forall g, t \quad (6.11)$$

$$r_t^{req} \leq \sum_g \left(r_{gt}^{SP} + r_{gt}^{NS}\right) \quad \forall t \quad (6.12)$$

$$0.5 r_t^{req} \leq \sum_g r_{gt}^{SP} \quad \forall t \quad (6.13)$$

$$0 \leq r_{gt}^{SP} \leq P_g^{max} - P_{gt} \quad \forall g, t \quad (6.14)$$

$$r_{gt}^{SP} \leq R_g^{10} u_{gt} \quad \forall g, t \quad (6.15)$$

$$0 \leq r_{gt}^{NS} \leq P_g^{max}(1 - u_{gt}) \quad \forall FS_g = 1, g, t \quad (6.16)$$

$$r_{gt}^{NS} \leq R_g^{10}(1 - u_{gt}) \quad \forall FS_g = 1, g, t \quad (6.17)$$

$$-P_{nt}^{inj} + \sum_{g \in g(n)} P_{gt} = d_{nt} \quad \forall n, t \quad (6.18)$$

$$-P_k^{max} \leq \sum_n P_{nt}^{inj} PTDF_{nk}^{REF} \leq P_k^{max} \quad \forall k, t \quad (6.19)$$

$$\sum_n P_{nt}^{inj} = 0 \quad \forall t \quad (6.20)$$

$$-P_k^{max,C} \leq \sum_n P_{nt}^{inj} PTDF_{nk}^{REF} + LODF_{kj} \sum_n P_{nt}^{inj} PTDF_{nj}^{REF} \leq P_k^{max,C} \quad \forall j, k, t \quad (6.21)$$

$$0 \leq v_{gt} \leq 1 \quad \forall g, t \quad (6.22)$$

$$0 \leq w_{gt} \leq 1 \quad \forall g, t \quad (6.23)$$

$$u_{gt} \epsilon \{0,1\} \quad \forall g, t \quad (6.24)$$

6.2.2. SCUC reformulation with reserve relaxation schemes

Two different reserve relaxation schemes, a fixed-price scheme and staircase curve price scheme are examined. In this work, similar to [47], spinning reserve was assumed to be 25% of the last operating cost segment and non-spinning reserve was assumed to be 5% of the last operating cost segment, such that the non-spinning price would be less than the spinning. As a result, the price for spinning reserve ranged from 0 $/MW to approximately 25 $/MW, while non-spinning reserve was approximately 10 $/MW. To include reserve relaxations in the SCUC means that the objective (6.1), reserve requirement for total reserves (6.12), and reserve requirement requiring half come from spinning reserve (6.13) must be modified.

For fixed-price relaxations, the following modifications needed for (6.1) and (6.12)-(6.13) are shown in (6.25)-(6.28). The prices for relaxing spinning and non-spinning reserves are listed in Table 6.1 and Table 6.2 below.

$$Minimize \ \sum_g \sum_t \sum_i \left(c_{gi}^{op} P_{git}\right) + \sum_g \sum_t (c_g^{NL} u_{gt} + c_g^{SU} v_{gt} + c_g^{SD} w_{gt}) + \sum_g \sum_t (0.25 c_{gI}^{op} r_{gt}^{sp} + 0.05 c_{gI}^{op} r_{gt}^{NS}) + \sum_t (c^{SP} s_t^{SP} + c^{NS} s_t^{NS}) \quad (6.25)$$

$$r_t^{req} \leq \sum_g \left(r_{gt}^{SP} + r_{gt}^{NS}\right) + s_t^{SP} + s_t^{NS} \quad \forall t \quad (6.26)$$

$$0.5r_t^{req} \le \sum_g r_{gt}^{SP} + s_t^{SP} \qquad \forall t \quad (6.27)$$

$$s_t^{SP}, s_t^{NS} \ge 0 \qquad \forall t \quad (6.28)$$

For staircase curve price relaxations, the following modifications needed for (6.1) and (6.12)-(6.13) are shown in (6.29)-(6.34). The index q represents the number of steps, which is assumed to be three, and the price for each step monotonically increases from the previous step. The prices for relaxing spinning and non-spinning reserves are listed in Table 6.1 and Table 6.2 below. Note that for the staircase relaxation scheme, a fourth iteration was solved, but the solution did not produce any relaxations and therefore its results were not reported.

$$Minimize \ \sum_g \sum_t \sum_i \left(c_{gi}^{op} P_{git}\right) + \sum_g \sum_t \left(c_g^{NL} u_{gt} + c_g^{SU} v_{gt} + c_g^{SD} w_{gt}\right) + \sum_g \sum_t (0.25 c_{gI}^{op} r_{gt}^{sp} + 0.05 c_{gI}^{op} r_{gt}^{NS}) + \sum_t \sum_q (c_q^{SP} s_{tq}^{SP} + c_q^{NS} s_{tq}^{NS}) \quad (6.29)$$

$$r_t^{req} \le \sum_g \left(r_{gt}^{SP} + r_{gt}^{NS}\right) + \sum_q (s_{tq}^{SP} + s_{tq}^{NS}) \qquad \forall t \quad (6.30)$$

$$0.5r_t^{req} \le \sum_g r_{gt}^{SP} + \sum_q s_{tq}^{SP} \qquad \forall t \quad (6.31)$$

$$0 \le s_{tq}^{SP}, s_{tq}^{NS} \le 2 \qquad \forall q = 1, t \quad (6.32)$$

$$0 \le s_{tq}^{SP}, s_{tq}^{NS} \le 5 \qquad \forall q = 2, t \quad (6.33)$$

$$s_{tQ}^{SP}, s_{tQ}^{NS} \ge 0 \qquad \forall t \quad (6.34)$$

Table 6.1 Spinning reserve relaxation prices

Scheme Type		Price 1	Price 2	Price 3	Price 4
Fixed		50 $/MW	100 $/MW	200 $/MW	400 $/MW
Staircase-price	Set 1 (2 MW allowed)	50 $/MW	100 $/MW	200 $/MW	N/A
	Set 2 (5 MW allowed)	100 $/MW	200 $/MW	400 $/MW	N/A
	Set 3 (unlimited)	500 $/MW	1000 $/MW	2000 $/MW	N/A

Table 6.2 Non-spinning reserve relaxation prices

Scheme Type		Price 1	Price 2	Price 3	Price 4
Fixed-price		40 $/MW	80 $/MW	200 $/MW	400 $/MW
Staircase-price	Set 1 (2 MW allowed)	40 $/MW	80 $/MW	160 $/MW	N/A
	Set 2 (5 MW allowed)	80 $/MW	160 $/MW	320 $/MW	N/A
	Set 3 (unlimited)	400 $/MW	800 $/MW	1600 $/MW	N/A

6.2.3. Contingency Analysis with Acquired Reserves

As part of testing the potential impacts of reserve relaxations, the non-relaxed SCUC, fixed-priced relaxed SCUC, and the staircase relaxed SCUC solutions were tested for *N*-1 violations with a contingency analysis tool (6.35)-(6.42) that only allows acquired reserve from the market solution to alleviate the *N*-1 contingency. This model allows for infinite transmission capability by including the slack variables s_{kt}^{+} and s_{kt}^{-}. However, if either of these variables is greater than zero, the dispatch is not *N*-1 secure. Note the model presented is for generator contingencies and can be easily modified for non-radial transmission line contingencies. However, with the LODFs formulation in the SCUC, non-radial transmission contingencies are already accounted; i.e. the event and the recourse action are taken into account in the market solution.

$$minimize \ \sum_k \sum_t s_{kt}^{+} + s_{kt}^{-} \tag{6.35}$$

$$N1_g \bar{u}_{gt}\left(\bar{P}_{gt} - \overline{R_{gt}^{SP}}\right) \le \hat{P}_{gt} \le N1_g \bar{u}_{gt}\left(\bar{P}_{gt} + \overline{R_{gt}^{SP}}\right) \quad \forall g,t \tag{6.36}$$

$$N1_g P_g^{min} \bar{u}_{gt} \le \hat{P}_{gt} \le N1_g P_g^{max} \bar{u}_{gt} \quad \forall g,t \tag{6.37}$$

$$0 \le \hat{P}_{gt} \le N1_g \overline{R_{gt}^{NS}} \quad \forall g,t,FS_g = 1 \tag{6.38}$$

$$-P_k^{max,C} - s_{kt}^{-} \le P_{kt} \le P_k^{max,C} + s_{kt}^{+} \quad \forall k,t \tag{6.39}$$

$$P_{kt} - B_k(\theta_{nt} - \theta_{mt}) = 0 \quad \forall t \tag{6.40}$$

$$\sum_{\forall \in \delta^{+}(n)} P_{kt} - \sum_{\forall \in \delta^{-}(n)} P_{kt} + \sum_{g \in g(n)} P_{gt} = d_{nt} \quad \forall n,t \tag{6.41}$$

$$s_{kt}^{+}, s_{kt}^{-} \ge 0 \quad \forall k,t \tag{6.42}$$

6.2.4. Benders' Decomposition

After evaluating the market solutions based on *N*-1 violations (6.35)-(6.42), both relaxed and non-relaxed market solutions are corrected for *N*-1 violations using a Benders' decomposition algorithm similar to [48]-[49], except non-spinning reserve was allowed to participate in mitigating *N*-1 violations. The original dispatch solutions (relaxed and non-relaxed) were all corrected such that no post-contingency violations occurred. After obtaining the *N*-1 secure solutions, market outcomes were compared. Finally, it should be noted that these *N*-1 secure solutions will no longer contain any reserve relaxations.

6.3. Results

The modified RTS-96 test case was solved by using the model presented above without relaxations (non-relaxed), fixed-priced relaxations (fixed-price), and staircase-priced relaxations (staircase). Furthermore, fixed-priced and staircase-priced relaxations cases were solved multiple times with increasing penalty prices, which were given in Table 6.1 and Table 6.2. In all three cases, the conservative reserve rule, (6.10), captured the same amount of total operating reserves

(approximately 701,000 MW) summed over all study days. This includes spinning and non-spinning reserves. With the fixed-price and staircase relaxations, not all of total reserve was truly acquired. Although the reserve required was approximately the same, the amount acquired from the market was less. Results regarding the number of relaxations for both cases (fixed-price and staircase), total system cost from the initial market solutions, the N-1 security violations, and the market outcomes corrected N-1 secure solutions obtained from utilizing the Benders' decomposition algorithm were compared.

The amount of reserve relaxed for each price iteration can be seen in Table 6.3. From these results, the fixed-price relaxation penalty scheme has more relaxations because the slack variable allows for any amount of reserve to be relaxed. On the other hand, the staircase relaxation scheme has less relaxations overall because the first two stairs of relaxations are constrained to be at most 2 and 5 MWs, respectively, and the final stair allows for any amount. As a result, the staircase scheme market solution only exhibits relaxations for the first three sets of prices, as seen in Table 6.1 and Table 6.2.

Table 6.3 Reserve relaxations distinguished by penalty scheme and reserve type (MWs)

Penalty Type	Reserve Type	Price 1	Price 2	Price 3	Price 4
Fixed-price	Spin	6033.94	103.5	28.2	0
	Non-spin	7819.8	876.5	243.8	77.5
Staircase-price	Spin	99.7	38.3	29.5	None
	Non-spin	131.1	65.6	58.1	None

Both relaxed solutions (fixed-price and staircase-price) have lower total system costs compared to the non-relaxed solution. In Table 6.4 below, the total system costs of the market solution summed over days with reserve relaxations for each price iteration is displayed. For the relaxed solutions, fixed-price and staircase, not all days in the data set had market solutions with relaxations. Furthermore, as the penalty price increased, the number of days with reserve relaxations decreased. For comparison, the non-relaxed market solution is summed over the same days of each relaxed solution separately, which is why there are two entries for the non-relaxed solution. From Table 6.4, it can be seen that the market solution for the non-relaxed case always has a slightly higher cost than both relaxed cases, which is expected because the market solutions that were relaxed (both fixed-priced and staircase) should be no worse off than the non-relaxed solution.

Table 6.4 Total system cost summed over days with relaxations ($k) for initial market solutions for relaxed and non-relaxed cases

Penalty Type	Price 1	Price 2	Price 3	Price 4
Fixed-price	47,832	27,761	21,782	13,291
Non-relaxed (compare w/ fixed)	48,024	27,777	21,791	13,292
Staircase-price	34,263	17,684	17,716	N/A
Non-relaxed (compare w/ staircase)	34,321	17,710	17,729	N/A

When testing these solutions for N-1 violations using (6.35)-(6.42), only the operating reserve acquired was allowed to participate in attempting to mitigate the potential violations from the N-1 contingency. In Table 6.5 below, the N-1 violations for hours with relaxations are reported for the fixed-priced and staircase-priced relaxed market solutions for hours with relaxations. The N-1 violations are compared to the non-relaxed case for the same hours. As the price increases, the relaxed solutions will have less relaxations and thus fewer hours are compared when testing for N-1 violations. Also, from Table 6.5, it can be seen that these relaxed solutions still have a greater number of potential N-1 violations than the non-relaxed case. Regardless, all initial market solutions, including the non-relaxed market solution, must be corrected such that the dispatch solutions are N-1 secure.

While the total system costs are similar, the non-relaxed solution exhibits considerably less N-1 security violations than the relaxed solutions – fixed-priced and staircase-priced – for days with reserve relaxations because the non-relaxed solution has acquired more reserves, whereas both relaxed solutions have acquired artificial resources (through the slack variables) and thus cannot dispatch as much reserve. Therefore, even with a small difference in total system cost, the dispatch solutions are quite different in their level of N-1 security; i.e. the non-relaxed case is always more secure than the relaxed cases because for hours with relaxations, the relaxed cases have less reserves to deliver.

Table 6.5 Total N-1 violations for hours with relaxations (MWs)

Case	Price 1	Price 2	Price 3	Price 4
Fixed-price	24217.8	3232.9	2409.6	828.0
Non-relaxed (same hours as fixed)	4111.0	2998.9	2381.4	721.5
Staircase-price	2700.4	2217.6	906.1	N/A
Non-relaxed (same hours as staircase)	2477.7	2203.5	858.6	N/A

After utilizing Benders' decomposition algorithm to correct the market solutions, N-1 secure solutions for all cases (fixed-price relaxed, staircase relaxed, and non-relaxed) were obtained. Table 6.6 has the total system cost after utilizing Benders' algorithm to achieve an N-1 secure solution. Only days that have relaxations were included. As before, the non-relaxed case is compared separately over the same days for each relaxed case. Therefore, there are two entries because days with relaxations for the fixed-priced solution are not always the same as those as the staircase-priced solution.

The difference between the total system cost from the market solutions, in Table 6.4, to the N-1 secure solutions, shown in Table 6.6, range from 1.75% to 3.34%. The change for the fixed-price solution going from market to N-1 secure was the greatest for the highest penalty prices at 3.34% and the lowest for the third penalty price set at 2.27%. Comparing the non-relaxed solution for the same days as the fixed-price relaxed solutions, the greatest change was at 2.75% for the same days of the fourth price set and 1.75% for the first price set days. For the staircase relaxed solution, the greatest change in total system cost from the initial market solution to the N-1 secure solution was for the second price set and the least was for the first price set. Comparing

the same days of the non-relaxed case, the greatest change in total system cost was for the same days of the second price set and the least was with the first price set.

When comparing the *N*-1 secure solutions, the non-relaxed solution for the same days is on whole cheaper than both of the previously relaxed cases that are now also *N*-1 secure. This is a result of the initial market solutions of both the previously relaxed cases needing more corrections to get to the *N*-1 secure solution and the fewer changes needed for the non-relaxed solution. Small differences in the initial market solutions lead to significant differences in the final outcomes, which can be seen in the differences in total cost for *N*-1 secure solutions in Table 6.6.

Table 6.6 *N*-1 secure solutions' total system costs summed over days that had relaxations in ($k)

Penalty Type	Price 1	Price 2	Price 3	Price 4
Fixed-price	49,041	28,529	22,277	13,735
Non-relaxed (compare w/ fixed)	48,864	28,348	22,232	13,657
Staircase-price	35,045	18,182	18,150	N/A
Non-relaxed (compare w/ staircase)	34,928	18,071	18,084	N/A

6.4. Conclusions

In this work, the effect of reserve relaxations on system *N*-1 security was investigated based on the static reserve rules utilized in the SCUC models employed by ISOs and RTOs today. Reserve requirements in the SCUC are proxy requirements and attempt to ensure *N*-1 security, but do not guarantee it. In this work, the reserve rule used was more conservative where the models were required to procure more reserve than the largest generator contingency. Furthermore, the use of the LODF formulation modeled the transmission contingencies in the SCUC formulation.

Reserve relaxations allowed in the market SCUC mean that less reserve has been procured because an artificial resource was acquired instead. Reserve requirements are proxy requirements that attempt to meet *N*-1 security. The use of a more conservative demand curve in this work does not mean that all the acquired reserve is deliverable for all potential post-contingency states. Reserve deliverability, i.e. network congestion in the post-contingency states, inhibits the deliverability of reserves. Therefore, market solutions with reserve relaxations can have *N*-1 violations not only due to a lack of reserves, but also the approximate nature of the reserve requirement. When testing for *N*-1 violations, the relaxed solutions had more violations than the non-relaxed solutions, which had a greater number of reserves than relaxed solutions. That said, it should be noted that the non-relaxed solution must also be corrected because of *N*-1 violations. Nevertheless, the non-relaxed *N*-1 secure solution is cheaper than the *N*-1 secure solutions that were previously relaxed because the relaxed solutions had more violations to correct. Because relaxed cases will typically need more corrections, more adjustments will be needed to arrive at a secure solution for relaxed cases than non-relaxed cases, which will typically require fewer corrections.

Even though the relaxed and non-relaxed cases have small deviations in total cost within the mipgap, a trend still exists in the number of N-1 violations that lead to a higher cost for the originally relaxed N-1 secure solutions. There is no trend or statistical significance in how much the relaxation costs, which is likely attributable to the fact that the SCUC is an approximation itself. The SCUC market solution is the starting point for Benders' algorithm, which is used to arrive at N-1 security for all solutions. As a result, the relaxed vs non-relaxed cases will have similar solutions, but the relaxed cases are always higher because of the need for more corrections. Yet a difference in the number of N-1 violations for both relaxed and non-relaxed cases still exists.

With that said, the present nature of the market models means that current relaxation practices are justifiable. This is especially true for reserve requirements, which are proxy constraints that attempt to guarantee N-1 security. Since a post-processing phase is already needed to meet other requirements not incorporated in the market model, being overly precise with the reserve requirement is not justifiable and thus allowing the reserve requirement constraint to sometimes be relaxed for a reason such as price control is justifiable.

7. Conclusions

System operators manage various market optimization models in market management systems to ensure a reliable and continuous supply of electric energy in the most efficient manner. Even though the software and algorithmic performance have been improved, market models cannot fully capture all the complexities inherent in operating the complex power system. Therefore, market models to date approximate complex operating, reliability, and transmission requirements while trying to optimize the dispatch of the generation fleet. Some common approximations include a linearized direct current power flow, linear ramping constraints, and proxy reserve requirements. Moreover, system operators employ constraint relaxations practices, which allow certain constraints to be relaxed for penalty prices, in their market model. To incorporate a constraint relaxation within a market model, the ISO or RTO adds a slack variable to a constraint in the market model. The slack variable is then added to the objective function multiplied by a pre-determined penalty price. To date, the practice of establishing what is an acceptable penalty price for a particular constraint has been primarily driven based on the results from stakeholder negotiations, without as much basis related to how to best choose these prices related to the impacts on market performance and operational security.

The prior research, PSerc project M-29, investigated the impacts of constraint relaxations on market solutions, reliability, and stability of the system while acknowledging the presence of out-of-market correction phase that corrects constraint relaxations that occur within dispatch models. This research extends the prior work based on confirmation from industry advisors that these constraint relaxations can and do occur in real-time, actual, operations; this research investigates the impact of constraint relaxations that propagate into actual operations.

First, this work has investigated the effect of post-contingency constraint relaxations on system performance end energy markets. The results presented in this work show that relaxations in energy market models have negative effects on real-time system performance in general since constraint relaxations are a form of violations in the market DC model. Base-case relaxations appeared consistently in real-time system as line flow violations. Base-case relaxations are based on the continuous normal thermal ratings of lines; therefore, they appeared as continuous violations in the real-time system. Scenarios that were base-case relaxed also encountered voltage violations caused by the limited availability of reactive power as a result of committing fewer generating units in the relaxed cases. Post-contingency constraint relaxations on the other hand were based on the emergency thermal ratings of lines following a contingency. Therefore, post-contingency relaxations appear as line flow violations in real-time system only following the event of a certain contingency. Hence, post-contingency relaxations are much less likely to appear in the real-time system as line flow violations compared to base-case relaxations. However, similar to base-case relaxations, voltage violations appeared in post-contingency relaxed cases because of reactive power deficiency. Allowing base-case and post-contingency constraint relaxations simultaneously had the largest impact on real-time system performance. Line flow violations caused by base-case relaxations and voltage violations caused by both types of relaxations appeared in real-time system. Moreover, allowing both types of relaxations simultaneously could result in cascading violation events. This could happen when a single line

is relaxed in base-case and post-contingency simultaneously. Therefore, that line could encounter large violations as a result of base-case and post-contingency relaxations overlapping at the same time following a specific contingency.

Second, this research has investigated a risk-based penalty price determination approach that considers the impact of constraint relaxations when accounting for the probability of contingencies. Transmission lines were categorized into three distinctive groups depending on their risk indices. Risk indices were determined depending on the length of the lines (outage frequency) and, the impact on system operational security (post-contingency overloads) following a credible contingency. Increasing the penalty price for high capacity lines resulted in decreasing total relaxations magnitude. Therefore, more generating units were committed in the risk based penalty price SCUC solution, compared to the traditional single penalty price scenario. As a result, voltage violations were reduced because of the additional reactive power availability. Moreover, none of the high-risk lines (long and high capacity lines) were relaxed when risk based penalty prices were used.

Third, this research proposed an online penalty price determination model that provides staircase penalty prices for thermal constraint relaxations to a real-time SCED model at each execution interval. The model accounts for the magnitude and duration of the relaxations simultaneously; moreover, the model captures the trade-off between relaxing transmission thermal limits and its impact on conductor materials. The numerical analysis results show that the proposed model can provide an automated and systematic mean to set staircase penalty prices on an online basis.

Lastly, the effect of reserve relaxations on system N-1 security was investigated based on the static reserve rules utilized in the SCUC models employed by ISOs and RTOs today. Reserve relaxations allowed in the market SCUC mean that less reserve has been procured because an artificial resource was acquired instead. Reserve requirements are proxy requirements that attempt to meet N-1 security. The use of a more conservative demand curve in this work does not mean that all the acquired reserve is deliverable for all potential post-contingency states. Reserve deliverability, i.e., network congestion in the post-contingency states, inhibits the deliverability of reserves. Therefore, market solutions with reserve relaxations can have N-1 violations not only due to a lack of reserves, but also the approximate nature of the reserve requirement. When testing for N-1 violations, the relaxed solutions had more violations than the non-relaxed solutions, which had a greater number of reserves than relaxed solutions. That said, it should be noted that the non-relaxed solution must also be corrected because of N-1 violations. Nevertheless, the non-relaxed N-1 secure solution is cheaper than the N-1 secure solutions that were previously relaxed because the relaxed solutions had more violations to correct. Because relaxed cases will typically need more corrections, more adjustments will be needed to arrive at a secure solution for relaxed cases than non-relaxed cases, which will typically require fewer corrections. However, there was no trend or statistical significance in how much the relaxation costs, which is likely attributable to the fact that the SCUC is an approximation itself. With that said, the present nature of the market models means that current relaxation practices are justifiable. This is especially true for reserve requirements, which are proxy constraints that attempt to guarantee N-1 security. Since a post-processing phase is already needed to meet other requirements not incorporated in the market model, being overly precise with the reserve

requirement is not justifiable and thus allowing the reserve requirement constraint to sometimes be relaxed for a reason such as price control is justifiable.

References

[1] A. J. Wood and B. F. Wollenberg, Power Generation Operation and Control, 2nd Ed., Hoboken, NJ: Wiley, 1996.

[2] B. Stott, J Jardim, and O. Alsaç, "DC power flow revisited," *IEEE Transactions on Power Systems*, vol. 24, no. 3, pp. 1290-1300, Aug. 2009.

[3] Y. M. Al-Abdullah, A. Salloum, K. W. Hedman, and V. Vittal, "Analyzing the impacts of constraint relaxation practices in electric energy markets," *IEEE Transactions on Power Systems*, vol. 31, no. 4, pp. 2566-2577, Oct. 2015.

[4] Midcontinent Independent System Operator, "Energy and operating reserve markets business practices manual," [Online]. Available: https://www.misoenergy.org/Library/BusinessPracticesManuals/Pages/BusinessPracticesManuals.aspx.

[5] Midcontinent Independent System Operator, "Transmission constraint control logic in market clearing engines," [Online]. Available: http://www.pjm.com/~/media/committees-groups/committees/mic/20170308/20170308-informational-only-transmission-constraint-control-logic-in-mces.ashx.

[6] Electric Reliability Council of Texas, "SCED penalty factor," [Online]. Available: www.ercot.com/content/meetings/natf/keydocs/2010/0809/08_sced_penalty_factor_100809.ppt.

[7] D. B. Patton, P. L. VanSchaick, and J. Chen, "2015 State of the market report for the New York ISO markets," Potomac Economics, Fairfax, VA, May 2016.

[8] California Independent System Operator, "Business practice manual for market operations," [Online]. Available: https://www.caiso.com/rules/Pages/BusinessPracticeManuals/Default.aspx.

[9] Southwest Power Pool, "VRL analysis," [Online]. Available: https://www.spp.org/documents/29222/2014_2015%20vrl%20analysis.pdf.

[10] University of Washington, "Power system test case archive," Dept. of Elect. Eng., 2007. [Online]. Available: http://www.ee.washington.edu/research/pstca. Accessed on August 2015.

[11] Y. Li and J. McCalley, "A general Benders' decomposition structure for power system decision problems," *IEEE International Conference on Electro/Information Technology*, pp. 72-77, 2008.

[12] S. Cvijic and J. Xiong, "Security constrained unit commitment and economic dispatch through Benders' decomposition: A comparative study," *IEEE PES General Meeting*, pp. 1-8, 2001.

[13] M. Shahidehpour and Y. Fu, "Benders' decomposition in restructured power systems," *IEEE Power and Energy Magazine*, pp. 20-21, 2005.

[14] M. Cadoli and F. Patrizi, "On the separability of subproblems in Benders' decompositions," [Online], Available: http://www.dis.uniroma1.it/~patrizi/docs/papers/cadoli-patrizi-CPAIOR06-final.pdf. Accessed on: August 2015.

[15] NERC Reliability Assessment Guidebook, Version 3.1, 2012, [Online], Available: http://www.nerc.com/files/Reliability%20Assessment%20Guidebook%203%201%20Final.pdf.

[16] P. Kundur, V. Ajjarapu, V. Vittal, *et al*., "Definition and classification of power system stability," *IEEE Transactions on Power Systems*, vol. 19, no. 3, pp. 1387-1401, Aug. 2004.

[17] Canadian Electricity Association, "Annual report - forced outage performance of transmission equipment," 2012.

[18] PJM, Interconnection Training Program, 2011, [Online], Available: https://www.pjm.com/~/media/training/nerc-certifications/to1-transmissionops.ashx.

[19] K. W. Hedman and V. Vittal, "Constraint relaxations: analyzing the impacts on system reliability, dynamics, and markets (M-29)," Power Systems Engineering Research Center, PSerc Project M-29, Sep. 2015.

[20] B. Clairmont, D. A. Douglass, E. C. Bascom, III, and T. C. Raymond, "Increased power flow guidebook: increasing power flow on transmission and substation circuits," Electric Power Research Institute, Palo Alto, CA, Tech. Rep. 1010627, Nov. 2005.

[21] IEEE Standard for Calculating the Current-Temperature of Bare Overhead Conductors, IEEE Standard 738-2006, Jan. 2006.

[22] Aluminum Electrical Conductor Handbook, 2nd ed. Washington, DC: The Aluminum Association, 1982.

[23] H. A. Smolleck and J. P. Sims, "Guidelines for the selection and operation of bare ACSR conductors with regard to current-carrying capacity," *Electric Power Systems Research*, vol. 5, no. 3, pp. 179-190, Sep. 1982.

[24] M. M. I. Bhuiyan, P. Musilek, J, Heckenbergerova, and D. Koval, "Evaluating thermal aging characteristics of electric power transmission lines," *23rd IEEE Canadian Conference on Electrical and Computer Engineering*, Calgary AB, pp. 1-4, May 2010.

[25] PJM Overhead Conductor Ad Hoc Committee, "Bare overhead transmission conductor rating," [Online]. Available: http://www.pjm.com/~/media/planning/design-engineering/maac-standards/bare-overhead-transmission-conductor-ratings.ashx.

[26] J. R. Harvey, "Effect of elevated temperature operation on the strength of aluminum conductors," *IEEE Transactions on Power Apparatus and Systems*, vol. PAS-91, no. 5, pp. 1769–1772, Sep.-Oct. 1972.

[27] IEEE Guide for Determining the Effects of High-Temperature Operation on Conductors, Connectors, and Accessories, IEEE Std. 1283-2013, Aug. 2013.

[28] Southwire Company, "ACSR," [Online]. Available: http://www.southwire.com/products/ACSR.htm.

[29] NERC Criteria for Reliability Coordinator Actions to Operate Within IROLs, NERC Standard IRO-009-1, Feb. 2014.

[30] NERC Criteria for Reliability Coordinator Actions to Operate Within IROLs, NERC Standard IRO-008-1, Feb. 2014.

[31] Y. Al-Abdullah, M. Abdi-Khorsand, and K. W. Hedman, "Analyzing the impacts of out-of-market corrections," *2013 IREP Symposium*, pp. 1-10, Crete, Greece, Aug. 2013.

[32] Y. M. Al-Abdullah, M. Abdi-Khorsand, and K. W. Hedman, "The role of out-of-market corrections in day-ahead scheduling," *IEEE Transactions on Power Systems*, vol. 30, no. 4, pp. 1937-1946, Jul. 2015.

[33] A. Papalexopoulos, "Theoretical and practical considerations in implementing and using a reliability unit commitment (RUC) in restructured electricity markets," *IEEE PES General Meeting*, pp. 1-2, Montreal, Canada, 2006.

[34] G. L. LaBove, R. B. Hytowitz, and K. W. Hedman, "Market implications of reliability unit commitment formulations for day-ahead scheduling," *IEEE PES General Meeting*, pp. 1-5, Washington, DC, USA, Jul. 2014.

[35] A. D. Papalexopoulos and P. E. Andrianesis, "Market design for the simultaneous optimization of the day-ahead market and the re-liability unit commitment applications," *2013 IREP Symposium*, pp. 1-8, Crete, Greece, Aug. 2013.

[36] Y. M. Al-Abdullah, A. Salloum, K. W. Hedman, and V. Vittal, "Analyzing the impacts of constraint re-laxation practices in electric energy markets," *IEEE Transactions on Power Systems*, vol. 31, no. 4, pp. 2566-2577, Jul. 2016.

[37] A. Salloum, Y. M. Al-Abdullah, V. Vittal, and K. W. Hedman, "Impacts of constraint relaxations on power system operational security," *IEEE Power and Energy Technology Systems Journal*, vol. 3, no. 3, pp. 99-108, Sep. 2016.

[38] A. Salloum, K. W. Hedman, and V. Vittal, "Pre- and post-contingency constraint relaxations analysis and results," *Electric Power Systems Research*, submitted for publication.

[39] ERCOT, "ERCOT nodal protocols – section 4: day-ahead operations," Electric Reliability Council of Texas, March 2014. [Online]. Available: http://www.ercot.com/content/mktrules/nprotocols/current/04-030114_Nodal.doc.

[40] J. D. Lyon, M. Zhang, and K. W. Hedman, "Locational reserve disqualification for distinct scenarios," *IEEE Transactions on Power Systems*, vol. 30, no. 1, pp. 357-364, Jan. 2015.

[41] University of Washington, "Power system test case archive," Dept. of Elect. Eng., 2007. [Online]. Available: http://www.ee.washington.edu/research/pstca/.

[42] MATLAB, "K-means," Mathworks documentation. [Online]. http://www.mathworks.com/help/stats/kmeans.html?s_tid=gn_loc_drop.

[43] K. W. Hedman, R. P. O'Neil, and S. S. Oren, "Analyzing valid inequalities of the generation unit commitment problem," *IEEE Power Systems Conference and Exposition,* pp. 1-6, Seattle, WA, Mar. 2009.

[44] D. Rajan and S. Takriti, "Minimum up/down polytopes of the unit commitment problem with start-up costs," IBM Research Report, June 2005. [Online]. http://domino.research.ibm.com/library/cyberdig.nsf/papers/CDCB02A7C809D89E8525702300502AC0/$File/rc23628.pdf.

[45] CAISO, "Spinning reserve and non-spinning reserve," California Independent System Operator, Jan. 2006. [Online]. Available: http://www.caiso.com/docs/2003/09/08/2003090815135425649.pdf.

[46] P. A. Ruiz, A. Rudkevich, M. C. Caramanis, E. Goldis, E. Ntakou, and C. R. Philbrick, "Reduced MIP formulation for transmission topology control," *50th Annual Allerton Conference on Communication, Control, and Computing*, pp. 1073-1079, Oct. 2012.

[47] J. D. Lyon, F. Wang, K. W. Hedman, and M. Zhang, "Market implications and pricing of dynamic re-serve policies for systems with renewables," *IEEE Transactions on Power Systems*, vol. 30, no. 3, pp. 1593-1602, May 2015.

[48] K. W. Hedman, M. C. Ferris, R. P. O'Neill, E. B. Fisher, and S. S. Oren, "Co-optimization of generation unit commitment and transmission switching with N-1 reliability," *IEEE Transactions on Power Systems*, vol. 25, no. 2, pp. 1052-1063, May 2010.

[49] F. Bouffard, F. D. Galiana, and A. J. Conejo, "Market-clearing with stochastic security (parts I and II)," *IEEE Transactions on Power Systems*, vol. 20, no. 4, pp. 1818-1835, Nov. 2005.

APPENDIX

A. SCUC Formulation

Extensive Form *N*-1 Reliable Unit Commitment Formulation:

$$\text{Min: } \sum_{g,t}\begin{pmatrix} c_g P_{gt} + c_g^{NL} u_{gt} + c_g^{SU} v_{gt} + PF_M(S_M^+ + S_M^-) \\ + PF_S(S_{NK}^- + S_{NK}^+ + S_{NG}^- + S_{NG}^+) \end{pmatrix} \quad \text{A.1}$$

s.t.:

Base-case modeling of generation:

$$P_g^{min} u_{gt} \le P_{gt}, \qquad \forall g,t \quad \text{A.2}$$

$$P_{gt} + r_{gt} \le P_g^{max} u_{gt}, \qquad \forall g,t \quad \text{A.3}$$

$$0 \le r_{gt} \le R_g^{10} u_{g,t}, \qquad \forall g,t \quad \text{A.4}$$

$$\sum_{q \in G} r_{qt} \ge P_{gt} + r_{gt}, \qquad \forall g,t \quad \text{A.5}$$

$$P_{gt} - P_{g,t-1} \le R_g^{hr} u_{g,t-1} + R_g^{SU} v_{gt}, \qquad \forall g, t \ge 2 \quad \text{A.6}$$

$$P_{g,t-1} - P_{gt} \le R_g^{hr} u_{g,t} + R_g^{SD}(v_{gt} - u_{gt} + u_{g.t-1}), \qquad \forall g, t \ge 2 \quad \text{A.7}$$

$$P_{g1} - P_{g,T} \le R_g^{hr} u_{g,T} + R_g^{SU} v_{g1}, \qquad \forall g \quad \text{A.8}$$

$$P_{g,T} - P_{g1} \le R_g^{hr} u_{g,1} + R_g^{SD}(v_{g1} - u_{g1} + u_{g,T}), \qquad \forall g \quad \text{A.9}$$

$$\sum_{q=t-UT_g+1}^{t} v_{g,q} \le u_{gt}, \qquad \forall g, t \ge UT_g \quad \text{A.10}$$

$$\sum_{q=T+t-UT_g+1}^{T} v_{g,q} + \sum_{q=1}^{t} v_{g,q} \le u_{gt}, \qquad \forall g, t \le UT_g - 1 \quad \text{A.11}$$

$$\sum_{q=t+1}^{t+DT_g} v_{g,q} \le 1 - u_{g,t}, \qquad \forall g, t \le T - DT_g \quad \text{A.12}$$

$$\sum_{q=1}^{t+DT_g-T} v_{g,q} + \sum_{q=t+1}^{T} v_{g,q} \le 1 - u_{g,t}, \qquad \forall g, t \ge T - DT_g + 1 \quad \text{A.13}$$

$$v_{gt} \ge u_{gt} - u_{g,t-1}, \qquad \forall g, t \ge 2 \quad \text{A.14}$$

$$v_{g1} \ge u_{g1} - u_{g,T}, \qquad \forall g \quad \text{A.15}$$

$$0 \le v_{gt} \le 1, \qquad \forall g,t \quad \text{A.16}$$

$$u_{gt} \in \{0,1\}, \qquad \forall g,t \quad \text{A.17}$$

Base-case modeling of power flow:

$$P_{kt} - b_k(\theta_{nt} - \theta_{mt}) = 0, \qquad \forall k,t \quad \text{A.18}$$

$$-(S_M^- + P_k^{max}) \leq P_{kt} \leq (S_M^+ + P_k^{max}), \qquad \forall k,t \quad \text{A.19}$$

$$\sum_{g\in g(n)} P_{g,t} + \sum_{k\in\delta^+(n)} P_{k,t} - \sum_{k\in\delta^-(n)} P_{k,t} = d_{n,t}, \qquad \forall n,t \quad \text{A.20}$$

The formulation of the slave problem for each contingency and for each hour.

Min: s A.21

s.t.:

For each line contingency ($\forall\, c \in N^k$) in each hour ($\forall\, t$):

$$-P_g + s\left(R_g^{10}\overline{u_g} - \overline{P_g}\right) \leq R_g^{10}\overline{u_g} - \overline{P_g}, \qquad \left(\alpha_{gct}^-\right) \quad \forall g \quad \text{A.22}$$

$$P_g + s\left(R_g^{10}\overline{u_g} + \overline{P_g}\right) \leq R_g^{10}\overline{u_g} + \overline{P_g}, \qquad \left(\alpha_{gct}^+\right) \quad \forall g \quad \text{A.23}$$

$$-P_g + s\left(-P_g^{min}\overline{u_g}\right) \leq -P_g^{min}\overline{u_g}, \qquad \left(\zeta_{gct}^-\right) \quad \forall g \quad \text{A.24}$$

$$P_g + s\left(P_g^{max}\overline{u_g}\right) \leq P_g^{max}\overline{u_g}, \qquad \left(\zeta_{gct}^+\right) \quad \forall g \quad \text{A.25}$$

$$P_k - N_{c,k}^k b_k(\theta_n - \theta_m) = 0, \qquad \left(s_{kct}^k\right) \quad \forall k \quad \text{A.26}$$

$$-P_k \leq N_{c,k}^k(\overline{S_{NK}^-} + P_k^{max,c})(1-s), \qquad \left(F_{kct}^{k-}\right) \quad \forall k \quad \text{A.27}$$

$$P_k \leq N_{c,k}^k(\overline{S_{NK}^+} + P_k^{max,c})(1-s), \qquad \left(F_{kct}^{k+}\right) \quad \forall k \quad \text{A.28}$$

$$\sum_{g\in g(n)} P_g + \sum_{k\in\delta^+(n)} P_k - \sum_{k\in\delta^-(n)} P_k + s(d_n) = d_n, \qquad (LMP_{nct}) \quad \forall n \quad \text{A.29}$$

For each generator contingency ($\forall\, c \in N^g$) in each hour ($\forall\, t$):

$$-P_g + s\left(R_g^{10}\overline{u_g} - N_{c,g}^g\overline{P_g}\right) \leq R_g^{10}\overline{u_g} - N_{c,g}^g\overline{P_g}, \qquad \left(\beta_{gct}^-\right) \quad \forall g \quad \text{A.30}$$

$$P_g + s\left(R_g^{10}\overline{u_g} + N_{c,g}^g\overline{P_g}\right) \leq R_g^{10}\overline{u_g} + N_{c,g}^g\overline{P_g}, \qquad \left(\beta_{gct}^+\right) \quad \forall g \quad \text{A.31}$$

$$-P_g + s\left(-P_g^{min}\overline{u_g}N_{c,g}^g\right) \leq -P_g^{min}\overline{u_g}N_{c,g}^g, \qquad \left(\gamma_{gct}^-\right) \quad \forall g \quad \text{A.32}$$

$$P_g + s\left(P_g^{max}\overline{u_g}N_{c,g}^g\right) \leq P_g^{max}\overline{u_g}N_{c,g}^g, \qquad \left(\gamma_{gct}^+\right) \quad \forall g \quad \text{A.33}$$

$$P_k - b_k(\theta_n - \theta_m) = 0, \qquad \left(s_{kct}^g\right) \quad \forall k \quad \text{A.34}$$

$$-P_k \leq (\overline{S_{NG}^-} + P_k^{max,c})(1-s), \qquad \left(F_{kct}^{g-}\right) \quad \forall k \quad \text{A.35}$$

$$P_k \leq (\overline{S_{NG}^+} + P_k^{max,c})(1-s), \qquad \left(F_{kct}^{g+}\right) \quad \forall k \quad \text{A.36}$$

The formulation of feasibility cuts for line contingency:

$$\sum_g \left(R_g^{10} u_{g,t} - P_{gt}\right)\alpha_{gct}^{r-} + \sum_{\forall g}\left(R_g^{10} u_{g,t} + P_{g,t}\right)\alpha_{gct}^{r+} + \sum_{\forall g}\left(-P_g^{min} u_{gt}\right)\eta_{gct}^{r-} + \sum_{\forall g}\left(P_g^{max} u_{gt}\right)\eta_{gct}^{r+} + C_{c,t}^{r} \leq 0, \qquad \forall r, c \in N^k, t \quad \text{A.37}$$

where,

$$C_{c,t}^{r} = \sum_{\forall k}\left(N_{c,k}^{k}(S_{NK}^{-} + P_k^{max,c})\right)F_{kct}^{r\,k-} + \sum_{\forall k}\left(N_{c,k}^{k}(S_{NK}^{+} + P_k^{max,c})\right)F_{kct}^{r\,k+} + \sum_{\forall n}\left(d_{n,t}\right)LMP_{nct}^{r}\,, \qquad \forall r, c \in N^k, t \quad \text{A.38}$$

The formulation of feasibility cuts for generator contingency:

$$\sum_{\forall g}\left(R_g^{10} u_{g,t} - N_{c,g}^{g} P_{gt}\right)\beta_{gct}^{r-} + \sum_{\forall g}\left(R_g^{10} u_{g,t} + N_{c,g}^{g} P_{g,t}\right)\beta_{gct}^{r+} + \sum_{\forall g}\left(-P_g^{min} u_{gt} N_{c,g}^{g}\right)\gamma_{gct}^{r-} + \sum_{\forall g}\left(P_g^{max} u_{gt} N_{c,g}^{g}\right)\gamma_{gct}^{r+} + C_{c,t}^{r} \leq 0, \qquad \forall r, c \in N^g, t \quad \text{A.39}$$

where,

$$C_{c,t}^{r} = \sum_{\forall k}\left(S_{NG}^{-} + P_k^{max,c}\right)F_{kct}^{r\,g-} + \sum_{\forall k}\left(S_{NG}^{+} + P_k^{max,c}\right)F_{kct}^{r\,g+} + \sum_{\forall n}\left(d_{n,t}\right)LMP_{nct}^{r}\,, \qquad \forall r, c \in N^g, t \quad \text{A.40}$$

Part II

Risk-based Predictive Constraint Relaxation

Xian Guo
James McCalley

Iowa State University

For information about this project, contact

James McCalley
Iowa State University
Electrical and Computer Engineering Department
111 Coover
Ames, IA 50011
Phone: 515 294-4844
Fax: 515 294-4263
Email: jdm@iastate.edu

Power Systems Engineering Research Center

The Power Systems Engineering Research Center (PSERC) is a multi-university Center conducting research on challenges facing the electric power industry and educating the next generation of power engineers. More information about PSERC can be found at the Center's website: http://www.pserc.org.

For additional information, contact:

Power Systems Engineering Research Center
Arizona State University
527 Engineering Research Center
Tempe, Arizona 85287-5706
Phone: 480-965-1643
Fax: 480-727-2052

Notice Concerning Copyright Material

Table of Contents

List of Figures

List of Tables

Nomenclature

Indices and Sets

i	Generator id number, $1, \dots, NG$
k	Post-contingency condition, $1, \dots, NC$
$k = 0$	Pre-contingency condition, i.e., normal condition
l	The l th circuit/line/ branch, $1, \dots, NL$
m	Bus ID number, $1, \dots, N$
N	Number of total buses
NC	Number of total post-contingency conditions
NG	Number of total generators
NI	Number of total time periods in the predictive control horizon
T	Time period for predictive control horizon, $1, \dots, NI$

Parameters

c_i	Marginal generation cost for unit i
$D_{m,T}$	Nodal load of bus m at time period T
$GSF_{l.m}^{k}$	Power transfer distribution factor
$Limit_{l}^{k}$	Transmission thermal limit of circuit l under event k, MW
$P_{i,min}$, $P_{i,max}$	Generation output limits for conventional unit i
$REG_{req,T}^{down}$	Regulation reserve (down) requirement, MW
$REG_{req,T}^{up}$	Regulation reserve (up) requirement, MW
RMP_{i}^{down}	Ramp down capability of conventional unit, MW/min
RMP_{i}^{up}	Ramp up capability of conventional unit, MW/min
ρ_{Ctg}^{k}	The probability of event k

Variables

$h_{l,T}^{k}$	Power flow on branch l
$P_{i,T}$	Generation output for unit i at time-period T
$REG_{G,i,T}^{down}$	Regulation down provided by conventional unit i, MW
$REG_{G,i,T}^{up}$	Regulation up provided by conventional unit i, MW
$sev_{C,l,T}^{k}$	Severity value for conductor temperature along line l under event k
$sev_{P,l,T}^{k}$	Severity value for flow along line l under event k

$\alpha_{l,T}^{k}$	The slack variable for branch flow constraints

Terms

SCED	Security constrained economic dispatch
CR	Constraint relaxation
OPF	Optimal power flow
LMP	Locational marginal price
ISOs	Independent system operators
NYCA	New York Control Area
A-CR	Applied constraint relaxation (CR methodology in industry)
P-RBCR	Risk-based predictive constraint relaxation
DAM	Day-ahead market
RTM	Real-time market
OMCs	Out-of-market corrections
EMS	Energy management system
BMS	Business management system
CRM	Constraint reliability margin
VRLs	Violation relaxation limits

1. Introduction

1.1 Research premise

Security constrained economic dispatch (SCED) serves as the market engine for current-day real-time electricity markets. Congestion issues are observed frequently and they are the result of supply and demand location and amount, network topology, and circuit limits under normal and contingency conditions. Congestion usually results from a circuit flow being bound at its normal or contingency limit. However, it is possible that such a binding constraint will cause the SCED to be infeasible. These situations result in a constraint violation, and constraint relaxation (CR) is necessary to solve the optimization problem. Such infeasibilities have to be addressed appropriately, since generation schedules and locational marginal prices (LMPs) resulting from the SCED solutions are required to operate the system.

Industry has experienced challenges in implementing a CR methodology to handle the infeasible SCED problem. Generally, the approach used by most market operators is to impose a pre-determined penalty price within on the objective function. Thus, selecting an appropriate penalty price has received significant attention within the industry, since large values can cause under-relaxation (i.e., infeasibilities still exist and cannot be solved) and low values can cause over-relaxation which may expose a system to risk and lowered security level.

Conductor temperature is the actual factor limiting the power flow capability of a transmission line. Heavily-loaded lines generate heat and subsequently increase conductor temperature, thus causing sag of overhead conductors. Thus, conductor temperature, if it can be estimated with reasonable accuracy, is an effective assessment metric for characterizing the risks of constraint relaxation. Accurate estimation of conductor temperature requires knowledge of initial flow conditions and time duration of changes from that condition, which can account for the delay in temperature rise following a change in flow. Thus, CR action should be treated with consideration of the several sequential dispatch and market solutions.

This report develops, proposes and illustrates a methodology of risk-based predictive constraint relaxation (P-RBCR), which is free-of penalty price and applies temperature limits to those overloads with constraint relaxation. This report successfully shows that P-RBCR has significant advantages in arriving at better relaxation decisions in terms of system security and economics.

1.2 Report organization

This report includes six chapters:

- Chapter 2 describes the background of constraint relaxation practices applied in industry, including market mechanisms of ISOs, congestion management, and

statistical analysis of constraint relaxation in industry, which provides the motivation and foundation for our research.

- Chapter 3 formulates the methodology of risk-based predictive constraint relaxation, based on linearization of dynamic heat balance equation, integration of model predictive control theory and risk assessment.
- Chapter 4 illustrates risk-based predictive constraint relaxation on a testing system, comparing the industry-based constraint relaxation approach and the risk-based constraint relaxation, providing insights based on examinations of the effects on LMPs.
- Chapter 5 is the development of an 11-zone mini-NYISO testing system, sourced from open access public data for New York Independent System Operators (NYISO) administrative control areas; it is used to test the risk-based predictive constraint relaxation.
- Chapter 6 summarizes the achievements, draws conclusions, and proposes future work.

2. Background

The security constrained economic dispatch (SCED) is the critical component of the electricity market engine (for example, this market engine is referred to as the Market Information System in the Mid-continent ISO (MISO) and the Business Management System (BMS) in NYISO). The objective of SCED is to minimize production costs, subject to network and generation limitations. The model formulation is complex, including tens of thousands of nodes and hundreds of thousands of constraints. Slack variables are employed within the constraints with a pre-defined penalty price, to guarantee that the market software may always obtain a feasible market solution. This action is called constraint relaxation (CR). In this document, the industry-based CR methodology is referred to as applied constraint relaxation and given the acronym A-CR.

2.1 ISO market mechanisms

The wholesale electricity market consists of two settlement systems—day-ahead market (DAM, or forward market) and real-time market (RTM, or spot market). Figure 2-1 shows the energy market process timeline for the NYISO and is representative of timelines used by other market operators. The DAM is a financially binding market, in which the energy is purchased or sold one day prior to the operating day and accounts for around 94% of energy transactions. Based on the forecast input data, the DAM schedules the available generators by an hourly basis for the next operating day. The RTM is the balancing market, which balances the DAM schedule and actual energy consumption during the operating day based on five-minute time intervals. Currently, both the unit commitment and the economic dispatch algorithm utilized in all ISOs, to administer the competitive auction processes, are deterministic.

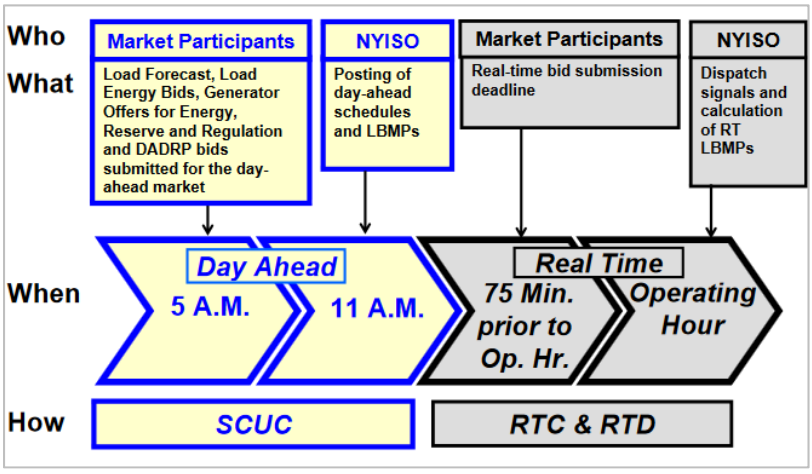

Figure 2-1: Energy market timeline in NYISO [1]

Motivated by the specific market situations among various ISOs, different functionalities have been added on top of this basic market structure. NYISO employs the real-time commitment (RTC) approach, which allows commitment of additional fast-response resources (such as gas-turbine units, GTs) and provides advisory commitment-dispatch decisions for the reminder of the optimization period, before implementing the real-time

dispatch (RTD, which is conducted on 5-min time interval) [1]. In addition, the NYISO energy market algorithm co-optimizes energy consumption and ancillary services, reflecting a feature that is common among most ISOs. The California ISO (CAISO) conducts market power mitigation tests to determine whether bids and offers are valid; the residual unit commitment (RUC) is established following the basic security-constrained unit commitment (SCUC) process. The RUC provides additional resources to make available during the real-time operating stage [2]. MISO runs the reliability assessment commitment (RAC) after the DAM results have been published; the purpose of the RAC is to allocate generator scheduling motived by reliability requirements [3].

Multiple passes (runs) are deployed in executing the RTD. In the NYISO market software, the RTD procedures consists of Physical Pass and Ideal Pass. Physical Pass is a mixed-integer optimization program which includes non-convex ramping products and quadratic production cost. The purpose of Physical Pass is to simulate the system as realistically as possible to produce the base point for energy dispatching. Ideal pass is a linear program which approximates the complex non-linear modeling and is capable to compute LMPs. In particular, GTs have distinctly different pricing logic in these passes: in Physical Pass, blocked bid limits are utilized for GTs; in Ideal Pass, GTs are dispatched across the entire operating range to set prices [4]. A similar mechanism is implemented in the CAISO market, which are referred to as Scheduling Run and Pricing Run. In Scheduling Run, self-schedule curtailment and relaxation of constraints can help market software arrive at a solution when simply considering the energy bid is not possible, subject to system energy balance, congestion management and ancillary service requirements. The significant feature distinguishing the CAISO approach from the NYISO's multiple-pass approach is that both dispatch schedules and price signals are provided in Scheduling Run and Pricing Run. However, for the settlement purposes, dispatch schedules are taken from Scheduling Run, and nodal prices are achieved from Pricing Run [5].

Out-of-market corrections (OMCs) are the actions necessary to correct or adjust market solutions, which cannot satisfy reliability or operational requirements. Those market solutions achieved by relaxation will be evaluated by the corresponding test and review procedures, and this guarantees that the solution is feasible. The review and resulting necessary OMCs ensure that the CR methodology is applicable to achieve a market solution. The terminology for OMCs among ISOs includes "uneconomic adjustments" and "exceptional dispatches" in CAISO and "out-of-merit energy/capacity" in ERCOT [6]. Figure 2-2 shows how OMCs are integrated into the market process. A deliverability test is performed to check the impacts on system reliability and stability, with adjustments and improvements being made if the test fails. No action is required if the market solution passes the testing and review procedures. Those solutions passing Operator Review are followed by submittal for DAM postings.

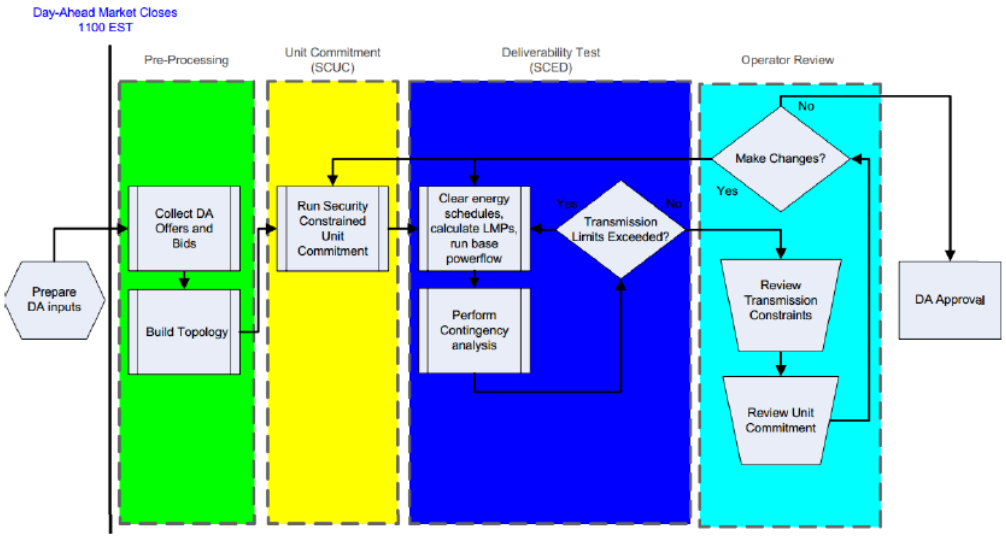

Figure 2-2: Day-ahead market process in MISO

2.2 Congestion management and constraint relaxation

Transmission congestion is a critical challenge facing system/market operators. Transmission congestion occurs due to the insufficient capability of transmission lines to deliver power from the generator (sources) to load serving entities (LSEs). The sources for transmission congestion include:

- Fuel price spreads among various locations: Production cost is significantly reduced when low-price fuel is procured in via economic dispatch. Thus, more generation is committed in the low-priced fuel region, less in the high-priced fuel region, and energy is transferred through transmission lines from the low-priced fuel region to the high-priced fuel regions. This can fully load the interfaces between low fuel-priced fuel regions and high-priced fuel regions.
- Transmission facilities outage: The occurrence of a single line-outage causes load to shift from the outage line to lines comprising parallel transfer paths; this has the potential to overload lines in the parallel transfer paths.
- Allocation of generation and demand: Load concentration and generation resource location can occur in a way that results in congestion. For example, in the New York Control Area, almost 50% of LSEs are located in the southeastern region of the state (including New York City and Long Island), typically has a high energy price due to oil-fueled units and GTs. In the remaining part of the state, cheaper energy is available from, for example, hydroelectric resources (either internal Niagara Falls or external Hydro Quebec power). Thus, the congestion pattern, which has been observed for decades, is that significant congestion exists along the interface between central and eastern New York, since less expensive power

transfers from the western/central area through the southeastern part of the state via these interfaces.

- Other reasons: Such reasons result in congested transmission facilities and include outage of generation fleet and increased demand requirements.

Transmission congestion can induce significant reliability issues while reducing market efficiency. Thus, actions to avoid or relieve congestion are available, referred to as congestion management. From an economic point of view, common congestion management approaches include 1) investment, including building new lines, upgrading existing transmission facilities, installing phase-shifters and/or flexible AC transmission system (FACTS) devices, which are result in costs borne by transmission owners; and 2) operational responses, which involves actions taken by generating companies (GenCos) and LSEs [7].

Congestion may be conceived as falling within two categories, depending on whether the flow limit associated with the congestion may be satisfied or not. If it can be satisfied, then a feasible SCED solution is obtained such that the flow equals the flow limit. If it cannot be satisfied, a feasible SCED solution can only be obtained if the flow is allowed to exceed the flow limit; this second category requires constraint relaxation and is considered a special kind of congestion management approach. However, both categories of congestion are typically identified in public postings from ISOs as binding constraints.

Significant benefits can be obtained through use of constraint relaxation:

1) Obtains a feasible solution: A generation dispatch/scheduling with appropriate LMPs are required for power system operations and market settlement. Adding slack variables to soften the network constraints to allow a limited and temporary violation is necessary in order to obtain the feasible operating solution that also has the corresponding market information.
2) Significant economic benefits: The constraints in SCED are approximated by the best applicable knowledge about the network and modelling capabilities; however, imposing them strictly, independent of their economic impact, can result in very large increases in operation costs. Thus, judicious softening of these limits following careful consideration of the impact on reliability can greatly reduce production costs.
3) Price management is available with CR action. Penalty prices associated with slack variables can cause LMPs to increase significantly when CR is implemented. These LMP increases are direct reflections of congestion, and they serve as a price signal to the market agents to modify their bids and offers accordingly, actions which invariably result in decreasing the corresponding (violating) flow.

2.3 Constraint relaxation practice in ISOs

Based on literature review and personal contact with several ISO representatives, the formulation of CR is to introduce slack variables in the transmission circuit thermal limit

constraints for both normal conditions and contingency conditions. The slack variables are included in the objective function with a pre-defined penalty price. Thus, the determination of penalty price is vital in the CR practice. In our previous research, we have summarized the formulation of the industry-based CR method and presented the penalty price methodology in our M-29 PSerc report [8]. In this section, we extend that summary. The materials of this section are supplemental to the materials provided in the M-29 report on industry practices. This implies that, the industry practices materials of the M-29 report are still accurate, and, relative to the materials given here, they are distinct (not redundant) and should be considered primary.

1. Constraint relaxation practice in MISO

CR occurrences in the real-time market are relatively frequent; it can occur for both normal condition and contingency conditions [9]. The constraint relaxation practice in MISO's market operations starts with a two-step solving process. The first step is to assign a relatively high penalty (on the scale of several thousand dollars) to reduce the constraint violations; the shadow price for the corresponding constraint is set at the penalty price once violations are necessary. However, the above step cannot reflect the true cost of managing the congested lines; at some point, the violations cannot be mitigated independent of how high a penalty price is selected. The second step determines the incremental re-dispatch costs of relieving transmission line congestion, in which transmission line thermal limits are updated by adding slack variables, produced in the first step, and the reliability margin on top of the original limit.

The disadvantage of the two-step CR approach is that it may not identify the best relaxation and pricing values for the violated constraints, resulting in over- or under-relaxation. Over-relaxation (and under-pricing) for transmission violations has been frequently observed. Furthermore, the shadow price is set to zero when there are no available resources for re-dispatch actions. Thus, the independent market monitor suggested to discontinue the second step for Non-Market-to-Market constraints (effective February 1, 2012), and it specified that appropriate penalty price mechanisms should be developed to reflect the congestion and resource scarcity. Flat default marginal value limits (MVLs) were proposed by voltage level. The two-step transmission constraint demand curve (TCDC) was deployed to achieve the tradeoff between violation frequency/quantity and the magnitude of shadow price [10]. MVLs with TCDC are currently utilized as CR mechanisms in MISO markets. Additional information regarding MVLs and TCDC were covered in the M-29 report.

2. Constraint relaxation practice in NYISO

In the economic logic of the NYISO BMS, the transmission line limit is associated with the constraint reliability margin (CRM). CRM is introduced for critical transmission facilities, to guarantee system reliability and operational security. Normally, NYISO sets a CRM of 20 MW on its transmission facilities. Facilities having a different CRM value are indicated in [11]. The procedure of "feasibility screening" is implemented to determine whether a transmission line constraint is re-dispatched feasible or not. If the constraint is re-dispatched feasible with non-zero CRM, then the graduated transmission

demand curve (GTDC, also known as Transmission Shortage Prices), as shown in Figure 2-3, is imposed on the violated constraints. If the constraint is re-dispatched infeasible or CRM is zero, the penalty cap is set to $4000/MWh in the market software.

Recently, an inconsistency between the GTDC approach and the NYISO tariff has been observed[1].. This inconsistency may result in inflation of the real-time shadow prices and increased market risk [12]. Starting in the June 2017 EMS/BMS deployment, "feasibility screening" is eliminated and the second step of the graduated Transmission Shortage Price is modified to $1,175/MWh, as shown in Figure 2-3[13].

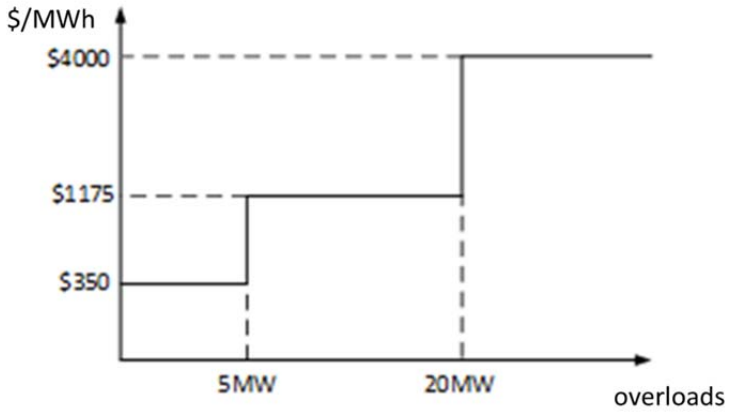

Figure 2-3: GTDC in NYISO market

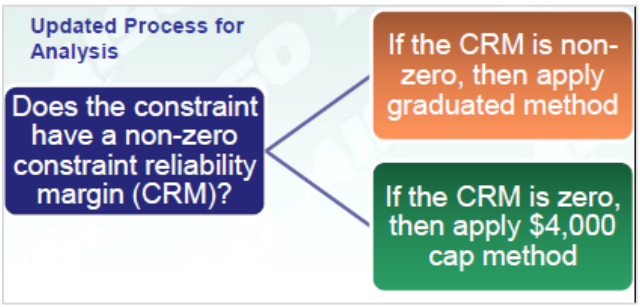

Figure 2-4: Updated Process for CR methodology in NYISO

3. Updates of constraint relaxation practices in other ISOs

To the authors' best knowledge, the basic essence of CR has not been significantly modified relative to the literature review in the M-29 report; the exceptions focus on the determination and selection of penalty price and are provided below.

(1) Transmission constraint relaxation parameter in CAISO [14]: Transmission constraint relaxation parameter is implemented in CAISO market to avoid

[1] Some observed high shadow price outcomes seem to conflict with the provision in NYISO MST that: "[The GTDC] is the maximum shadow price that will be used in calculating LBMPs under various levels of relaxation."

expensive and ineffective market solutions, by relaxing internal transmission constraints. Previously, the relaxation parameter is set according to voltage level and the level of flow violation. Motivated by stakeholder input, CAISO proposed to eliminate the relaxation tier prices below the bid cap in February 2017. In response to the increased energy bid cap required by FERC, CR for small violations at the lower voltage levels were discontinued.

(2) Violation relaxation limits (VRLs) in Southwest Power Pool (SPP): VRLs are activated when the shadow price to satisfy a constraint exceeds the corresponding VRLs, which includes spinning reserve requirement, operating constraints, resource ramping constraints, global power balance constraints, and resource capacity constraints. Based on the historical data and sensitivity analysis on market performance, SPP recommends no changes to VRLs, expect for setting the first VRL block of operating constrain as $750/MWh, which achieves a good trade-off between production costs and operational reliability [15].

2.3 Statistics of constraint relaxation practices in industry

Motivated to provide more insights of constraint relaxation practices in industry, we assess publicly available CR data from NYISO. With the implementation of the updated GTDC starting in June 1, 2017, we are able to map shadow price of binding constraints to corresponding values for flow violation. The detailed mapping criteria is prescribed by the GTDC as:

- If the constraint cost (also known as shadow price of a constraint) = $350/MWh, the flow violation of the corresponding constraint is <= 5MW;
- If the constraint cost = $1175/MWh, the violation is between 5MW~20MW;
- If the constraint cost is between $1175~$4000/MWh, the violation is above 20MW (here, we assume that the CRM is 20MW).

The NYISO publishes limiting constraints for both the DAM and the RTM. Considering that the updated GTDC methodology is integrated into the BMS and deployed as of June 2017, we extract the "OASIS_Real_Time_Dispatch_Limiting_Constraints.csv" files from NYISO market and operations data [16], which covers data within the range from June 1, 2017, to July 21, 2017. Within this specific time duration, the total number of CR occurrences is 1643, where each occurrence is based on a five-minute interval), including 203 occurrences observed under normal conditions with the remaining 1440 occurrences observed under contingency conditions. The average frequency of CR action is 32.2 per day. Figure 2-5 summaries the occurrences by the amount of flow violations. It can be observed that the low-violation event is the dominant category responsible for CR action, followed by around 25% in medium-violation events and 12.5% associated with high-

violation events. Transmission line limits for the normal conditions and for 28 additional pre-defined contingency conditions are involved in this investigation, as summarized in Table 2-1. Figure 2-6 plots the distribution of shadow prices for the events among the top 12 contingency conditions with high-occurrences of CR actions.

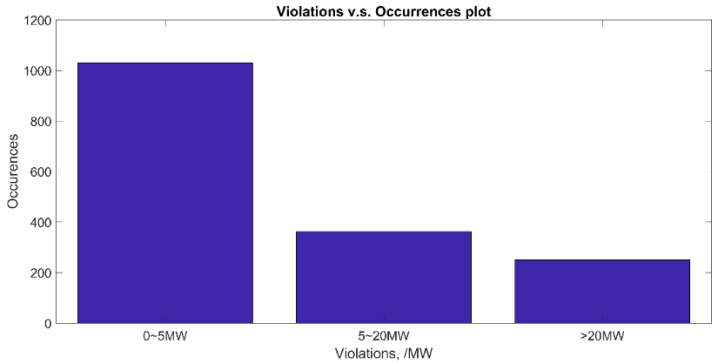

Figure 2-5: Plot of CR occurrences for each violation category

Table 2-1: Contingency list and CR occurrences

Contingency List	**Total occurrences of CR**	**Contingency List**	**Total occurrences of CR**
TWR:GOETHALS 22 & 21	432	FOXHLLS-WILLWBRK_138_29212&BK1	12
BUS:PACKARD BK3 & 61 & 78	254	TSA:CE80 91&301	10
NORMAL CONDITION	203	SIN:MSU1&7040& HQ GN&LD PROXY	8
SHORE_RD-LAKSUCSS_138_368	169	SCB:GOWANUS(22):42231&G27&BEC	7
ALCOA_PA-ALCOA____115_R8105	116	NIAGARA_-ROBNSNRD_230_64	4
SHORE_RD-LAKSUCSS_138_367	112	SCB:SPBK(RNS2):Y49&M29&Y49_ST	3
PACKARD_-SAWYER___230_77	69	TWR:NIAGARA 61 & 64	3
FOXHLLS-WILLWBRK_138_29211&BK2	67	TSA:CE41 F30& 31&W79&80&81&93	2
BUS:BARRETT 292&459&G2&IC9-12	53	TWR:UCC2-41&EF24-40	1
SCB:GOWANUS(2):41&42231&R4	25	ATHENS__-PLSNTVLY_345_91	1
TWR:HOLTSVLLE 881& 882	24	TSA_E:CE80 91&301	1
TWR:PACKARD 62 & BP76	19	BUCHAN_S-MILLWOOD_345_W97	1
SCB:NEWBRDG 1380 461&BK6+4	18	NEPTUNE HVDC TIE LINE	1
SCB:GOWANUS(14):42&42232&R14	14	TSA:CE09 F38&F39&Y86&Y87&W75	1
SCRIBA__-VOLNEY___345_21	13		

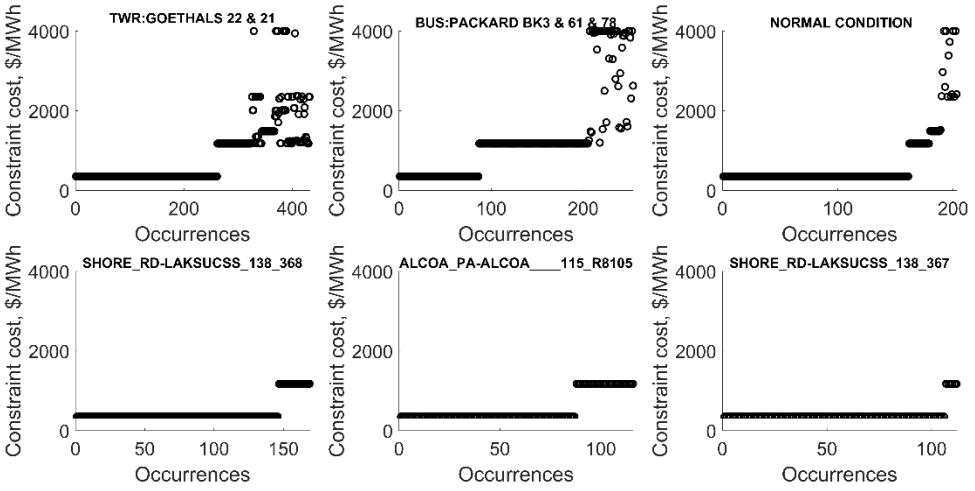

(a) Top 1-6

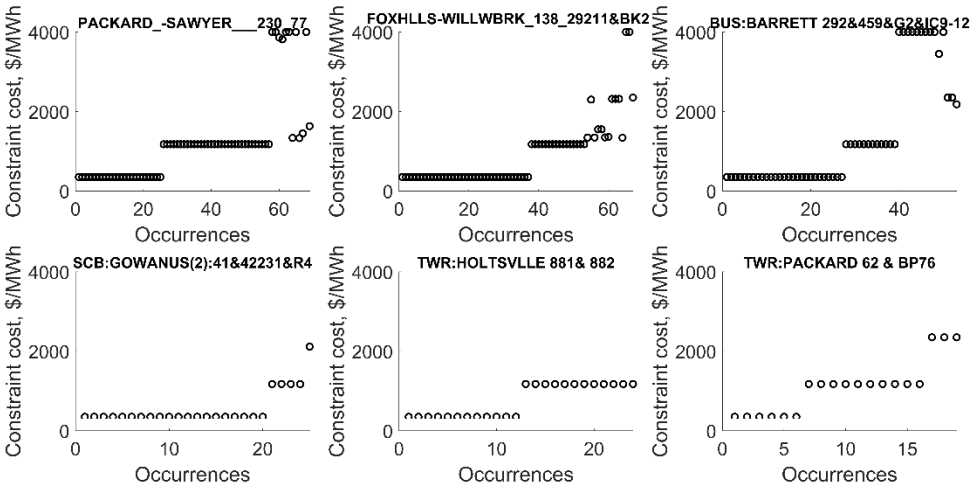

(b) Top 7-12

Figure 2-6: Distribution of shadow price for contingency cases with high CR occurrences

The contingency event "*TWR: GOETHALS 22& 21*" contributes the most to the overloads violating transmission line limits, followed by contingency "*BUS: PACKARD BK3 & 61 & 78*" and the normal condition.

Among these cases, 33 transmission facilities participated in CR actions, as summarized in Table 2.2. Figure 2.7 plots the distribution of shadow price for the transmission lines among the top 12 for number of occurrences.

Table 2-2: Congested line list and CR occurrences

Line List	Total Occurrences of CR	Line List	Total Occurrences of CR
PACKARD 230 SAWYER 230 1	327	KENTAVE 138 VERNON 138 1	6
GREENWD 138 VERNON 138 1	310	ADIRNDCK 230 MOSES 230 1	5
GOWANUS 138 GREENWD 138 1	232	FARRAGUT 138 HUDS_AVE 138 1	5
LAKSUCSS 138 SHORE_RD 138 1	169	ADIRNDCK 230 MOSES 230 2	3
MALONE 115 WILLIS 115 1	116	NIAGARA 230 PACKARD 230 2	3
LAKSUCSS 138 SHORE_RD 138 2	112	BUCHAN_S 345 LADENTWN 345 1	2
FOXHILLS 138 GREENWD 138 1	82	FRESHKLS 138 WILLWBRK 138 1	2
EGRDNCTY 138 VALLYSTR 138 1	74	E179THST 138 HELLGATE 138 1	2
E179THST 138 DUNWOODS 138 1	63	MOTTHAVN 345 DUNWODIE 345 1	2
GREENWD 138 KENTAVE 138 1	30	RAINEY 138 VERNON 138 1	2
C._ISLIP 138 HAUPPAUG 138 1	24	GOWANUS 138 GOWANUS 138 1	1
NIAGARA 230 PACKARD 230 1	19	LAFAYTTE 345 CLRKSCRN 345 1	1
SCRIBA 345 VOLNEY 345 1	13	FARRAGUT 345 GOWANUS 345 1	1
PLSNTVLY 345 LEEDS 345 1	12	BUCHAN_S 345 MILLWOOD 345 2	1
GOETHALS 345 GOWANUS 345 1	8	EGRDNCTY 345 EGRDNCTY 138 1	1
GOETHALS 345 GOWANUS 345 2	8	CARLPLCE 138 EGRDNCTY 138 1	1
DUNWODIE 345 SHORE_RD 345 1	6	KENTAVE 138 VERNON 138 1	6

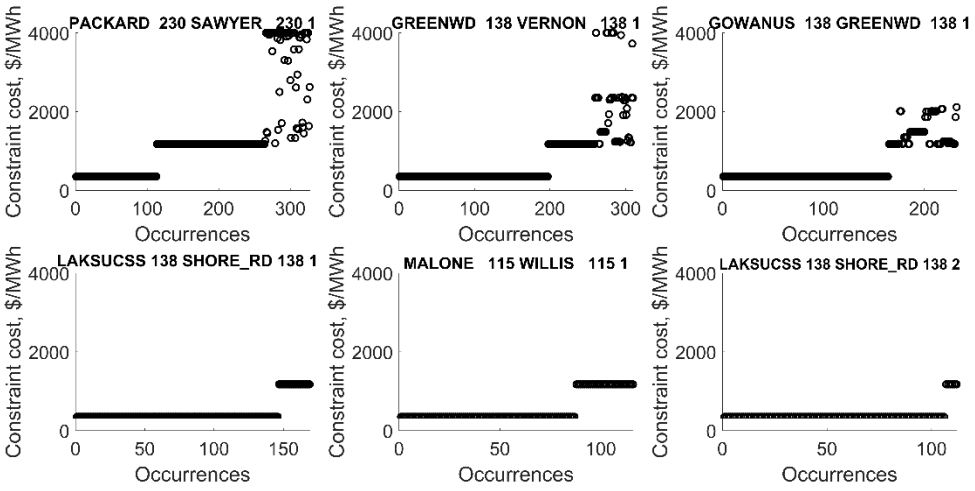

(a) Top 1-6

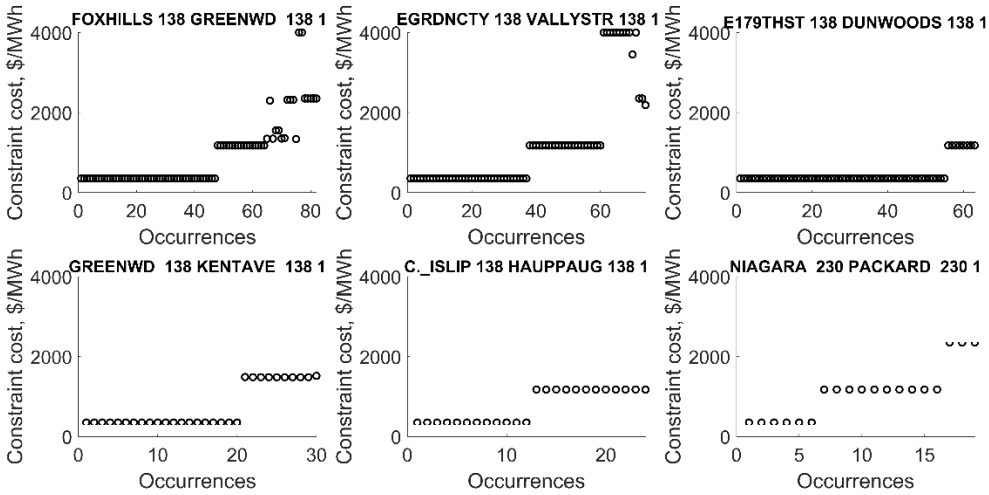

(b) Top 7-12

Figure 2-7: Distribution of shadow price for transmission lines with high occurrences

As indicated in the Table 2-2 and Figure 2-7, line "*PACKARD 230 SAWYER 230 1*" has the highest occurrences in congestion, followed by line "*GREENWD 138 VERNON 138 1*" and "*GOWANUS 138 GREENWD 138 1*". Either transmission upgrades can improve the transfer capability for those lines or congestion patterns can be alleviated by applying efficient congestion management to the NYISO network.

To illustrate the relationship between high LMP price and transmission congestion, we describe a situation obtained from publicly available data on the NYISO website. This

situation occurred at *3:35pm, August 11, 2016*[2]. At 3:35pm, the shadow price reaches $546.5/MWh along transmission line "*DUNWODIE 345 SHORE_RD 345 1*", which is the tie-line connecting Dunwoodie (Zone I) and Long Island (Zone K) in the New York Control Area [17]. Correspondingly, we observe high LMP in -Zone K, which is the receiving area, of $1222.38/MWh (the congestion component is $546.5/MWh, contributing to this LMP spike). The data sources for this example are shown in Figure 2-8. Considering that the actual load for that specific time-interval in Zone K is 5228.5 MW, the cost induced by the CR-related congestion (implemented with high penalty price) is approximately $3 million. This is the cost associated with a single CR action, and the average CR occurrences is 32.2/per day, so roughly $100 million is procured in recovering the cost for constraint relaxation and congestion management.

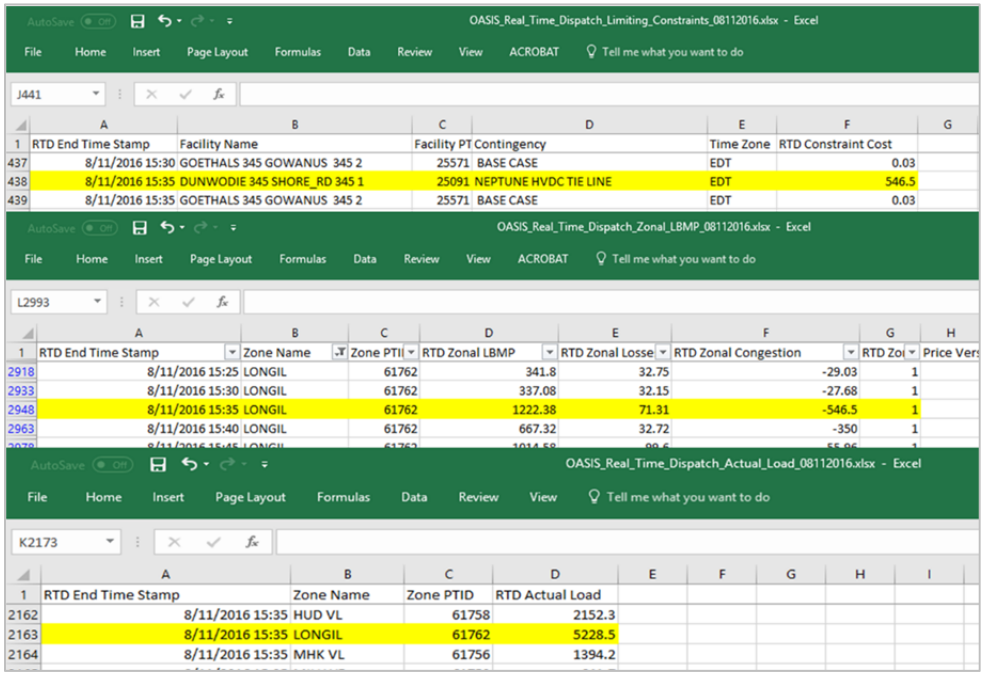

Figure 2-8: Example for investigation relationship between LMP price and transmission congestion

2.4 Summary

This chapter summarizes the state of art for CR practice in ISO/RTOs, indicating that CR is applicable to handling SCED with infeasibilities caused by overloads. The industry has made significant effort over the past decade in selecting reasonable penalty prices. From the analysis of industry data performed in this section, the insight has been obtained that CR practice occurs quite frequently in real-time operations, and they are associated with huge amount of costs. That motivates us to propose a systematic methodology to

[2] August 11, 2016 is the recorded summer peak of NYISO in calendar year 2016. The network is more congested than most if not all other days of the year.

implement CR action, which should be penalty-free and is able to make better use of the potential capacity of transmission lines. We describe this methodology in the next section.

3. Risk-based predictive constraint relaxation

3.1 Literature review

3.1.1 Model predictive control in power system

Model predictive control (MPC) is a control scheme, which has been widely applied in multiple disciplines, especially power system operation and control. The essence is to solve a fast look-ahead optimization problem at each time step. As shown in Figure 3-1, in our Risk-based Predictive CR model, the control decision (generation dispatch) for the entire operation horizon is determined, considering the predictive evolution of system state parameters. Only the control decision for the first time-step is executed; the remaining is for advisory purposes.

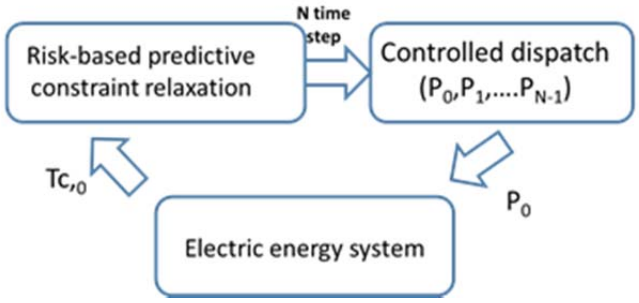

Figure 3-1: Structure of Predictive RBCR

3.1.2 Dynamic thermal ratings in power system

The power transfer limits of overhead transmission lines are critical constraints for both power system planning and operation. The actual limitation of allowable loading through transmission lines is conductor temperature, and this is related to current (flow) constraints via the dynamic heat balance equation (DHBE). Static line rating (SLR) has been implemented by most transmission owners and ISOs, and SLR corresponds to the most severe weather condition (for example, ambient temperature) and is calculated seasonally [18 , 19]. Thus, computing thermal ratings by SLR tends to result in conservative operating limits. Dynamic line rating (DLR) is determined based on real-time meteorology, indicating the maximum current permissible under a current situation. The benefits of DLR have already been identified and assessed for some study cases. A recent example is that Oncor electric delivery company has installed a DLR monitoring system for eight transmission lines; these systems are active in daily operations and their effects are accounted for in the electricity market. The demonstration shows that transmission capacity has been improved 8%~14% for 90% of the monitored time [20].

The significant challenge in implementing DLR is lack of real-time monitoring capability in current power systems [21]. To relieve concerns on this issue, Kim and Cho [22] propose prediction of DLR based on a time series weather model; this model enables calculation of thermal overload (TOL) risk. In [23], DLR is estimated using synchronized phasor measurements and verified under various weather conditions, indicating good performance in enhancing transfer capability. Reference [24] integrates conductor temperature dynamics with existing system control via the concept of electrothermal coordination (ETC), which enhances power transfer capability, emergency load shedding, and congestion management. Reference [25] adopts partial least square (PLS) to reduce error caused by parameter selection, in performing DLR estimation based on monitored data. To summarize, most of these methods rely on measurements from real-time monitoring, followed by probabilistic or statistical processing methods.

Application of DLR provide a cost-effective method to better utilize line capacity. Its use provides benefits for congestion management for integration of renewable energy. Reference [26] proposes a distributionally robust congestion management model, which imposes DLR on critical lines, providing the ability to control the risk of thermal overloading. References [27] and [28] develop simulation models, the implementation of which shows significant economic potential and system security enhancement of deploying DLR when integrating significant amounts of variable renewable integration.

DLR has been coordinated with optimal power flow (OPF) for addressing issues spanning several time-scales, from planning to power system scheduling. The main challenge is that DHBE adds a set of time-coupled nonlinear equality constraints to the optimization model. The studies in [29], [30] do not involve DHBE directly; instead, they model overloading risk as a deterministic function of the level of line current exceeding previous thermal rating and include it as a penalty function in the objective function, and they relax the reserves rating without significant increasing computation complexity. In reference [31], DHBE is simplified by assuming that the terms unrelated to transmission line loss are constant with temperature change. In [24] and [32], power flow and heat terms are linearized as functions of generation output and conductor temperature. Then, the iterative method of solving several linearized sub-problems generates the corresponding solution. Reference [33] introduces a feasible way to integrate DHBE with AC-based security constrained unit commitment (SCUC), but several assumptions are made, such as the conductor resistance is fixed at its value when at maximum temperature, and several internal relationships are linearized. Although many efforts were made to integrate DHBE in OPF, they tend to be oversimplified or non-convex, resulting in inappropriate results. The requirement of AC power flow also limits the scalability of extending to large-scale industry-grade power system models.

According to this literature review, three observable drawbacks of DLR are identified as follows: 1) real-time monitoring requires deployment of relatively expensive hardware; 2)

simplified or linearized DHBE may be not precise or even appropriate; and 3) application of AC power flow adds computational complexity.

3.2 Dynamic heat balance equation

Thermal rating calculations for conductors is performed today using the relations and process provided in IEEE Std. 738 [18]. According to IEEE Std. 738, line temperature for overhead transmission conductors is a function of 1) conductor material properties; 2) conductor diameter; 3) conductor surface conditions; 4) ambient weather conditions (ambient temperature, solar radiation and wind velocity); and 5) conductor electrical current. The first two items characterize chemical and physical properties of the conductor, which can be pre-determined and remain fixed over the life of the conductor. The DHBE imposes that heat gain from solar radiation and conductor thermal effects equals to heat loss through natural radiation and through convection cooling effects via ambient surface wind, as indicated by the differential equation of (3-1).

$$C_P \frac{dT_c}{dt} = I^2 R(T_c) + Q_s - Q_r(T_c, T_a) - Q_c(T_c, T_a) \tag{3-1}$$

Here, T_c is conductor temperature (^oC), T_a is ambient temperature (^oC), I is conductor current (A), Q_s is heat gain from solar radiation, Q_r is heat loss by natural radiation, Q_c is convection by wind cooling effects, and C_P is conductor heat capacity. The detailed calculation of each heat item can be found in [18].

The underlying concept for application of DLR in constraint relaxation is not to update the thermal rating according to real-time monitoring on ambient weather information but rather to account for the transient temperature variation using conservative weather information as currents change from one market interval to another. By using pre-determined, conservative weather data to compute thermal ratings [19], we can increase maneuverability for deploying constraint relaxation while maintaining secure conditions. Although data from real-time monitoring equipment can certainly be used, real-time monitoring equipment is not required.

We use DC power flow assumptions in the proposed model. It is well-known that in assessing circuit overload, the DC power flow assumptions provide reasonable estimates of power flow. This provides that our model has good scalability, enabling tractable computational burden even for large-size systems.

In what follows, we illustrate solution of the DHBE based on an assumed conservative weather conditions. Suppose we desire to assess the 2pm conditions of a particular Drake 795kcmil 26/7 ACSR conductor. From IEEE Std. 738, the value of emissivity, altitude and the azimuth of the sun can be determined. We conservatively assume ambient temperature to be $T_a = 40\ ^oC$ and wind velocity to be 2ft/s. Then the various heat terms are described by equations (3-2) ~ (3-5) [18]:

- Radiated heat loss: $q_r = 0.0765 \times \left(\frac{T_c + 273}{100} \right)^4 - 7.3424$ (3-2)
- Solar heat gain: $q_s = 4.3082 \ \ W / ft$ (3-3)
- Heat loss from current: $I^2 R = I^2 \times \left(\left(8.6 \times 10^{-8} T_c \right) + 2.005 \times 10^{-5} \right)$ (3-4)
- Heat loss from wind convection: $q_c = 0.4175 \times T_c - 16.7013$ (3-5)

We then substitute each heat term into (3-1) to obtain:

$$\frac{dT_c}{dt} = \left(0.0215 \times 10^{-8} \times I^2 \right) \times T_c - 1.9125 \times 10^{-4} \times \left(\frac{T_c + 273}{100} \right)^4 + \left(0.005 \times 10^{-5} \times I^2 + 0.0709 \right) \quad (3\text{-}6)$$

We conduct numerical experiments (under conditions of typical T_a and v_m values), deriving the relationship between $(T_{c,\Delta t} - T_{c,0})$ and $(T_{c,0}, I_{\Delta t})$ (Δt is a specific time step), as shown in Figure 3-2. This figure shows that the surface is convex; indeed, it can be shown that the resulting surface is convex independent of parameters selected. This fact facilitates fitting the surface with a piece-wise linear surface, resulting in a linearized relationship between current and conductor temperature change, as shown in (3-7).

$$T_{C,\Delta t} - T_{C,0} = a_i \times T_{C,0} + b_i \times I_{\Delta t} + c_i \quad (3\text{-}7)$$

where, a_i, b_i, c_i are coefficients obtained by linear regression. When there exists overloading along a specific transmission line, we allow the overloading as long as the conductor temperature is still within satisfactory limits as characterized by the linearized surface illustrated in Figure 3-2.

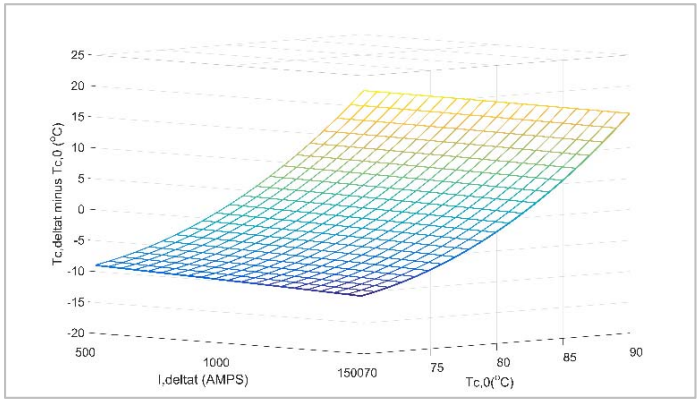

Figure 3-2: Relationship between circuit current and conductor temperature

We will use this piece-wise linear representation of the conductor limitations within our predictive control model. To facilitate on-line assessment, the conductor limitation equation (3-7) can be developed off-line for each conductor known to be a CR candidate.

3.3 Conceptual illustration

In this subsection, to illustrate the concept and projected outcomes for risk-based constraint relaxation under the framework of model predictive control, the dynamic thermal rating of a typical transmission line (Drake conductor-795 Kcmil 26/7 ACSR) is modeled over a 30 minute (1800 second) timeframe. Parameters used include ambient temperature $T_a = 40\ ^oC$, wind velocity is 2ft/s, maximum allowable current to carry is 1150A, and maximum allowable conductor temperature $T_{c,max} = 110\ ^oC$. We assume that loading level during each 5-minute time interval remains constant. The conductor temperature variation within a specific time-interval depends on the conductor temperature at the beginning of that interval and the current loading during that interval, so that at the end of the interval; we require that conductor temperature does not exceed the temperature limit for the conductor. The time constant of conductor temperature change is assumed to be 12 minutes, which is typical of ACSR conductors [18]; since the thermal time constant gives the time following a step-change in current necessary to reach 63.2% of the steady-state temperature, temperature will not reach steady state for any changes imposed during the 30-minute time frame. The differential equation is run in MATLAB/Simulink, and the corresponding curve of loading change and conductor temperature change with time is shown in Figure 3-3. In this figure, the green curve represents the imposed current, quantified by the right-hand axis, and the blue curve represents the resulting temperature, quantified by the left-hand axis. The horizontal line labeled I_{max} represents the maximum steady-state current as computed based on procedures and parameters provided in the IEEE Std. 738 [18]. The horizontal line labeled $T_{c,max}$ represents the maximum steady-state temperature for this conductor. The initial current loading is 1000 A at $t=0^-$ and 1050 A at $t=0^+$, and the initial conductor temperature is 80°C.

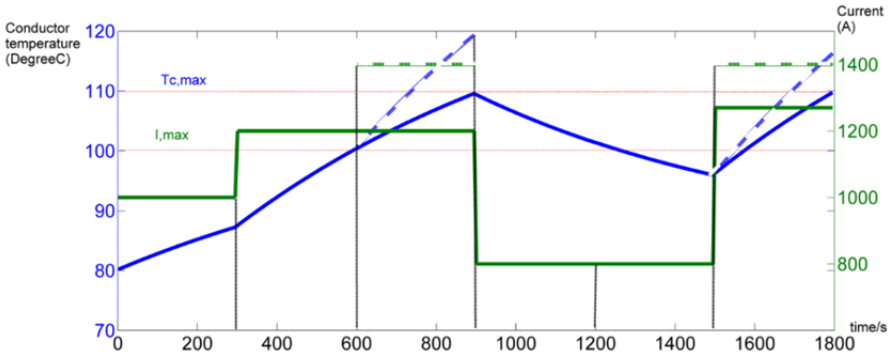

Figure 3-3: Change of load and conductor temperature

As shown in Figure 3-3，

- For the second time-interval, flow (green plot) violates the limit, but since there exists a delay in the change of conductor temperature, conductor temperature (blue plot) remains within its limits for this interval.
- For the third time-interval, since the initial temperature (obtained as the final value from the previous interval) is relatively high, the predicted future flow (dashed green plot) will cause conductor temperature to exceed the limits (dashed blue plot). Therefore, such a constraint relaxation is not acceptable.
- For the third interval and sixth interval, the predicted future flows (dashed green plots) are the same; however, the resulting conductor temperatures in the two intervals (dashed blue plots) are different. This difference results from the different initial temperatures for the third and sixth intervals; the sixth interval has a significantly lower initial temperature because of the depressed flow during the fourth and fifth intervals. This observation illustrates that use of conductor temperature during a constraint relaxation period increases flexibility in that conductor temperature during an interval depends not only on the flow during that interval but also on the flow in preceding intervals as well. Thus, it is the thermal dynamics that offer the possibility of using model predictive control to maneuver conductor temperature during periods where constraint relaxation is needed.
- The conductor temperature violation represented by the dashed blue plots of the third and sixth intervals may be avoided by limiting the current to the green solid plots during these time periods. This results in the blue solid plots, which maintain conductor temperature at or below the temperature limit in all intervals and would be achieved via model predictive control.

To summarize, conductor temperature at the end of time-interval is related to initial conductor temperature and the flow level through this time-interval.

- A constraint relaxation is considered to be acceptable if flow is violating the corresponding limits while conductor temperature is still within its limit;

A constraint relaxation is considered to be unacceptable if conductor temperature exceeds its limit. Although this approach provides additional maneuverability for CR necessitated by both normal and contingency conditions (due to the thermal dynamics), the benefit for CR necessitated by contingency conditions is generally larger than that necessitated by normal conditions because contingency conditions are always associated with a step change in flow following the contingency.

3.4 Methodology of risk-based predictive constraint relaxation

3.4.1 Risk assessment

1. Risk measurement

We evaluate the effects on *system* security of thermal overloads using risk[3]. Our risk metric accounts for both pre-contingency (normal condition) and post-contingency conditions. We identify each condition as a state, thus, we have the no-contingency state as well as a number of different contingency states. The risk metric is then computed as the summation across all states of the product of state probability and state severity (or impact). The severity of a particular state is the summation across all circuits of each circuit's severity, where a circuit's severity is a function of the circuit's power flow if not a CR circuit (NCR set), or a function of conductor temperature if a CR circuit (CR set), which are defined as sev_P and sev_C respectively. The calculation of risk value is according to (3-8).

$$Risk = \sum_{k=1}^{NC} \Pr^k \left(\sum_{l \in NCR} sev_{P,l}^k + \sum_{l \in CR} sev_{C,l}^k \right) \tag{3-8}$$

where $sev_{P,l}^k$ is the severity value of the particular line l under scenario k in NCR set, which is evaluated by loading level; $sev_{C,l}^k$ is the severity of a particular line l under scenario k in CR set, which is evaluated by level of conductor temperature.

1. Modelling of severity function

We utilize a piece-wise linear function to identify severity value, as shown in Figure 3-4.

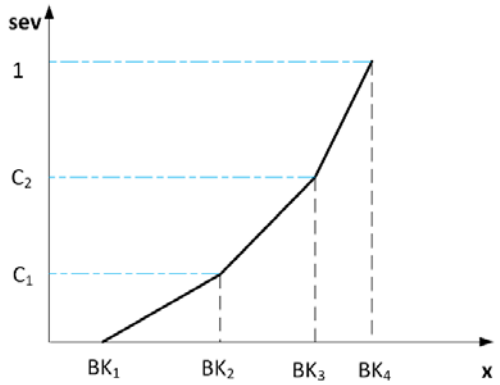

Figure 3-4: Relationship between severity and overloading (line flow/conductor temperature)

[3] More details about the application of risk metrics in power system steady state analysis can be referenced to M-29 report [9].

The severity function $g:\square^{+}\to\square^{+}, x\mapsto s$ is a continuous piecewise linear function defined by

$$s=g(x)=\begin{cases}0 & 0\le x<BK_1\\ a_1x+b_1 & BK_1\le x<BK_2\\ a_2x+b_2 & BK_2\le x<BK_3\\ a_3x+b_3 & BK_3\le x\le BK_4\end{cases} \tag{3-9}$$

where for each i, BK_i corresponds to the x-coordinate of an intersection of two adjacent segments as shown in Fig. x; $0<a_1<a_2<a_3$. The objective function has the additive structure:

$$f(\mathbf{s})=\sum_i f_i(s_i)=\sum_i f_i(g_i(x_i)) \tag{3-10}$$

where $\mathbf{s}=(s_1,s_2,\ldots)$, and f_i is increasing for all i. With this function, the piecewise linear severity function can be formulated by a set of linear constraints:

$$\begin{cases}s\ge 0\\ s\ge a_1x+b_1\\ s\ge a_2x+b_2\\ s\ge a_3x+b_3\\ 0\le x\le BK_4\end{cases} \tag{3-11}$$

We prove this equivalence by two steps. First, it will be shown that (3-11) exactly gives the epigraph of g, i.e., $\{(x,s):(3\text{-}11)\}=epig$, as illustrated in Figure 3-5.

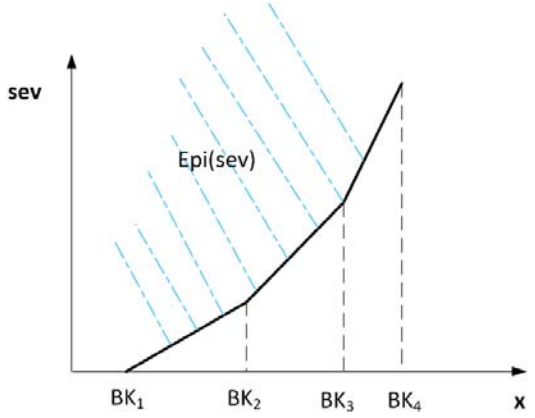

Figure 3-5: Piece-wise linear severity function

then we show that the optimal solution of the problem

$$\begin{aligned} \min_{x,s} \quad & f(\boldsymbol{s}) \\ \text{s.t.} \quad & (3-11) \\ & \text{other constraints with } \boldsymbol{s} \text{ not involved} \end{aligned} \tag{3-12}$$

satisfies $\boldsymbol{s}^* = \boldsymbol{g}(\boldsymbol{x}^*)$, where $\boldsymbol{g}(\boldsymbol{x}) = [g_1(x_1), g_2(x_2), \ldots]$, $(\boldsymbol{x}^*, \boldsymbol{s}^*)$ is an optimal solution. In other words, (3-11) is equivalent to (3-9) in for optimal solution(s).

Step 1:

1. $\{(x,s):(3-11)\} \subset epig$

This direction is trivial since $\text{epi}\, g$ is exactly (3-11) with restricted domain of x for each segment constraint.

2. $\{(x,s):(3-11)\} \supset epig$

Prove by contradiction. Suppose there exists (x',s') satisfying $(x',s') \in \text{epi}\, g$ and $(x',s') \notin \{(x,s):(3)\}$. The second condition implies $s' < a_i x' + b_i$ (let $a_0 = b_0 = BK_0 = 0$) for some i. Define a closed set

$$S = \{(x,s): s < a_i x + b_i, BK_i \le x \le BK_{i+1}\} \tag{3-13}$$

If $(x',s') \in S$, the contradiction follows immediately since $S \cap \text{epi}\, g = \varnothing$. If $(x',s') \notin S$, let (x'',s'') denote a point lies on the interior of i th segment, i.e., $s'' = a_i x'' + b_i, BK_i \le x'' \le BK_{i+1}$. Since (x',s') and (x'',s'') are both in $\text{epi}\, g$, and it is trivial to show that $\text{epi}\, g$ is convex, it follows that the straight line segment that connecting the two points is a subset of $\text{epi}\, g$. It is not difficult to show that this straight line segment must intersect the boundary of S, and since S is closed, the intersection is in S, which leads to the contradiction, given the fact that $S \cap \text{epi}\, g = \varnothing$.

Step 2:

Suppose $(\boldsymbol{x}', \boldsymbol{s}')$ is a feasible solution of (3-12). Then $(\boldsymbol{x}', \boldsymbol{g}(\boldsymbol{x}'))$ is also a feasible solution, because $\boldsymbol{s}$ is only involved in (3-11). And since f is increasing and $\boldsymbol{g}(\boldsymbol{x}') \le \boldsymbol{s}'$, we have $f(\boldsymbol{g}(\boldsymbol{x}')) \le f(\boldsymbol{s}')$. Thus, no matter what $\boldsymbol{x}^*$ is, $\boldsymbol{s}^* = \boldsymbol{g}(\boldsymbol{x}^*)$.

3.4.2 Formulation

A three-stage solving procedure is implemented in risk-based predictive constraint relaxation (P-RBCR), including stage 0, stage 1 and stage 2. These stages are described in what follows:

1. Stage 0 - initialization

Initialize the infeasible problem (identifies initial set of CR lines and NCR lines). The starting point is the implementation of industry-based CR method, defined as the applied CR method (A-CR). Non-negative slack variables are introduced to the transmission line constraints, and the associated penalty cost is incorporated into the objective function. DC power flow is utilized in the optimization problem, and power loss is neglected. Detailed formulations are provided in (3-14) to (3-23).

$$Min \sum_{T=1}^{NI}\sum_{i=1}^{NG} c_i \times P_{i,T} + \sum \text{Penalty} \times \alpha_{l,T}^{k} \tag{3-14}$$

subject to:

$$\sum_{m=1}^{N}\left(\sum_{i=m} P_{i,T}\right) - \sum_{m=1}^{N} D_{m,T} = 0, T \in \{1,...,NI\} \tag{3-15}$$

$$h_{l,T}^{k} = \sum_{m=1}^{N} GSF_{l,m}^{k}\left(\sum_{i=m} P_{i,T} - D_{m,T}\right), k \in \{0,1,...,NC\}, l \in, T \in \{1,..,NI\} \tag{3-16}$$

$$h_{l,T}^{k} - \alpha_{l,T}^{k} \le Limit_{l}^{k}, k \in \{0,1,...,NC\}, l \in \{1,..,NL\}, T \in \{1,..,NI\} \tag{3-17}$$

$$P_{i,T} - REG_{i,T}^{down} \ge P_{i,\min}, T \in \{1,...,NI\}\ i \in \{1,...NG\} \tag{3-18}$$

$$P_{i,T} + REG_{i,T}^{up} \le P_{i,\max}, T \in \{1,...,NI\}\ i \in \{1,...NG\} \tag{3-19}$$

$$-RMP_{i}^{up} \le \Delta T\left(P_{i,T} - P_{i,T-1}\right) \le RMP_{i}^{up}, T \in \{1,..,NI\}, i \in \{1,...NG\} \tag{3-20}$$

$$-RMP_{i}^{down} \le \Delta T\left(P_{i,T} - P_{i.T-1}\right) \le RMP_{i}^{down}, T \in \{1,..,NI\}, i \in \{1,...NG\} \tag{3-21}$$

$$\sum_{i=1}^{NG} REG_{i,T}^{up} \ge REG_{req,T}^{up}, T \in \{1,..,NI\} \tag{3-22}$$

$$\sum_{i=1}^{NG} REG_{i,T}^{down} \ge REG_{req,T}^{down}, T \in \{1,..,NI\} \tag{3-23}$$

Here, (3-15) is the system power balance equation, which guarantees that the generation output is able to satisfy load consumption. Equation (3-16) is the calculation of line flow, which are restricted by thermal limits in (3-17). Equations (3-18) ~ (3-19) constrain minimum and maximum generation output with sufficient space for regulation movements. Equations (3-20) ~ (3-21) are ramping constraints, which are applicable to be operated in multiple time-interval horizon, since distinct base points are setting up for each individual time-interval. Equations (3-22) ~ (3-23) indicate the system demand for regulation products.

Lines with non-zero slack variables are included in the CR set; the remaining transmission line constraints are automatically identified as NCR lines.

2. Stage 1 - feasibility

Stage 1 searches the infeasible SCED problem for a feasible solution. In this stage, the effects on system security imposed by allowing overloads are controlled by system risk. The objective is to identify the feasible solution, with minimization of risk. This problem is formulated as follows:

$$Min\ Risk = \sum_{k=1}^{NC} \Pr^k \left(\sum_{l \in NCR} sev_{P,l,T}^k + \sum_{l \in CR} sev_{C,l,T}^k \right) \tag{3-24}$$

Subject to:

$$(3\text{-}15) \sim (3\text{-}16)$$

$$T_{C,l,T}\left(h_{l,T}^k, T_{C,l,T_0}\right) \le T_{C,l,\max}, k \in \{0,1,...,NC\}, l \in CR, T \in \{1,..,NI\} \tag{3-25}$$

$$h_{l,T}^k - \alpha_{l,T}^k \le Limit_l^k, k \in \{0,1,...,NC\}, l \in NCR, T \in \{1,..,NI\} \tag{3-26}$$

$$\begin{cases} sev_{P,l,T}^k \ge 0 \\ sev_{P,l,T}^k \ge a_{1l} \times h_{l,T}^k + b_{1l} \\ sev_{P,l,T}^k \ge a_{2l} \times h_{l,T}^k + b_{2l} \\ sev_{P,l,T}^k \ge a_{3l} \times h_{l,T}^k + b_{3l} \end{cases}, k \in \{0,1,...,NC\}, l \in NCR, T \in \{1,..,NI\} \tag{3-27}$$

$$\begin{cases} sev_{C,l,T}^k \ge 0 \\ sev_{C,l,T}^k \ge a_{1l}^c \times h_{l,T}^k + b_{1l}^c \\ sev_{C,l,T}^k \ge a_{2l}^c \times h_{l,T}^k + b_{1l}^c \\ sev_{C,l,T}^k \ge a_{3l}^c \times h_{l,T}^k + b_{1l}^c \end{cases}, k \in \{0,1,...,NC\}, l \in CR, T \in \{1,..,NI\} \tag{3-28}$$

$$(3\text{-}18) \sim (3\text{-}23)$$

The overloading lines are included in the CR set, for which the DHBE is implemented, which constraint conductor temperature (and not conductor flow) for the CR set, as shown in (3-25). For lines assigned to the NCR set, which has no observed overloads, power flow is limited on the corresponding transmission facilities, as expressed in (3-26). Equations (3-27) ~ (3-28) represent the calculation of severity value performed for the NCR lines and CR lines, respectively.

3. Stage 2 – optimality

Stage 2 is formulated to obtain economic dispatch decision, based on feasible region determined by Stage 1. In comparison with Stage 0, Stage 2 works with the new limits which have been relaxed, and are free of penalty price. This problem is formulated as follows:

$$Min \sum_{T=1}^{NI} \sum_{i=1}^{NG} c_i \times P_{i,T} \tag{3-29}$$

subject to:

$$(3\text{-}15) \sim (3\text{-}16)$$

$$h_{l,T}^{k} \le Limit\_new_{l}^{k}, k \in \{0,1,...,NC\}, l \in \{1,..,NL\}, T \in \{1,..,NI\} \tag{3-30}$$

$$(3\text{-}18) \sim (3\text{-}23)$$

3.4.3 Solution approach

1. Solution procedure

The P-RBCR solution procedure is illustrated in the flow chart of Figure 3-6, it is illustrated using simplified optimization formulations in Figure 3-7, and it is described below.

- Stage 0, initialization: This stage initializes the infeasible problem. It identifies the locations and amounts of overloads through the slack variables that are non-zero; in addition, the CR and NCR sets of circuits are initialized in this stage.
- Stage 1, feasibility: This stage identifies the constraint relaxation decision by minimizing risk, iterates on the dynamic CR set until no further CR lines are found, and provides the feasible solution to stage 2. The iteration on the CR set occurs by forming linear relationships among T_0, ΔT and I to provide the conductor temperature limits; slack variables are minimized for the NCR set, and any line with positive slack becomes a new CR line, being added to the CR set. Based on the conductor temperature of CR lines, the dynamic HBEs are applied within the optimization to achieve the necessary relaxation to obtain the updated new flow limits. Those overloads are allowable since the conductor temperature does not exceed the corresponding limit; the distribution of overloads by optimization algorithm degrades the system security least which is evaluated in terms of risk value.
- Stage 2, optimality: This stage utilizes the new flow limits, and obtains the most economic dispatch decision among all feasible solutions to this predictive SCED problem, which is otherwise infeasible. As the predictive control methodology, the solution for the first time-interval is implemented; the solutions for the remaining intervals are considered as advisory dispatch decisions.

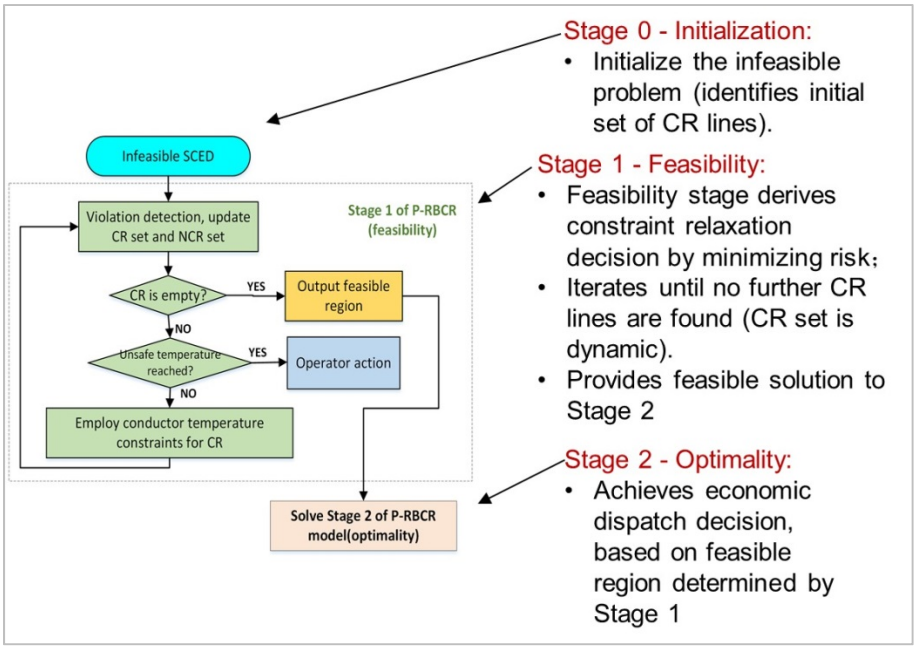

Figure 3-6: Flow chart of P-RBCR solution procedure

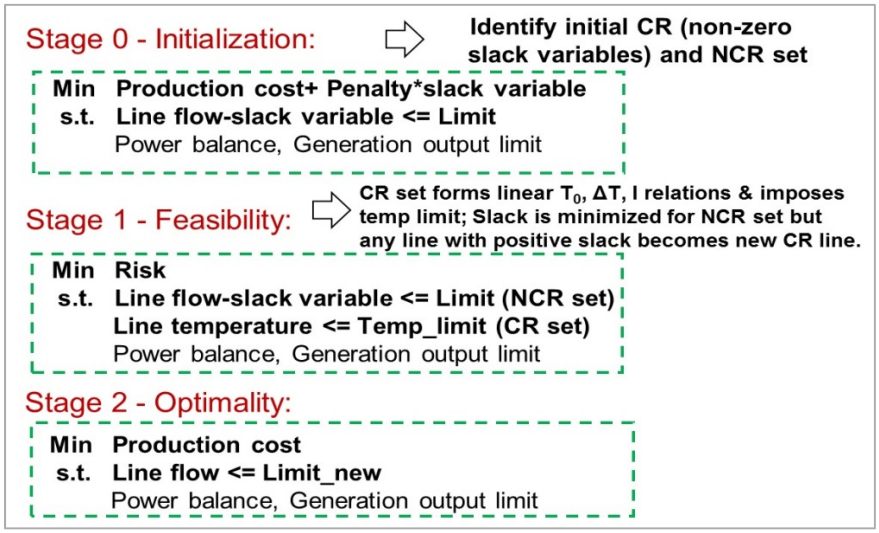

Figure 3-7: Simplified optimization formulations for solution procedure

2. Algorithm realization: interfacing GAMS with MATLAB

As a leading modelling and mathematical tool, the General Algebraic Modeling System (GAMS) has been widely used in operations research. It has the advantages of simplicity in implementation and convenience to debug, as well as it is easy to interface with other commonly used programming languages, such as MATLAB and Python. GAMS contains advanced solving algorithms for linear programs, mixed-integer programs, and other optimization problem types. Furthermore, GAMS has the ability to handle high-dimensional problems due to large quantities of constraints and decision variables. Thus, GAMS is selected to model and solve optimization models in P-RBCR which are linear programming problems. In addition, output processing and iterative updating sets are

interfaced using MATLAB, which has good flexibility for data processing. The functionality GDXMRW (GDX-MATLAB Read/Write) is utilized to exchange data between GAMS and MATLAB.

3.4.3 LMP calculation

LMPs varies among geographical locations, providing economic signals for wholesale electricity markets. LMPs are defined for each bus, as the incremental production cost to satisfy the next MW of withdrawal at that particular bus. As indicated in Chapter 2, the LMP spike is perceived in this work as undesirable, as it stresses the market in a way that is arguably arbitrary (owing to the lack of rigor behind choice of the penalty price) and thus motivates changes to the A-CR methodology. This section derives the LMP calculation for Stage 0 (A-CR) and Stage 2 (Optimality of P-RBCR).

(1) LMP calculation in A-CR

The formulation of A-CR is repeated here with corresponding Lagrange multipliers in the parentheses, as follows.

$$Min \sum_{T=1}^{NI}\left(\sum_{i=1}^{NG} c_i \times P_{i,T} + \sum_{k=0}^{NC}\sum_{l=1}^{NL} \text{Penalty} \times \alpha_{l,T}^{k}\right)$$

subject to:

$$\sum_{m=1}^{N}\left(\sum_{i=m} P_{i,T}\right) - \sum_{m=1}^{N} D_{m,T} = 0, T \in \{1,...,NI\} \qquad (\lambda_{1,T} \geq 0)$$

$$\begin{cases} \sum_{m=1}^{N} GSF_{l,m}^{k}(\sum_{i=m} P_{i,T} - D_{m,T}) - \alpha_{l,T}^{k} \leq Limit_{l}^{k}, \\ k \in \{0,1,...,NC\}, l \in \{1,..,NL\}, T \in \{1,..,NI\} \end{cases} \quad (\beta_{1,l,T}^{k} \geq 0)$$

$$P_{i,T} - REG_{i,T}^{down} \geq P_{i,\min}, T \in \{1,...,NI\}\ i \in \{1,...NG\} \quad (\mu_{1,i,T}^{min} \geq 0)$$

$$P_{i,T} + REG_{i,T}^{up} \leq P_{i,\max}, T \in \{1,...,NI\}\ i \in \{1,...NG\} \qquad (\mu_{1,i,T}^{max} \geq 0)$$

$$-RMP_{i}^{up} \leq \Delta T\left(P_{i,T} - P_{i,T-1}\right) \leq RMP_{i}^{up}, T \in \{1,..,NI\}, i \in \{1,...NG\} \quad (\delta_{1l,i,T}^{up}, \delta_{1u,i,T}^{up} \geq 0)$$

$$-RMP_{i}^{down} \leq \Delta T\left(P_{i,T} - P_{i.T-1}\right) \leq RMP_{i}^{down}, T \in \{1,..,NI\}, i \in \{1,...NG\} \quad (\delta_{1l,i,T}^{down}, \delta_{1l,i,T}^{down} \geq 0)$$

$$\sum_{i=1}^{NG} REG_{i,T}^{up} \geq REG_{req,T}^{up}, T \in \{1,..,NI\} \quad (\eta_{1,T}^{up} \geq 0)$$

$$\sum_{i=1}^{NG} REG_{i,T}^{down} \geq REG_{req,T}^{down}, T \in \{1,..,NI\} \quad (\eta_{1,T}^{down} \geq 0)$$

According to the LMP definition, the LMP at bus i for period T can be obtained as the partial derivative of Lagrange function. The Lagrange function across the entire operation horizon is indicated in (3-31).

$$
\begin{aligned}
L_1 = & \sum_{T=1}^{NI}\left(\sum_{i=1}^{NG} c_i \times P_{i,T} + \sum_{k=0}^{NC}\sum_{l=1}^{NL} \text{Penalty} \times \alpha_{l,T}^{k}\right) - \sum_{T=1}^{NI} \lambda_{1,T} \times \left(\sum_{i=1}^{N} P_{i,T} - \sum_{i=1}^{N} D_{i,T}\right) \\
& + \sum_{T=1}^{NI}\sum_{k=0}^{NC}\sum_{l=1}^{NL} \beta_{1,l,T}^{k} \times \left(\sum_{m=1}^{N} GSF_{l,m}^{k}(\sum_{i=m} P_{i,T} - D_{m,T}) - \alpha_{l,T}^{k} - Limit_{l}^{k}\right) \\
& + \sum_{T=1}^{NI}\sum_{i=1}^{NG} \mu_{1,i,T}^{\min} \times \left(-P_{i,T} + REG_{i,T}^{down} + P_{i,\min}\right) + \sum_{T=1}^{NI}\sum_{i=1}^{NG} \mu_{1,i,T}^{\max} \times \left(P_{i,T} + REG_{i,T}^{up} - P_{i,\max}\right) \\
& + \sum_{T=2}^{NI}\left(\delta_{1l,i,T}^{up} \times \left(-RMP_{i}^{up} - \Delta T\left(P_{i,T} - P_{i,T-1}\right)\right) + \delta_{1u,i,T}^{up} \times \left(\Delta T\left(P_{i,T} - P_{i,T-1}\right) - RMP_{i}^{up}\right)\right) \\
& + \sum_{T=2}^{NI}\left(\delta_{1l,i,T}^{down} \times \left(-RMP_{i}^{down} - \Delta T\left(P_{i,T} - P_{i,T-1}\right)\right) + \delta_{1u,i,T}^{down} \times \left(\Delta T\left(P_{i,T} - P_{i,T-1}\right) - RMP_{i}^{down}\right)\right) \\
& + \sum_{T=1}^{NI} \eta_{1,T}^{up} \times \left(-\sum_{i=1}^{NG} REG_{i,T}^{up} + REG_{req,T}^{up}\right) + \sum_{T=1}^{NI} \eta_{1,T}^{down} \times \left(-\sum_{i=1}^{NG} REG_{i,T}^{down} + REG_{req,T}^{down}\right)
\end{aligned}
\tag{3-31}
$$

We take the partial derivative of L_1 with respect to load $D_{i,T}$, i.e., the LMP at bus i for period T is calculated as (3-32).

$$
LMP_{i,T}^{1} = \frac{\partial L_1}{\partial D_{i,T}} = \lambda_{1,T} - \sum_{k=0}^{NC}\sum_{l=1}^{NL}\left(\beta_{1,l,T}^{k} \times \sum_{m=1}^{N} GSF_{l,m}^{k}\right) \tag{3-32}
$$

In reference to convex optimization theory, the Karush-Kuhn-Tucker (KKT) conditions are imposed at the optimal point. Thus,

$$
\frac{\partial L_1}{\partial \alpha_{l,T}^{k}} = \text{Penalty} - \beta_{1,l,T}^{k} = 0 \tag{3-33}
$$

Then, by substituting (3-33) into (3-32), the LMP can be converted into (3-34).

$$
LMP_{i,T}^{1} = LMP_{i,T}^{1,energy} + LMP_{i,T}^{1,congestion} = \lambda_{1,T} - \sum_{k=0}^{NC}\sum_{l=1}^{NL}\left(Penalty \times \sum_{m=1}^{N} GSF_{l,m}^{k}\right) \tag{3-34}
$$

We do not consider the power loss along transmission lines, making the loss component in LMP zero[4]. Therefore, the energy component is the shadow price of the power balance equation, which is set by the bid of the marginal unit, which is the unit that would supply the next MW of load over the requirements. The energy component is the same across the entire network. On the other hand, the congestion component is the by-product of transmission line limits, which reflects the congestion status of each specific line. The congestion component can have various values, which reflects the congestion level.

[4] This assumption is reasonable because the loss component takes a relatively small proportion of the whole LMP value; the dominant component of the LMP is the congestion component, which can be a significant contributor to the LMP spike caused by CR.

Another observation from (3-34) is that the selection of penalty price has significant impact on the value of the congestion component. That is the source for the LMP spike if the penalty is too high, or under pricings if the penalty is too low.

(2) LMP calculation in stage 2 of P-RBCR

The formulation of Stage 2 of P-RBCR is repeated here with the corresponding Lagrange multipliers in parentheses, as follows:

$$Min \sum_{T=1}^{NI} \sum_{i=1}^{NG} c_i \times P_{i,T}$$

subject to:

$$\sum_{m=1}^{N} \left(\sum_{i=m} P_{i,T} \right) - \sum_{m=1}^{N} D_{m,T} = 0, T \in \{1,..., NI\} \qquad (\lambda_{2,T} \geq 0)$$

$$\begin{cases} \sum_{m=1}^{N} GSF_{l,m}^{k} (\sum_{i=m} P_{i,T} - D_{m,T}) \leq Limit\_new_{l}^{k}, \\ k \in \{0,1,..., NC\}, l \in \{1,.., NL\}, T \in \{1,.., NI\} \end{cases} \qquad (\beta_{2,l,T}^{k} \geq 0)$$

$$P_{i,T} - REG_{i,T}^{down} \geq P_{i,\min}, T \in \{1,..., NI\}\ i \in \{1,...NG\} \quad (\mu_{2,i,T}^{min} \geq 0)$$

$$P_{i,T} + REG_{i,T}^{up} \leq P_{i,\max}, T \in \{1,..., NI\}\ i \in \{1,...NG\} \qquad (\mu_{2,i,T}^{max} \geq 0)$$

$$-RMP_{i}^{up} \leq \Delta T \left(P_{i,T} - P_{i,T-1} \right) \leq RMP_{i}^{up}, T \in \{1,.., NI\}, i \in \{1,...NG\} \quad (\delta_{2l,i,T}^{up}, \delta_{2u,i,T}^{up} \geq 0)$$

$$-RMP_{i}^{down} \leq \Delta T \left(P_{i,T} - P_{i.T-1} \right) \leq RMP_{i}^{down}, T \in \{1,.., NI\}, i \in \{1,...NG\} \qquad (\delta_{2l,i,T}^{down}, \delta_{2l,i,T}^{down} \geq 0)$$

$$\sum_{i=1}^{NG} REG_{i,T}^{up} \geq REG_{req,T}^{up}, T \in \{1,.., NI\} \quad (\eta_{2,T}^{up} \geq 0)$$

$$\sum_{i=1}^{NG} REG_{i,T}^{down} \geq REG_{req,T}^{down}, T \in \{1,.., NI\} \quad (\eta_{2,T}^{down} \geq 0)$$

According to the incremental cost definition of price, the LMP at bus i for period T can be calculated by taking the partial derivative of Lagrange function. The Lagrange function across the entire operation horizon is indicated in (3-35).

$$
\begin{aligned}
L_2 = & \sum_{T=1}^{NI}\left(\sum_{i=1}^{NG} c_i \times P_{i,T} + \sum_{k=0}^{NC}\sum_{l=1}^{NL} \text{Penalty} \times \alpha_{l,T}^{k}\right) - \sum_{T=1}^{NI} \lambda_{2,T} \times \left(\sum_{i=1}^{N} P_{i,T} - \sum_{i=1}^{N} D_{i,T}\right) \\
& + \sum_{T=1}^{NI}\sum_{k=0}^{NC}\sum_{l=1}^{NL} \beta_{2,l,T}^{k} \times \left(\sum_{m=1}^{N} GSF_{l,m}^{k}(\sum_{i=m} P_{i,T} - D_{m,T}) - Limit\_new_{l}^{k}\right) \\
& + \sum_{T=1}^{NI}\sum_{i=1}^{NG} \mu_{2,i,T}^{\min} \times \left(-P_{i,T} + REG_{i,T}^{down} + P_{i,\min}\right) + \sum_{T=1}^{NI}\sum_{i=1}^{NG} \mu_{2,i,T}^{\max} \times \left(P_{i,T} + REG_{i,T}^{up} - P_{i,\max}\right) \\
& + \sum_{T=2}^{NI}\left(\delta_{2l,i,T}^{up} \times \left(-RMP_{i}^{up} - \Delta T\left(P_{i,T} - P_{i,T-1}\right)\right) + \delta_{2u,i,T}^{up} \times \left(\Delta T\left(P_{i,T} - P_{i,T-1}\right) - RMP_{i}^{up}\right)\right) \\
& + \sum_{T=2}^{NI}\left(\delta_{2l,i,T}^{down} \times \left(-RMP_{i}^{down} - \Delta T\left(P_{i,T} - P_{i,T-1}\right)\right) + \delta_{2u,i,T}^{down} \times \left(\Delta T\left(P_{i,T} - P_{i,T-1}\right) - RMP_{i}^{down}\right)\right) \\
& + \sum_{T=1}^{NI} \eta_{2,T}^{up} \times \left(-\sum_{i=1}^{NG} REG_{i,T}^{up} + REG_{req,T}^{up}\right) + \sum_{T=1}^{NI} \eta_{2,T}^{down} \times \left(-\sum_{i=1}^{NG} REG_{i,T}^{down} + REG_{req,T}^{down}\right)
\end{aligned}
\tag{3-35}
$$

We take the partial derivative of L_2 with respect to load $D_{i,T}$, i.e., the LMP at bus i for period T is calculated as (3-36).

$$
LMP_{i,T}^{2} = \frac{\partial L_2}{\partial D_{i,T}} = \lambda_{2,T} - \sum_{k=0}^{NC}\sum_{l=1}^{NL}\left(\beta_{2,l,T}^{k} \times \sum_{m=1}^{N} GSF_{l,m}^{k}\right) \tag{3-36}
$$

The LMP in P-RBCR is free of an influence from the penalty price, reducing the potential to cause an LMP spike. Transmission constraints in the CR set are binding under the updated limits with relaxation, resulting in non-zero congestion component. The congestion components still have the ability to reflect price signals for a congested network.

3.5 Summary

Based on the theoretical foundation of the DHBE and model predictive control, we have developed the framework of a three-stage P-RBCR, including initialization, feasibility, and optimality. For each stage, the optimization model has been formulated, and the corresponding solving algorithm with software architecture has been proposed. We also describe the calculation of LMP for A-CR and P-RBCR. This theoretical development will be illustrated in the next two chapters using case studies. Chapter 4 will provide a case study using an IEEE test system. Chapter 5 will provide a case study using a system emulating the NYISO system, contrived using publicly available data.

4. Case study on IEEE test system

4.1 Parameter and data preparation for IEEE test system

1. IEEE six-bus system

For the purpose of verification on the proposed optimization for handling the infeasible predictive SCED problem, we tested the methodology of P-RBCR and associated solution algorithm on the modified IEEE six-bus system [34]. The single-line diagram for network configuration is indicated in Figure 4-1. There are 11 transmission lines with 3 generators at buses 1, 2, and 3, respectively. System loads are located at buses 4, 5, and 6, respectively. The operating horizon for predictive control is six 5-minute time-intervals.

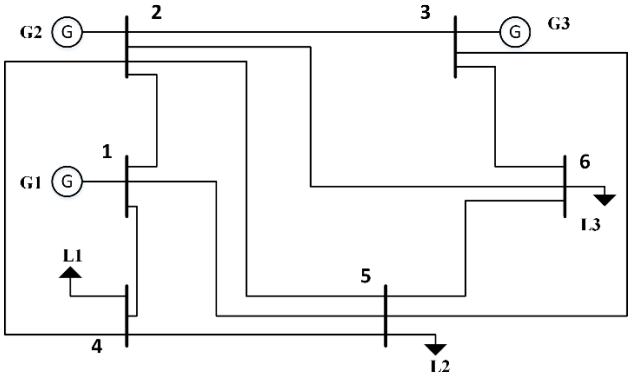

Figure 4-1: Network topology of IEEE six-bus system

Tables 4-1~4-3 provides generator attributes, load variations and parameters for each line (including thermal ratings and pre-defined probabilities of 'N-1' contingency states). One state represents the normal condition and 11 states represent 'N-1' contingency conditions; 6 time-intervals are considered in the predictive SCED. Thus, 726 inequalities are utilized to represent and model the transmission line constraints. This large number of constraints indicates the complexity of the optimization problem, given the fact that this is such a small system.

Table 4-1: Generator attributes

	Pmax (MW)	Pmin (MW)	Marginal Cost ($/MW)	Ramping up rate (MW/min)	Ramping up rate (MW/min)	Regulation cost ($/MWh)
G1	200	50	30	2	2	10
G2	150	37.5	20	2	2	10
G3	180	45	40	2	2	10

Table 4-2: Load attributes (/MW)

	Period 1	Period 2	Period 3	Period 4	Period 5	Period 6
Load 1	78	79.3	80.6	79.3	78	79.3
Load 2	78	79.3	80.6	79.3	78	79.3
Load 3	78	79.3	80.6	79.3	78	79.3

Table 4-3: Transmission line parameters

From Bus	To Bus	Normal Rating (MW)	Long-term emergency Rating (MW)	Short-term emergency Rating (MW)	Prob. of contingency
1	2	100	110	130	0.077
1	4	100	110	130	0.077
1	5	100	110	130	0.115
2	3	60	66	78	0.096
2	4	60	66	78	0.038
2	5	60	66	78	0.115
2	6	60	66	78	0.077
3	5	60	66	78	0.100
3	6	60	66	78	0.038
4	5	60	66	78	0.153
5	6	60	66	78	0.115

2. Linear representation of dynamic heat balance equation

Suppose the initial temperature at the beginning of the time interval $T_{c,0} = 30\ ^oC$, and the maximum temperature that the conductor can withstand is $T_{c,max} = 100\ ^oC$. By conducting numerical experiments, we derive the relationship between $(T_{c,\Delta t} - T_{c,0})$ and $(T_{c,0}, I_{\Delta t})$ (Δt is a specific time step), as shown in Figure 4-2. Furthermore, the convex surface is fit by linear regression; the coefficients are indicated in (4-1) with an R-square of 0.99, which verifies that the linear relationship has a satisfactory performance in approximating the complex differential formulation.

$$T_{C,\Delta t} - T_{C,0} = -0.4004 \times T_{C,0} + 0.0129 \times I_{\Delta t} + 12.97 \quad (4\text{-}1)$$

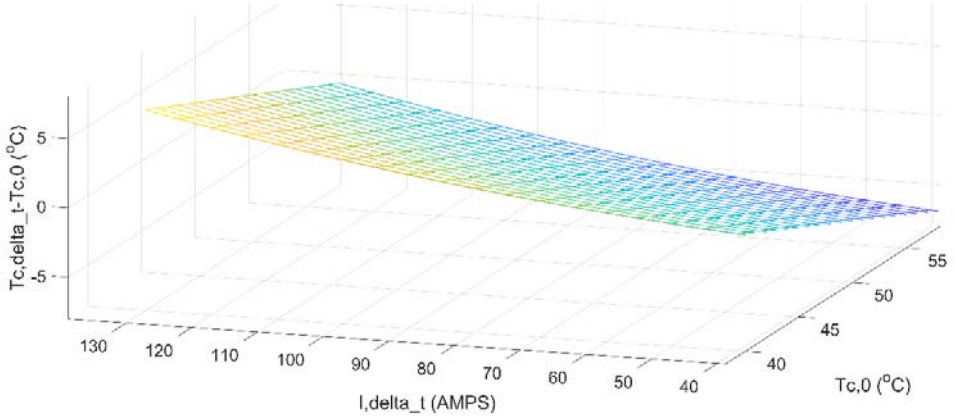

Figure 4-2: Relationship between current flow and conductor temperature

Solving the infeasible SCED problem under A-CR, which is Stage 0 of P-RBCR, the violated thermal constraints (line2, contingency 2 through the first time-interval ~ the sixth time-interval, denoted as P1~P6) are identified by evaluating non-zero slack variables. Then, those violated lines are added to the CR set (constrained by conductor temperature limits), and the remaining lines remain in the NCR set (constrained by flow limits), with the objective to minimize the system risk. This process is iteratively repeated until an iteration occurs where no additional violated lines are identified; in the specific case studied here, only 2 iterations are necessary. Finally, the new limits required to be relaxed are computed by the thermal DHBE, and the predictive SCED is re-solved. With the feasible region determined by the relaxed limits, the most economic re-dispatch decisions have been identified. The results and analysis are conducted in the following sections.

4.2 Risk-based predictive constraint relaxation results

1. Flow/temperature change

In the feasibility stage, the thermal limits for line 24 (contingency 2, P1~P6) has been assigned to CR set. By shifting from flow limits to temperature limits, those lines are no longer violated constraints. Figure 4-3 illustrates flow/temperature change along line 24 under contingency 2.

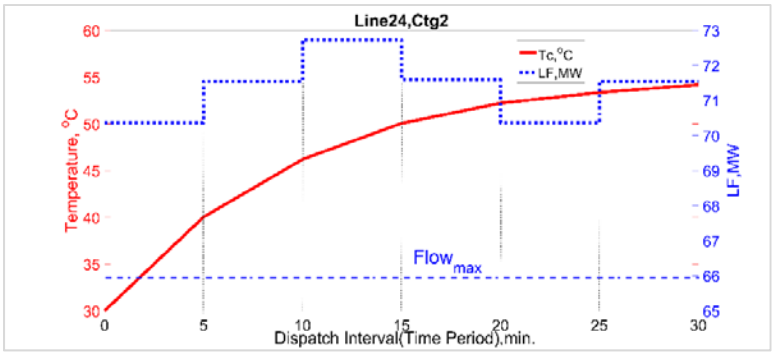

Figure 4-3: Flow/Temperature change for line 24 under contingency 2

As shown in Figure 4-3, for those time intervals, power flows (indicated by the dashed lines) exceed corresponding limits; while conductor temperature (indicated by the solid lines) are within the temperature boundary. This effect arises from the fact that conductor temperature change is delayed relative to power flow change. Thus, constraint relaxations, where power flow exceeds its limit, can be safe if the power flow increase is reduced before the temperature exceeds its limit.

It is observed that the slope of temperature change within each interval is decreasing with time; this results from the pattern of flow change, where the flow increases in the first three intervals and decreases in the fourth and fifth intervals. This observation indicates that the nature of flow change can be step-wise, which follows the control signal immediately; while temperature change is a gradual and slow dynamic process. Another observation is that flow change and temperature change are not simply positively or negatively correlated. The behavior of temperature change is determined by the initial temperature at the beginning of the time duration, together with the accumulated thermal effects imposed on the conductor during the time duration. As shown in the fourth interval, flow decrease does not result in immediate temperature drop; on the contrary, temperature continues to increase but with a decreasing rate, until the end of the time horizon.

2. Production cost and risk

Economy and security are the criteria to consider when making dispatch decisions. Table 4-4 lists production cost and risk for A-CR and P-RBCR for this illustration. As provided in Table 4-4, P-RBCR results in a solution that has both lower production cost and lower risk. The reason for the lower cost is that there is no penalty (which is in thousands-scale) in the formulation of P-RBCR. However, P-RBCR re-dispatches available resources and reflects the true costs to alleviate congested lines. P-RBCR sends LMP signals which reflect the system congestion status but avoids price spikes; this feature will be discussed in the next subsection. The feasible solution is identified through the risk minimization of stage 1; this provides that P-RBCR has better performance in risk evaluation.

Table 4-4: Comparisons on cost and risk

	Production cost ($/30min)	**Risk**
A-CR	179,616	135.6
P-RBCR	51,168	130.8

3. LMP comparison between A-CR and P-RBCR

Based on the LMP calculation presented in Section 3.4.3, we calculated LMP under A-CR and P-RBCR, as shown in Table 4-5 and Figure 4-4.

Congestion on line 24 results in relatively high LMP at buses 4 and 5. The reason that bus 2 has a negative congestion component is that one additional MW withdrawal at bus 2 reduces the congestion along line 24, thus decreasing the total cost.

The LMP components in Table 4-5 are plotted in Figure 4-4 (some of the price values exceed $3000 and so have been cut off at the top in order to ensure the lower values are readable); from this, it can be observed that the A-CR and P-RBCR share the unique energy component, since the generator and load attributes for those two models are the same. Another observation is that P-RBCR decreases the congestion component, which avoids the artificially high LMP spike yet still retains the congestion pattern of A-CR.

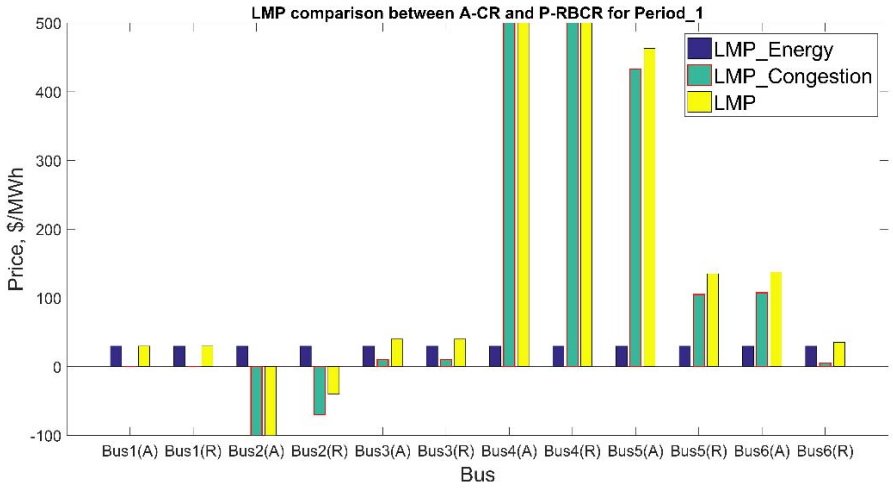

Figure 4-4: Breakdown and comparisons of LMP between A-CR and P-RBCR

Table 4-5: Breakdown of LMP for A-CR and P-RBCR

Bus	Period	A-CR			P-RBCR		
		LMP_ Energy	LMP_ congestion	LMP	LMP_ Energy	LMP_ congestion	LMP
1	P1	30	0.00	30.00	30	0.00	30.00
2		30	-287.44	-257.44	30	-70.04	-40.04
3		30	10.00	40.00	30	10.00	40.00
4		30	3057.24	3087.24	30	757.65	787.65
5		30	433.24	463.24	30	105.06	135.06
6		30	107.51	137.51	30	5.45	35.45
1	P2	30	0.00	30.00	30	0.00	30.00
2		30	-287.44	-257.44	30	-70.04	-40.04
3		30	10.00	40.00	30	10.00	40.00
4		30	3057.24	3087.24	30	757.65	787.65
5		30	433.24	463.24	30	105.06	135.06
6		30	107.51	137.51	30	5.45	35.45
1	P3	30	0.00	30.00	30	0.00	30.00
2		30	-287.44	-257.44	30	-70.04	-40.04
3		30	10.00	40.00	30	10.00	40.00
4		30	3057.24	3087.24	30	757.65	787.65
5		30	433.24	463.24	30	105.06	135.06
6		30	107.51	137.51	30	5.45	35.45
1	P4	30	0.00	30.00	30	0.00	30.00
2		30	-287.44	-257.44	30	-70.04	-40.04
3		30	10.00	40.00	30	10.00	40.00
4		30	3057.24	3087.24	30	757.65	787.65
5		30	433.24	463.24	30	105.06	135.06
6		30	107.51	137.51	30	5.45	35.45
1	P5	30	0.00	30.00	30	0.00	30.00
2		30	-287.44	-257.44	30	-70.04	-40.04
3		30	10.00	40.00	30	10.00	40.00
4		30	3057.24	3087.24	30	757.65	787.65
5		30	433.24	463.24	30	105.06	135.06
6		30	107.51	137.51	30	5.45	35.45
1	P6	30	0.00	30.00	30	0.00	30.00
2		30	-287.44	-257.44	30	-70.04	-40.04
3		30	10.00	40.00	30	10.00	40.00
4		30	3057.24	3087.24	30	757.65	787.65
5		30	433.24	463.24	30	105.06	135.06
6		30	107.51	137.51	30	5.45	35.45

4.3 Summary

This chapter illustrates and verifies the methodology of P-RBCR using an IEEE test system by utilizing a combined MATLAB/GAMS framework. The temperature/flow curve verifies that overloads are allowable when the incurred conductor temperatures do not hit the limits; cost and risk analysis shows that P-RBCR identifies good re-dispatch solutions to remove constraint violations. In addition, P-RBCR reduces occurrence of the LMP spike, while the price signals necessary to provide congestion management remain.

5. Case study on contrived NYISO system

In order to test our methodology on an empirically-grounded and real-life system, we have developed the 11-zone mini-NYISO system, based on publicly available data and information. The development procedure is similar to what was done for the New England system in [35]. Although what we have produced is certainly simplified and approximate, we have tuned the parameters to reflect the network performance as close as possible. The resulting "mini-NYISO test system" can be used to illustrate wholesale market operation via SCED and associated LMP calculation. This chapter describes the development of the mini-NYISO system and the application CR action to it.

5.1 Development of mini-NYISO test system

This section describes the development of the mini-NYISO test system, based on the publicly available data and information. The intent of this effort is to provide a system having transmission configuration, generation fleet, load attributes, and reserve requirements that reasonably reflect at a high-level corresponding features in the actual NYISO system.

5.1.1 Transmission grid

NYISO operates the competitive wholesale market across New York State, managing nearly 11,000 miles of high-voltage transmission lines and dispatching more than 500 electric generators. The footprint of the New York Control Area (NYCA) covers 11 aggregated loading zones, as shown in Figure 5-1. The identification of load zones is based on interface transfer capability and the regulatory area of Transmission Owners.

To reflect this network configuration, we found in the Reliability Needs Requirement Assessment report [36] that the NYISO was represented by an 11-zone bubble model, as indicated in Figure 5-2.In our work, each zone is aggregated to a single bus, and those buses are connected by 345kV transmission lines[5]. In summary, the simplified network has the topology of 11-buses and 11 lines. For the exchange with neighboring areas, i.e., PJM, ISO-NE, Hydro Quebec and Ontario, the external transaction is modeled as fixed injection or withdrawal at the corresponding bus. For example, about 800MW of power is imported to Capital Zone from ISO-NE (see Figure 5-2). Thus, we model the external injection as a blocked generator (800MW) with zero production cost, which is connected at Bus 6. Similarly, exports are modeled as either a blocked unit with negative output or a load injection at the corresponding bus. The proposed mini-NYISO system is presented in Figure 5-3.

[5] The backbone of critical transmission lines internal to NYISO area is 345kV; there are no 500kV lines internal to NYCA.

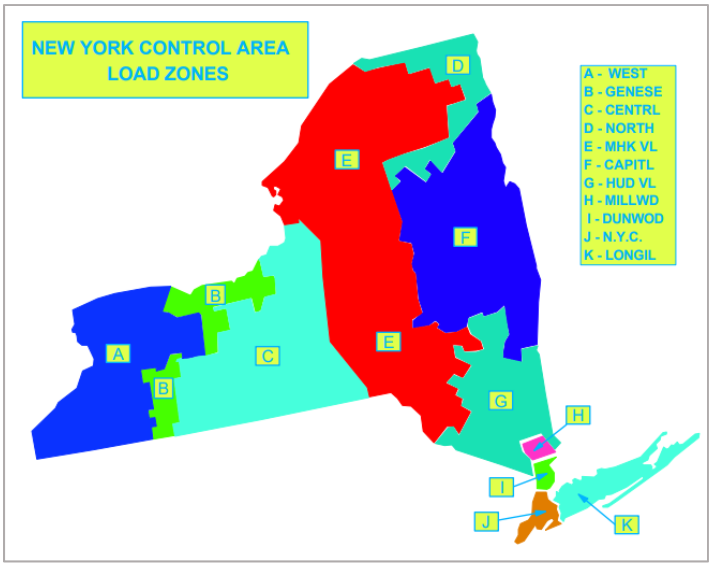

Figure 5-1: New York Control Area Load zones

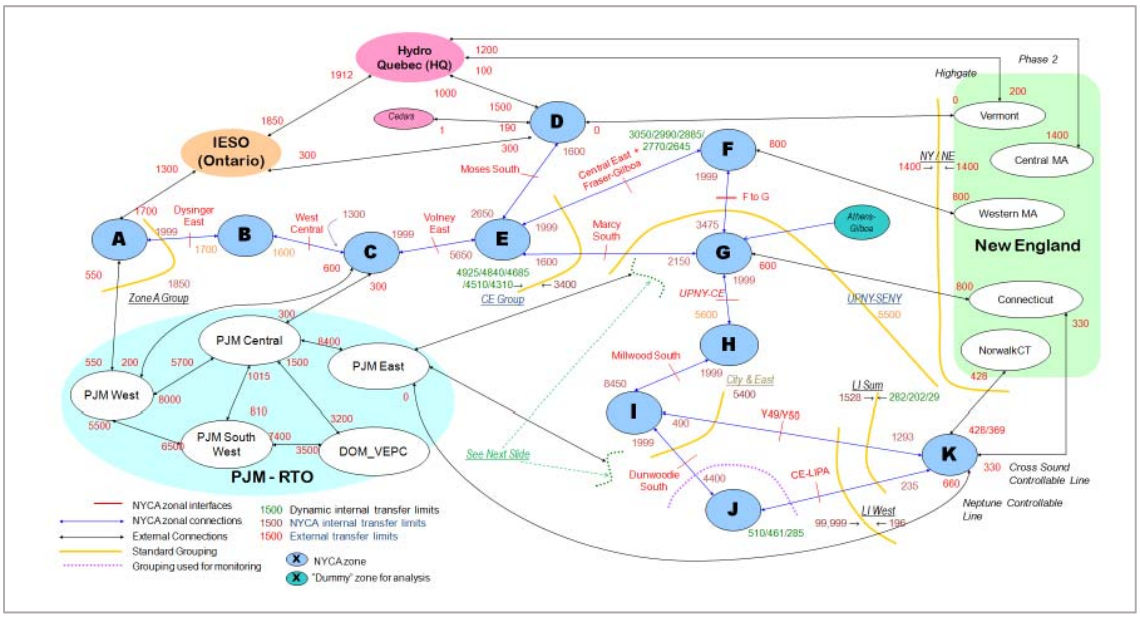

Figure 5-2: MARS Preliminary normal condition topology [36]

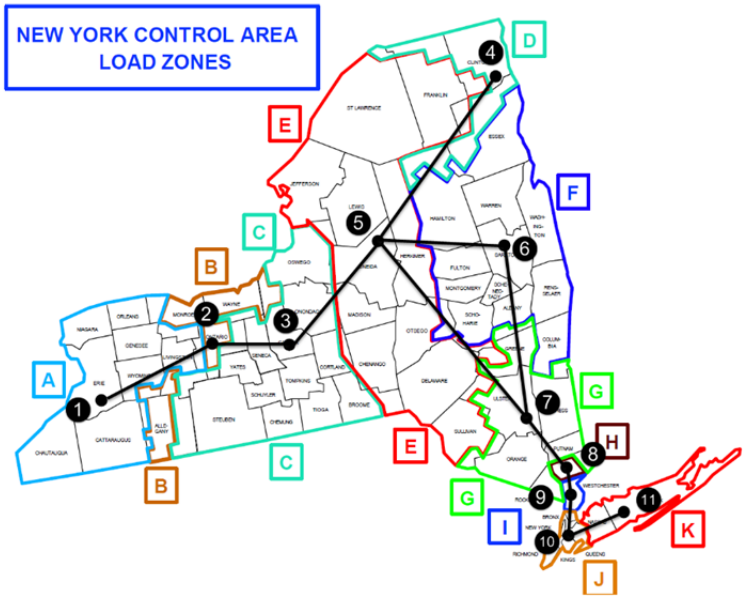

Figure 5-3: Mini-NYISO testing system

The benchmark values of resistance and reactance are approximated for those 11 lines, with consideration of physical properties of transmission lines. As mentioned above, the voltage level is 345kV. Thus, the impedance per unit (meter/mile) is determined by the conductor type, conductor bundling, conductivity of materials, and temperature. We assume that physical parameters of the 345kV AC transmission line are as listed in Table 5-1 [35]. Thus, per unit data for impedance is derived from ACSR tables for overhead transmission lines.

Table 5-1: Physical parameters of 345kV transmission line

	Conductor Type	**Conductor Bundling**	**Constant temperature (^{o}C)**
345kV AC lines	Dove (556 kcmil)	6-conductor bundle per phase with 2.5' diameter and 45' to separate phases	25 ^{o}C

Another attribute contributing to impedance of the entire transmission line is the total length of each modeled line. Several counties are located in the footprint of each load zone, and the geographical information (pairs of latitude and longitude) for each county is available online. Thus, each bus is assumed to be located at the centered county of that zone. Furthermore, the length of each line can be calculated using the two pairs of latitudes and longitudes. The attributes for transmission lines are summarized in Table 5-2.

Table 5-2: Benchmark values of impedance for the 11-zone mini-NYISO test system

Interface name	From Zone	To Zone	Distance (miles)	Resistance (ohms)	Reactance (ohms)	Reactance (per unit)
DYSINGER EAST	West	Genessee	76	12.70	35.95	0.03
West Central	Genessee	Central	36	5.95	16.85	0.01
Volney East	Central	Mohawk Valley	62	10.24	29.00	0.02
MOSES South	Mohawk Valley	North	139	23.06	65.30	0.05
Central EAST	Mohawk Valley	Capital	79	13.16	37.26	0.03
UPNY/SENY	Capital	Hudson valley	84	13.91	39.40	0.03
UPNY/CONED	Hudson valley	Millwood	39	6.42	18.17	0.02
MILLWOOD SOUTH	Millwood	Dunwoodie	21	3.43	9.73	0.01
SPRAINBROOK/DUNWOODIE SOUTH	Dunwoodie	NYC	29	4.76	13.46	0.01
CON ED/LILCO	NYC	Long Island	52	8.63	24.44	0.02
Marcy South	Mohawk Valley	Hudson valley	108	17.94	50.80	0.04

5.1.2 Generator attributes

The next step is to represent the capacity mix in NYISO. To achieve a reasonable trade-off between generality and complexity, generators with the same technology type and located in the same zone is modeled as a single generator, which has the aggregated capacity.

EIA [37] provides operating generator capacity by state. The generators affiliated to NY state are filtered and are then mapped to zones based on its geographical location[6]. There are 1038 units located in NYCA, and the breakdown by technology type is represented by the pie chart in Figure 5-4. As shown in the pie chart, gas turbines dominate the capacity mix, followed by nuclear power units and hydro units. Biomass, solar PV and storage (flywheel units) are neglected since those units do not have much contribution to the total capacity.

[6] Since some county are across several load zones, especially in the southeastern area, the zonal information of some units involved are approximated to our best knowledge.

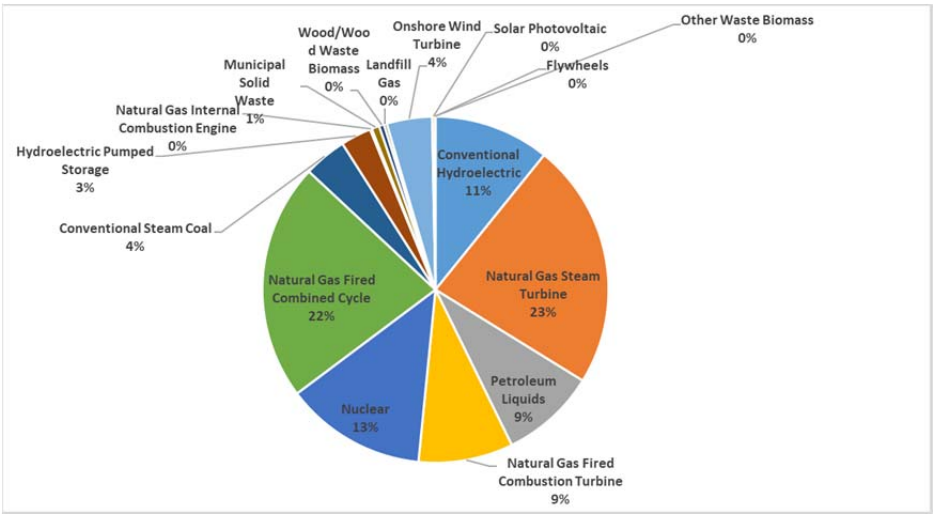

Figure 5-4: Pie chart of generation capacity by technology type

We re-categorize technology type to common types—natural gas, hydro (conventional hydro or pumped storage), nuclear, coal, wind and oil. Thus, the capacity mix in mini-NYISO system is provided in Figure 5-5. In comparison with the actual capacity mix of the NYISO system [38], as shown in Figure 5-5, we determined that the capacity mix in the mini-NYISO system reflects the fuel structure for the real-life system. Figure 5-6 represents the capacity proportion by fuel type for each zone.

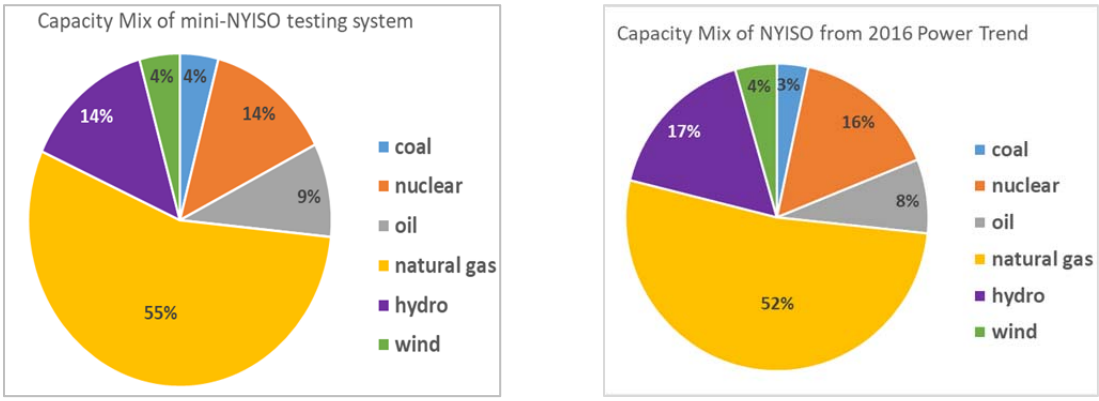

(a) Capacity mix of mini-NYISO testing system (b)Capacity mix of NYISO from 2016 Power Trend

Figure 5-5: Capacity mix comparison between mini-NYISO and actual NYISO system

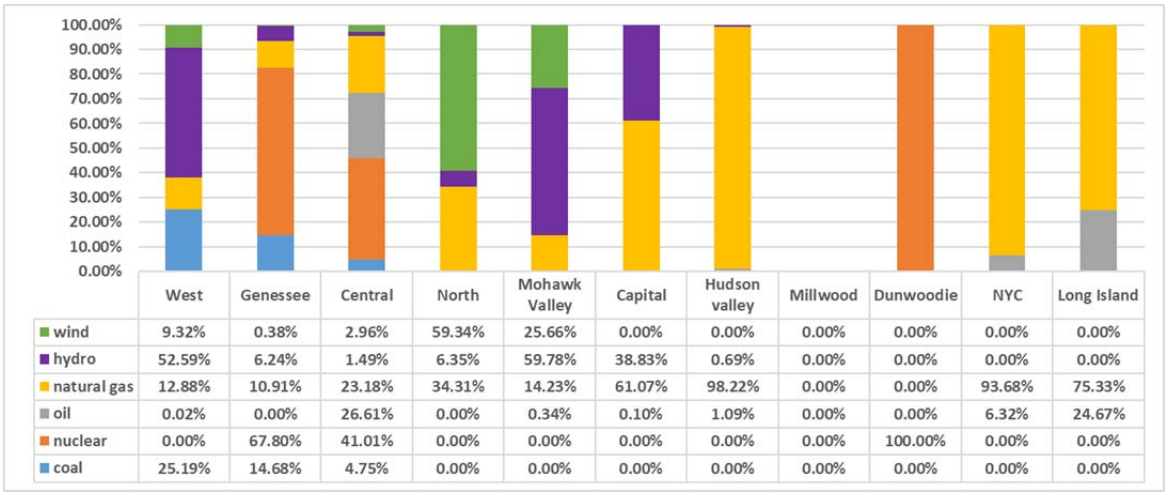

	West	Genessee	Central	North	Mohawk Valley	Capital	Hudson valley	Millwood	Dunwoodie	NYC	Long Island
wind	9.32%	0.38%	2.96%	59.34%	25.66%	0.00%	0.00%	0.00%	0.00%	0.00%	0.00%
hydro	52.59%	6.24%	1.49%	6.35%	59.78%	38.83%	0.69%	0.00%	0.00%	0.00%	0.00%
natural gas	12.88%	10.91%	23.18%	34.31%	14.23%	61.07%	98.22%	0.00%	0.00%	93.68%	75.33%
oil	0.02%	0.00%	26.61%	0.00%	0.34%	0.10%	1.09%	0.00%	0.00%	6.32%	24.67%
nuclear	0.00%	67.80%	41.01%	0.00%	0.00%	0.00%	0.00%	0.00%	100.00%	0.00%	0.00%
coal	25.19%	14.68%	4.75%	0.00%	0.00%	0.00%	0.00%	0.00%	0.00%	0.00%	0.00%

Figure 5-6: Capacity proportion for fuel type by zone

To reflect the fact that the capacity of some generators is not fully utilized, the capacity factor is used to represent the relationship between the actual output and rated capacity. Those generators participate in SCED and incur production cost; they have the limitations on ramping capabilities. Table 5-3 lists typical values for the generator marginal cost (per EIA data [39]) and ramping rate.

Table 5-3: Generator attributes by resource type

Technology type	Nuclear	Coal	Hydro	Gas Turbine	Oil	Wind
Marginal cost ($/MWh)	25.71	37.26	13.42	33.24	45	0
Ramping rate (MW/min)	2.0	2.0	/	6.7	2.0	/

5.1.3 LSE attributes

Per requirements from the NYISO Tariff, the NYISO publishes hourly zonal load for the next several operating days and posts the actual load on a five-minute basis [40]. We have used these postings to generate load data appropriate for our test system.

5.1.4 Reserve requirement

Reserve products in NYISO include regulation, 10-minute spinning reserve, 10-minute non-synchronized reserve, and 30-minute reserve. Regulation reserve is necessary to continuously balance load procurement with generation output. The remaining reserve products are responsible for backup generation or demand response, following occurrence of a real-time contingency. NYISO has a nested requirement for operating reserves [41], as provided in Figure 5-7.

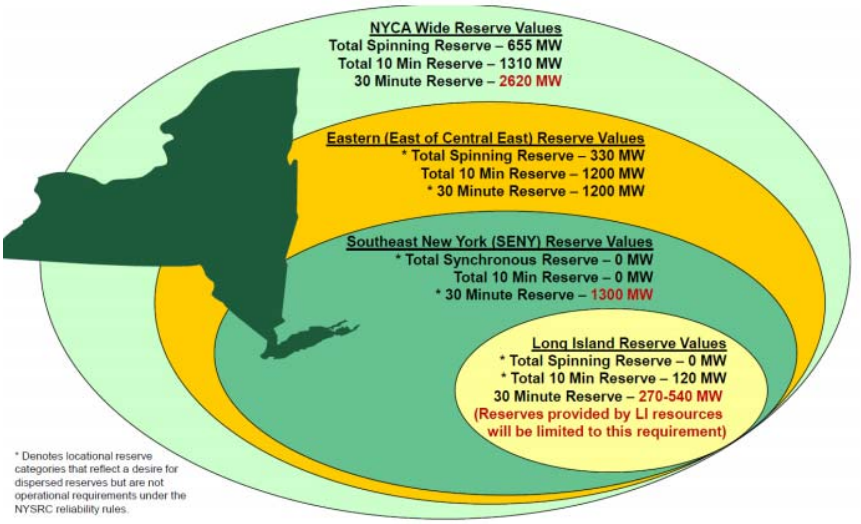

Figure 5-7: NYCA operating reserve requirements

5.2 Constraint relaxation on NYISO system

5.2.1 Evaluation on mini-NYISO system

June 13th, 2017 is the recorded peak day in the operation report for June 2017. Thus, we pick the time stamp from 20:00 to 20:25 as the examined operating horizon, since a LMP spike is observed to occur frequently during this time duration, which indicates a highly congested network. By manipulating the interface limit, we successfully repeat the congestion pattern that is observed in the actual NYISO system**.** Overloads have been observed in the initial condition, as shown as Table 5-4. The corresponding LMPs are listed in Table 5-5, where we have only provided these LMPs for Period 1 since the remaining periods have similar patterns. A high congestion price is shown for Zones Millwood, Dunwoodie, NYC and Long Island. Furthermore, the LMPs in the western and central zones tend to be lower than those in the southeastern zones. This is caused by the imbalanced allocation of resources and load in NYISO. Overall, Zone NYC and Long Island contribute to 50% of the total load; local units in these two zones are mainly expensive gas-turbines; cheap generation is concentrated in western and central zones, including the Niagara hydro units. Congestion on the Central-East interface has been historically challenging for NYISO. Thus, LMPs in those zones tend to be higher. This verifies that the mini-NYISO system we have developed is a reasonable approximation to the operation and market performance of the NYISO system.

Table 5-4: Limiting facilities

Periods	**Limiting facility**
P1	Hudson valley →Millwood ; Millwood → Dunwoodie ; Dunwoodie → NYC ; NYC → Long Island
P2	Hudson valley → Millwood ; Millwood → Dunwoodie ; Dunwoodie → NYC; NYC → Long Island
P3	Dunwoodie → NYC; NYC → Long Island
P4	Dunwoodie → NYC; NYC → Long Island
P5	Dunwoodie → NYC; NYC → Long Island
P6	Millwood → Dunwoodie; Dunwoodie → NYC ; NYC → Long Island

Table 5-5: Breakdown of LMP in A-CR

Bus	**Period No.**	**LMP_Energy**	**LMP_Congestion**	**LMP**
West	P1	33.24	0	33.24
Genessee	P1	33.24	4.02	37.26
Central	P1	33.24	0	33.24
North	P1	33.24	0	33.24
Mohawk Valley	P1	33.24	0	33.24
Capital	P1	33.24	0	33.24
Hudson valley	P1	33.24	11.76	45
Millwood	**P1**	**33.24**	**4011.76**	**4045**
Dunwoodie	**P1**	**33.24**	**8011.76**	**8045**
NYC	**P1**	**33.24**	**12011.76**	**12045**
Long Island	**P1**	**33.24**	**8011.76**	**8045**

5.2.2 Constraint relaxation results

We apply the methodology of P-RBCR on the mini-NYISO system. The results are presented and analyzed in the following subsections.

1. Flow/ temperature change

In the feasibility stage, the thermal limits for limiting constraints in the initial condition (Table 5-4) are assigned to the CR set. For those lines, temperature limits are applied instead of flow limits, and no further violations are observed. For example, the

Dunwoodie -NYC line exhibits interesting temperature/flow dynamics, as indicated in Figure 5-8.

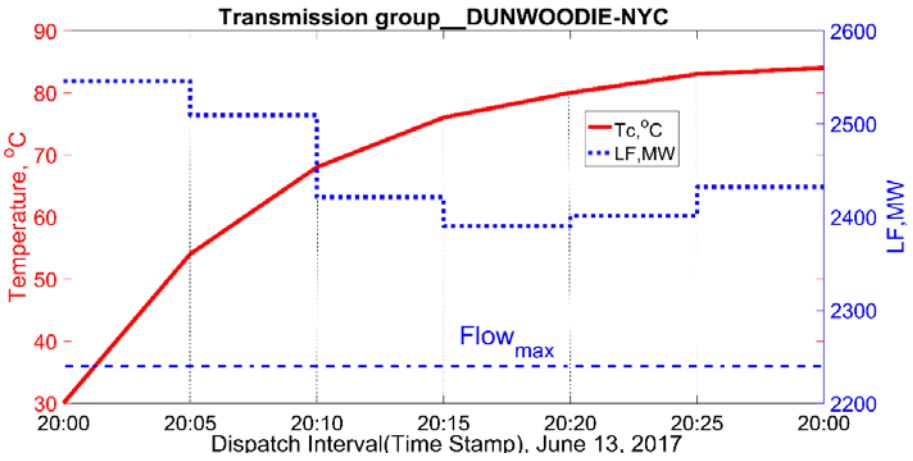

Figure 5-8: Flow/temperature change for the Dunwoodie-NYC line[7]

As shown in Figure 5-8, the flow significantly exceeds its limit, but the temperature does not, so such a constraint relaxation is acceptable.

2. Production cost and risk

Table 5-6 provides comparisons on production cost and risk for the A-CR and the P-RBCR constraint relaxation procedures. Inspection of these data result in observations that are similar to those made for the six-bus IEEE test system, i.e., the decisions obtained by the P-RBCR approach results in more economic and more secure operating conditions for handling infeasible SCED by actions of constraint relaxation.

Table 5-6: Comparisons on production cost and risk

	Production cost ($/30min)	**Risk**
A-CR	14,517,679	115
P-RBCR	4,086,710	5

3. LMP comparisons between A-CR and P-RBCR

Figure 5-9: LMP plots for A-CR v.s. P-RBCRplots the breakdown of LMP for A-CR and P-RBCR. Since other periods have the same conclusion and patterns, only the plots for periods 1 and 2 are provided. From these plots, we make observations consistent with those made from results of analysis on the six-bus system, that is to say, P-RBCR reduces price spikes while retaining the effects of a price signal to mitigate system congestion.

[7] The conductor temperature limit is 100 ^{o}C.

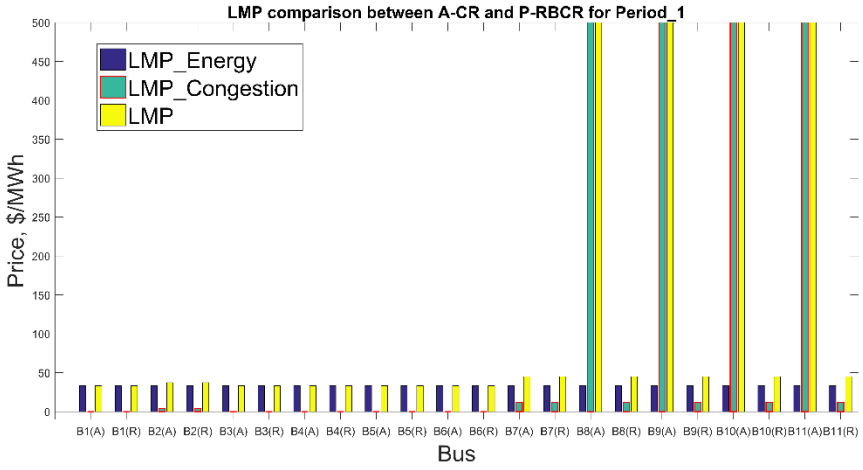

(a) Period 1

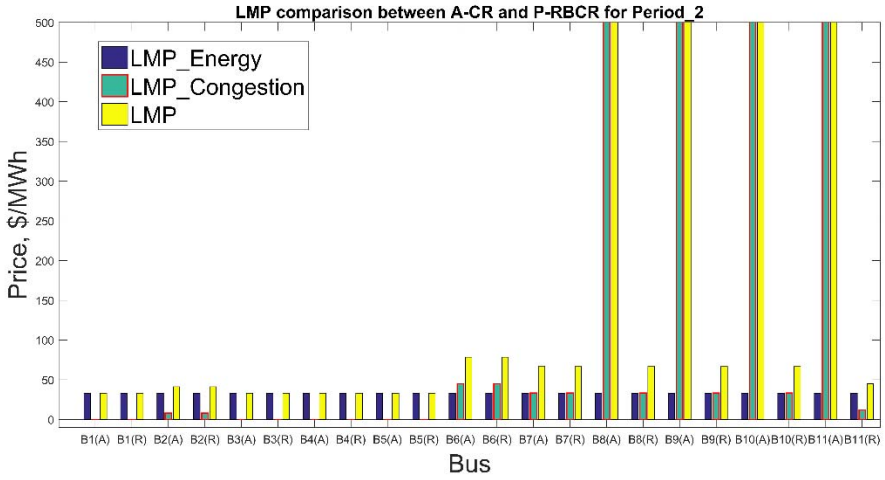

(b) Period 2

Figure 5-9: LMP plots for A-CR v.s. P-RBCR

5.3 Summary

This chapter describes the development process for mini-NYISO system, and tests the methodology of P-RBCR on this representative real-life system, which achieves the similar conclusions as that for the IEEE standard testing system.

6. Conclusions

The infeasible predictive-SCED, which results from constraint violations on transmission lines limits, can be solved successful by the proposed P-RBCR methodology. The properties of thermal dynamics enable conductor temperature limitations to be effectively used to safely provide increased maneuverability when deploying constraint relaxation. The predictive control strategy utilizes sequences of time-intervals, making the relaxation decision more economic and adaptive to future conditions. The fact that P-RBCR does not use penalty price reduces LMP spikes while maintaining good price signals for motivating market response to congestion.

In conclusion, as an efficient approach to manage congestion, the methodology of P-RBCR, is applicable and promising in handing infeasibilities of SCED in terms of overloaded transmission lines.

As the follow-up project to M-29, we have improved the CR methodology using the concept of dynamic heat balance equation. P-RBCR is also applicable to overloads under normal condition. The research and achievements obtained in this project are advancements in relation to the previous project.

References

[1] New York Independent System Operator. NYISO market participant user guide. http://www.nyiso.com/public/webdocs/markets_operations/documents/Manuals_and_Guides/Guides/User_Guides/mpug.pdf

[2] California Independent System Operator. Market process and products in CAISO. https://www.caiso.com/market/Pages/MarketProcesses.aspx

[3] Mid-continent Independent System Operator. MISO overview training. https://www.misoenergy.org/Library/Repository/Meeting%20Material/Stakeholder/Training%20Materials/100%20Level%20Training/Level%20100%20-%20MISO%20Overview.pdf

[4] New York Independent System Operator. NYISO Day-Ahead Scheduling Manual. http://www.nyiso.com/public/webdocs/markets_operations/documents/Manuals_and_Guides/Manuals/Operations/dayahd_schd_mnl.pdf

[5] California Independent System Operator. Price Inconsistency Market Enhancements-Issue Paper & Straw Proposal. https://www.caiso.com/Documents/IssuePaper_StrawProposalPriceInconsistencyMarketEnhancements.pdf

[6] Y. Al-Abdullah, "Energy Market Transparency: Analyzing the impacts of constraint relaxation and out-of-market correction practices in electric energy markets," Ph.D. Dissertation, Arizona State University, May 2016.

[7] A. Pillay, S. Karthikeyan, and D. Kothari, "Congestion management in power systems – a review," International Journal of Electrical Power and Energy Systems," 70 (2015): 83-90.

[8] K. Hedman, X. Guo , J. McCalley, etc. "PSerc report M-29, "Constraint relaxations: analyzing the impacts on system reliability, dynamics and markets," August, 2015, https://pserc.wisc.edu/documents/.../M-29_Final-Report_ExecSum_Sept-2015.pdf.

[9] Personal Communication with market expert, Dr. Yonghong Chen, Principal Advisor at MISO, conducted by Dr. J. McCalley. School of Electrical and Computer Engineering, Iowa State University, 2017.

[10] Mid-continent Independent System Operator. Transmission Constraint Demand Curve Proposal. Materials for November MSC, 2012.

[11] New York Independent System Operator. Transmission congestion pricing. MIWG materials.http://www.nyiso.com/public/webdocs/markets_operations/committees/bic_miwg/meeting_materials/2016-12-21/Constraint%20Reliability%20Margin%20CRM.pdf

[12] New York Independent System Operator. MMU Assessment of the Graduated Transmission Demand Curve Implementation. MIWG meetings. http://www.nyiso.com/public/webdocs/markets_operations/committees/bic_miwg/meeting_materials/2016-11-03/Evaluation%20of%20Potential%20Market%20Problem%20by%20MMU_11-02-2016_final.pdf

[13] New York Independent System Operator. Transmission constraint pricing. BIC meeting.

[14] California Independent System Operator. Stepped Constraint Parameters, Straw Proposal. May 2016. https://www.caiso.com/Documents/IssuePaper-SteppedConstraintParameters.pdf

[15] South Power Pool. 2016 Annual VRL Analysis for SPP market. https://www.spp.org/documents/40439/2015_2016%20vrl%20analysis.pdf

[16] New York Independent System Operator. Markets & Operations Data. http://www.nyiso.com/public/markets_operations/market_data/power_grid_data/ind ex.jsp

[17] New York Independent System Operator. Sub-zone boundaries. http://www.nyiso.com/public/webdocs/markets_operations/documents/Manuals_and_Guides/Manuals/Additional_Manuals/tablea1_subzone_boundaries.pdf

[18] "738-2006 - IEEE Standard for Calculating the Current-Temperature of Bare Overhead Conductors," IEEE, 2007.

[19] Procedures for determining and implementing transmission facility ratings in New England. ISO New England planning procedure No.7.

[20] Oncor's pioneering transmission dynamic line rating demonstration lays foundation for follow-up developments. Oncor, May 2014.

[21] D. Douglass; W. Chisholm; G. Davidson; I. Grant; K. Lindsey; M. Lancaster; D. Lawry; T. McCarthy; C. Nascimento; M. A. Pasha; J. Reding; T. Seppa; J. Toth; P. Waltz, "Real-Time Overhead Transmission Line Monitoring for Dynamic Rating," in IEEE Transactions on Power Delivery, vol.PP, no.99, pp.1-1

[22] D. M. Kim, J. M. Cho, H. S. Lee, H. S. Jung and J. O. Kim, "Prediction of Dynamic Line Rating Based on Assessment Risk by Time Series Weather Model," Probabilistic Methods Applied to Power Systems, 2006. PMAPS 2006. International Conference on, Stockholm, 2006, pp. 1-7.

[23] R. Mai, L. Fu and Xu HaiBo, "Dynamic Line Rating estimator with synchronized phasor measurement," Advanced Power System Automation and Protection (APAP), 2011 International Conference on, Beijing, 2011, pp. 940-945.

[24] H. Banakar, N. Alguacil and F. Galiana, "Electrothermal CoordinationPart I: theory and implementation schemes," IEEE Trans. Power Syst.,vol. 20, no. 2, pp. 798 - 805, 2005.

[25] Jiao Fu, S. Abdelkader, D. J. Morrow and B. Fox, "Partial least squares modelling for dynamic overhead line ratings," PowerTech, 2011 IEEE Trondheim, Trondheim, 2011, pp. 1-6.

[26] F. Qiu and J. Wang, "Distributionally Robust Congestion Management With Dynamic Line Ratings," in IEEE Transactions on Power Systems, vol. 30, no. 4, pp. 2198-2199, July 2015.

[27] C. J. Wallnerström, Y. Huang and L. Söder, "Impact From Dynamic Line Rating on Wind Power Integration," in IEEE Transactions on Smart Grid, vol. 6, no. 1, pp. 343-350, Jan. 2015.

[28] Bolun Xu, A. Ulbig and G. Andersson, "Impacts of dynamic line rating on power dispatch performance and grid integration of renewable energy sources," Innovative Smart Grid Technologies Europe (ISGT EUROPE), 2013 4th IEEE/PES, Lyngby, 2013, pp. 1-5.

[29] B. Banerjee, D. Jayaweera, and S. M. Islam, "Alleviating PostContingency Congestion Risk of Wind Integrated Systems with Dynamic Line Ratings," in Universities Power Engineering Conference (AUPEC), 2014 24th Australasian, 2014.

[30] B. Banerjee, D. Jayaweera, and S. M. Islam, "Optimal scheduling with dynamic line ratings and intermittent wind power," in PES General Meeting | Conference & Exposition, 2014 IEEE, 2014, pp. 1-5

[31] M. Wang and X. Han, "Study on Electro-thermal Coupling Optimal Power Flow Model and Its Simplification," in IEEE Power & Energy Soc. General Meeting, Minneapolis, 2010.

[32] N. Alguacil, M. Banakar and F. Galiana, "Electrothermal Coordination Part II: Case Studies," IEEE Trans. Power Syst., vol. 20, no. 4, pp. 1738-1745, 2005.

[33] M. Nick; O. Alizadeh-Mousavi; R. Cherkaoui; M. Paolone, "Security Constrained Unit Commitment With Dynamic Thermal Line Rating," in IEEE Transactions on Power Systems, vol.PP, no.99, pp.1-12

[34] A. Wood and B. Wollenberg, Power Generation, Operation and Control, 2nd. New York, NY, USA: Wiley, 1996.

[35] K., Dheepak, W. Li, and L. Tesfatsion. "An 8-zone test system based on ISO New England data: Development and application." IEEE Transactions on Power Systems 31.1 (2016): 234-246.

[36] New York Independent System Operator. 2016 Reliability Needs Assessment. http://www.nyiso.com/public/webdocs/media_room/press_releases/2016/Child_2016_RNA/2016RNA_Final_Oct18_2016.pdf

[37] EIA. Preliminary Monthly Electric Generator Inventory. https://www.eia.gov/electricity/data/eia860M/

[38] New York Independent System Operator. 2016 power trend for NYISO. http://www.nyiso.com/public/webdocs/media_room/publications_presentations/Power_Trends/Power_Trends/2016-power-trends-FINAL-070516.pdf

[39] EIA. https://www.eia.gov/electricity/annual/html/epa_08_04.html

[40] New York Independent System Operator. Actual load, Market & Operations Data Archive.

[41] New York Independent System Operator. Ancillary service, training materials for NYMOC courses.